2001-12

Performance analysis of OFDM in frequency selective, slowly fading Nakagami Channels

Count, Patrick A.

NAVAL POSTGRADUATE SCHOOL
Monterey, California

THESIS

PERFORMANCE ANALYSIS OF OFDM IN FREQUENCY-SELECTIVE, SLOWLY FADING NAKAGAMI CHANNELS

by

Patrick A. Count

December 2001

Thesis Co-Advisors: Tri T. Ha
R. Clark Robertson

Approved for public release; distribution is unlimited.

THIS PAGE INTENTIONALLY LEFT BLANK

REPORT DOCUMENTATION PAGE			Form Approved OMB No. 0704-0188
Public reporting burden for this collection of information is estimated to average 1 hour per response, including the time for reviewing instruction, searching existing data sources, gathering and maintaining the data needed, and completing and reviewing the collection of information. Send comments regarding this burden estimate or any other aspect of this collection of information, including suggestions for reducing this burden, to Washington headquarters Services, Directorate for Information Operations and Reports, 1215 Jefferson Davis Highway, Suite 1204, Arlington, VA 22202-4302, and to the Office of Management and Budget, Paperwork Reduction Project (0704-0188) Washington DC 20503.			
1. AGENCY USE ONLY *(Leave blank)*	**2. REPORT DATE** December 2001	**3. REPORT TYPE AND DATES COVERED** Master's Thesis	
4. TITLE AND SUBTITLE: Title (Mix case letters) Performance Analysis of OFDM in Frequency-Selective, Slowly Fading Nakagami Channels			**5. FUNDING NUMBERS**
6. AUTHOR(S) Count, Patrick A.			
7. PERFORMING ORGANIZATION NAME(S) AND ADDRESS(ES) Naval Postgraduate School Monterey, CA 93943-5000			**8. PERFORMING ORGANIZATION REPORT NUMBER**
9. SPONSORING / MONITORING AGENCY NAME(S) AND ADDRESS(ES) N/A			**10. SPONSORING / MONITORING AGENCY REPORT NUMBER**
11. SUPPLEMENTARY NOTES The views expressed in this thesis are those of the author and do not reflect the official policy or position of the Department of Defense or the U.S. Government.			
12a. DISTRIBUTION / AVAILABILITY STATEMENT Approved for public release; distribution is unlimited.			**12b. DISTRIBUTION CODE**

13. ABSTRACT ***(maximum 200 words)***

In an effort to offer faster, more reliable wireless communications services to the public, many wireless standardization committees have, in recent years, adopted Orthogonal Frequency Division Multiplexing (OFDM) as the modulation technique of choice. Given the incredible growth in the industry as manifest by the seemingly infinite demand for wireless products and services and the accompanying need for superior performance of these systems in congested and electronically demanding environments, it is evident that OFDM will be at the core of many future high data rate communications systems. This thesis examines the performance of OFDM in frequency-selective slowly fading Nakagami channels. The Nakagami channel is used in this study as it probably best models the propagation characteristics of the environments in which OFDM based systems will be applied.

14. SUBJECT TERMS OFDM, Nakagami, Modulation, Multiplexing, frequency-selective, slow, PSK, QAM, multipath fading, FEC coding, hard-decision decoding, soft-decision decoding			**15. NUMBER OF PAGES** 112
			16. PRICE CODE
17. SECURITY CLASSIFICATION OF REPORT Unclassified	**18. SECURITY CLASSIFICATION OF THIS PAGE** Unclassified	**19. SECURITY CLASSIFICATION OF ABSTRACT** Unclassified	**20. LIMITATION OF ABSTRACT** UL

NSN 7540-01-280-5500 Standard Form 298 (Rev. 2-89)
Prescribed by ANSI Std. 239-18

THIS PAGE INTENTIONALLY LEFT BLANK

Approved for public release; distribution is unlimited

PERFORMANCE ANALYSIS OF OFDM IN FREQUENCY-SELECTIVE, SLOWLY FADING NAKAGAMI CHANNELS

Patrick A. Count
Lieutenant, United States Navy
B.A., University of South Carolina, 1995

Submitted in partial fulfillment of the
requirements for the degree of

MASTER OF SCIENCE IN ELECTRICAL ENGINEERING

from the

NAVAL POSTGRADUATE SCHOOL
December 2001

Author: _____
Patrick A. Count

Approved by: _____
Tri T. Ha, Thesis Co-Advisor

_____
R. Clark Robertson, Thesis Co-Advisor

_____
Jeffrey B. Knorr, Chairman,
Department of Electrical and Computer Engineering

THIS PAGE INTENTIONALLY LEFT BLANK

ABSTRACT

In an effort to offer faster, more reliable wireless communications services to the public, many wireless standardization committees have, in recent years, adopted orthogonal frequency-division multiplexing (OFDM) as the signaling technique of choice. Given the incredible growth in the industry as manifest by the seemingly infinite demand for wireless products and services and the accompanying need for superior performance of these systems in congested and electronically demanding environments, it is evident that OFDM will be at the core of many future high data rate communications systems. This thesis examines the performance of OFDM in frequency-selective, slowly fading Nakagami channels. The Nakagami channel is used in this study as it best models the propagation characteristics of the environments in which OFDM based systems will be applied.

THIS PAGE INTENTIONALLY LEFT BLANK

TABLE OF CONTENTS

LIST OF FIGURES

LIST OF TABLES

THIS PAGE INTENTIONALLY LEFT BLANK

ACKNOWLEDGMENTS

In any undertaking of this magnitude one inevitably relies upon the guidance, counsel, and support of many. Academically, my deepest debts of gratitude go to my thesis co-advisors, Professors Tri T. Ha and R. Clark Robertson. Dr. Ha's vision in first acquiring a topic, then refining it and establishing goals and milestones kept me on schedule and was critical to the successful completion of this thesis. His encouragement gave me the confidence I needed to move forward.

For his ever informative and insightful mentoring and instruction I extend my heartfelt appreciation to Dr. Robertson. His approachable manner and superior technical insight into some of the most complicated portions of this thesis were irreplaceable and guaranteed my success. His enthusiasm transformed this thesis from an academic endeavor into a fun and enlightening experience.

Thanks go out as well to LCDR John. W. McKinstry, USN, LCDR Tom E. Newman, USN, and CTR1(NAC) Frank B. Williams, USN (Ret.), all of whom I credit with introducing me to the wonderful and exciting world of Electrical Engineering and it's applications. Their encouragement was vital in transforming myself from a linguist into a well rounded and technically competent Engineer and Naval Cryptologist.

To my many classmates and peers at the Naval Postgraduate School over the past two and a half years I give a great deal of the credit. Though I learned much in class, my classmates, through untold hours of evening and weekend study sessions, taught me more than any instructor ever could. Their camaraderie and professionalism as students and officers are what set the Naval Postgraduate School apart.

Certainly most critical to my work and my entire education for that matter is the unwavering support at home provided by my behind the scenes instructor, friend, and love, my wife Julie and my children Benjamin, Samuel, and Emma who have given my life such great joy and purpose. Their collective understanding during the many long often discouraging hours it took to complete this thesis and degree program have been the one constant in this process.

Finally, to the glory of God, I render the greatest degree of credit. For none of this would be possible without the graces so freely given through his son Jesus Christ.

THIS PAGE INTENTIONALLY LEFT BLANK

EXECUTIVE SUMMARY

Orthogonal frequency-division multiplexing (OFDM) has been adopted as the digital signaling technique for many new and emerging communications systems. For its ability to mitigate the most severe multipath propagation conditions, bandwidth efficiency, and simplicity of implementation, OFDM has become the standard in a number of applications world wide such as, Digital Video and Digital Audio Broadcast (DAB and DVB), ETSI HIPERLAN II, Asymmetric Digital Subscriber Line (ADSL), and the IEEE 802.11a wireless local area networking high speed physical layer standard.

In this thesis the IEEE 802.11a application of OFDM is closely examined. The sub-carrier modulation types, the forward error correction coding techniques, and achievable data rates called for in the 802.11a standard form the framework for a performance analysis of OFDM in a wide range of fading environments.

Since fading conditions vary wildly, a comprehensive statistical model must be used in order to analyze as many fading conditions as possible. The Nakagami-m distribution is chosen for its ability to emulate fading channels whose conditions are either less severe than, the same as, or more severe than the most common statistical fading model, the Rayleigh fading model. With the Nakagami we are able to analyze both line-of-sight (LOS) and non-LOS conditions. This flexibility is important in the WLAN application of OFDM since any one of these propagation characteristics may be encountered in such an application.

Since OFDM is a multi-carrier communications system in which multiple low data-rate sub-carriers are used to transmit a single high data-rate stream, conventional modulation techniques are used for sub-carrier modulation. Consideration of ease of implementation, error performance, and bandwidth efficiency led to the selection of binary phase-shift keying (BPSK), quadrature phase-shift keying (QPSK), and 16 and 64-quadrature amplitude modulation (MQAM) for the sub-carriers. This thesis examines the performance of each of these sub-carrier modulation types in the presence of Nakagami-m distributed fading. The convolutional code rates specified in the 802.11a

standard are also incorporated as they are in real communications systems to provide improved performance and a more realistic scenario.

The performance metric we use is the probability of bit error versus the average signal-to-noise ratio (SNR) per bit. We develop expressions for the probability of bit error for each modulation and code rate possible in the IEEE 802.11a standard. This approach to OFDM and an IEEE 802.11a-compliant system is designed to provide the reader with a comprehensive study of the performance of such a system with a variety of parameters already considered. The range of fading is studied from the most severe to the least. This is accomplished by adjusting the primary variable in the Nakagami-m distribution.

The dominance of the more severe fading conditions relative to the range of fading conditions considered across all 48 data sub-carriers is among the important results of this study. Further, the relatively large coding gains possible with the addition of error correction coding is also significant. Most of all the performance curves themselves give the reader and 802.11a system design engineer an idea of what kind of performance can be expected by such a system under a great many varied conditions. If this is in any way helpful in determining the best possible system trade-offs, then this thesis will have served its purpose.

I. INTRODUCTION

In an increasingly mobile society, the value placed on wireless communications grows daily. The revolution in wireless communications technology, brought about by high consumer demand for such products as cellular phones, pagers, and wireless networks, has elevated yesterday's dreams to today's reality. These advances, however, rely on increasingly complicated microelectronic fabrication processes, comprehensive propagation studies, and clever modulation techniques. Communications technology has advanced from the days of manual morse to amplitude modulation (AM) to the sophisticated digital signaling schemes of today. One digital signaling technique, orthogonal frequency-division multiplexing (OFDM), is the focus of this thesis. In an effort to offer faster, more reliable wireless communications services to the public, many wireless standardization committees have, in recent years, adopted OFDM as the modulation technique of choice for its ability to provide reliable high data rate communications in wireless environments. This thesis examines the performance of OFDM in a frequency-selective, slowly fading Nakagami channel, a channel which best models the propagation characteristics of the environments in which OFDM based wireless systems will be applied.

A. SCOPE

OFDM has been adopted as the standard for many wireless applications, Digital Video and Digital Audio Broadcast (DVB and DAB), ETSI HIPERLAN II, Asymmetric Digital Subscriber Line (ADSL), and IEEE 802.11a high data-rate wireless local area network (WLAN) applications just to name a few. Since the methods of implementing OFDM are numerous and the applications varied, this study focuses on the standard adopted by the Standards Association of the Institute of Electrical and Electronics Engineers, IEEE 802.11a. This standard for the medium access control (MAC) and physical layers (PHY) of WLANs in the 5 GHz band is the OFDM based system from which this thesis draws many of its assumptions.

1. Why OFDM?

OFDM has evolved from the earliest forms of frequency-division multiplexing (FDM). FDM was conceived in order to allow the simultaneous transmission of multiple signals over a wide bandwidth channel utilizing separate carrier frequencies. The trouble with conventional FDM systems is that they do not efficiently utilize the available bandwidth because there is no spectral overlap between adjacent carriers. This waste is further aggravated by the addition of guard bands (areas of no spectral content between carriers) necessary to ensure no frequency domain overlap and to make filtering at the receiver practical.

Rather than transmitting completely separate signals, each on their own carrier frequency, as with conventional FDM, the concept of OFDM is to divide the bits of a single high-data rate transmission into many lower-data rate bit streams through serial-to-parallel conversion. The resulting lower-data rate bit streams are then modulated and transmitted on multiple carrier frequencies. The orthogonality, or precise peak-to-null frequency spacing, of these multiple carriers, the so called "sub-carriers", and the ensuing spectral overlap is what sets OFDM apart from its predecessors. Modern signal processing techniques such as the fast Fourier transform (FFT) have made implementation of OFDM realizable.

More compelling still, and the most significant reason for adopting OFDM, is its ability to deal effectively with the most prevalent complicating factor in realistic wireless communications channels, inter-symbol interference (ISI) caused by multipath fading. In any mobile channel, multiple versions of the same signal arrive at the receiver because of reflection, refraction, or other phenomenon. These multiple signals arrive at the receiver at different times resulting in time domain overlap of individual symbols. The duration of this symbol overlap, usually quantified as "delay spread," causes the symbols to destructively interfere with one another resulting in wild fluctuations in received signal power. The resulting ISI can significantly degrade communications and thereby reduce the quality of service (QOS) provided.

The bottom line effect of multipath fading in today's wireless market is the reduction of maximum achievable data rates. As will be discussed in greater detail in

chapter two, OFDM, through a variety of remedies, combats this multipath fading effectively and enables the higher data rates sought by today's consumers.

2. Why Nakagami?

In any environment in which fading is present, wireless engineers must attempt to predict the effect of such fading on the transmitted signal as it passes through the transmission medium to the receiver. A variety of statistical models derived from probability theory and actual field observations help us model channel behavior and in so doing provide us with information essential to system design. If received signal amplitude levels can be predicted based on these models, then required transmitter power, system architecture, modulation technique, and a host of other parameters can be adjusted to compensate for the channel. The Nakagami-m distribution is one such model, which can be used to emulate fading channel conditions.

The Nakagami distribution, like other distributions, is used to describe the fluctuations in the envelope of the received signal due to multipath fading. The choice of the Nakagami distribution for the transmission channel in this thesis is based upon the fact that the Nakagami model has been found to best match observed signal statistics in fading environments [1]. In addition, this distribution offers a greater degree of flexibility to vary our statistical channel representation than many other popular channel models as it is a two-parameter distribution. Other distributions such as the more popular Rayleigh are single-parameter distributions and are generally more restrictive. In fact, the Rayleigh is a special case of the Nakagami-m distribution.

3. Frequency Selective, Slowly Fading Channels

There are many qualifiers where fading channels are involved. Fading channels may be described as either frequency non-selective (flat) or frequency-selective and as either fast or slowly fading. In order to make sense of these characteristics it is necessary to first define a few terms.

When the transmission channel exhibits constant gain and linear phase over a bandwidth much smaller than that of the signal, the channel is said to be frequency-

selective. If the opposite is true, it is frequency non-selective, or flat. The bandwidth over which the channel has linear phase and constant gain occurs is referred to as the "coherence bandwidth." In the time domain, this phenomenon is characterized by the "delay spread." In other words, a frequency-selective channel is one in which the coherence bandwidth is much smaller than the signal bandwidth. Equally true, if the root mean squared (RMS) delay spread is greater than the signal symbol period, the channel is frequency-selective [2].

A channel is said to be slowly fading if the impulse response (used to describe channel behavior) of the channel changes at a rate much slower than that of the signal. That is, the channel coherence time is much greater than the symbol duration. By the same token, fast fading describes a channel whose characteristics change rapidly relative to the transmitted signal. In this case, the channel coherence time is less than the symbol duration [2].

This thesis treats OFDM in frequency-selective, slowly fading channels. The reason for this choice of channel characteristics is precisely because OFDM was conceived and is employed to combat the multipath effects encountered in frequency-selective channels. If we did not have frequency-selective channels, OFDM would not be needed. Though frequency-selective channels are more difficult to analyze, as we have pointed out, they will most likely be the types of channels encountered by an OFDM signal.

For simplicity and breadth of application, the channel is assumed to be slowly fading; although, in any realistic mobile scenario, Doppler effects due to the motion of a mobile unit will further degrade signal strength. As this thesis does not restrict itself to mobile applications but rather incorporates the current WLAN applications of OFDM, the outstations are assumed here to be stationary. Naturally, when an outstation is not in motion, a channel is slowly fading. The treatment of fast fading channels and cellular specific applications of OFDM is the subject of further research.

4. Related Research

The analysis of OFDM in various types of fading is not a novel concept. There are numerous studies circulating regarding the performance of OFDM in many different fading channel characteristics. For instance, OFDM over frequency-nonselective, fast Rayleigh and Rician fading channels are addressed in [3] and [4] by Wan and Dubey; Miletik, Dimitrijevic, et. al. undertook an analysis of OFDM in Nakagami fading channels with differential frequency shift keying (DFSK) as the modulation in [5]; and in [6] Beaulieu, in a treatment on the effects of equal gain diversity on Nakagami fading channels has addressed the effects of soft decision decoding on Nakagami fading channels. These are just a few of the many related works.

In this thesis, we combine numerous concepts from communications theory along with novel analysis techniques to accomplish the goal of analyzing the performance of OFDM in frequency-selective, slowly fading, Nakagami fading channels. The combination of OFDM in Nakagami fading according to IEEE 802.11a standards has not, to the knowledge of the author, been addressed. Aside from this, our treatment is altogether different from other studies of OFDM performance. As will be explained in greater detail in Chapters III and IV, we will examine the uncoded performance of each OFDM sub-carrier as an independent channel, add error correction coding to the analysis, and account for the multiple sub-carriers by randomly distributing the Nakagami fading statistics and averaging them out over the total number of sub-carriers.

Further, we confine our approach to analyzing only those methods of OFDM implementation found in IEEE 802.11a-compliant systems. In so doing we address the four modulation types called for in the 802.11a standard specifically, along with their corresponding data rates and error correction coding rates. The benefit of such an approach is to assess the performance of an existing OFDM standard and gain some insight into how well we can expect these systems to perform as the first such devices begin to reach the public.

B. THESIS ORGANIZATION

After this introduction, this thesis is organized into four remaining chapters. In Chapter II we discuss OFDM basics. Chapter II will examine how OFDM works and

how OFDM symbols are generated. It will also cover many of the techniques involved in mitigating ISI and reducing probability of bit error. In Chapter III the performance of OFDM in a Nakagami channel will be developed analytically. This will begin with a treatment of BPSK, QPSK, 16-QAM, and 64-QAM as potential sub-carrier modulation techniques for OFDM as specified in the IEEE 802.11a standard. The performance of these modulation schemes in the presence of Nakagami fading will be the cornerstone of the chapter. In Chapter III we will also develop OFDM as a composite system of multiple sub-carriers and examine its performance. Chapter IV examines the effect of including forward error correction (FEC) coding. Finally, this study concludes with Chapter V and a brief review of the results obtained in the previous chapters followed by recommendations for further research.

II. OFDM FUNDAMENTALS

Before an analysis of OFDM in a Nakagami fading channel can be undertaken, it is first necessary to understand how OFDM works and how it is implemented. In this chapter we will cover basic OFDM concepts starting with some background, then moving into how to generate an OFDM signal, and finally discussing the implementation of OFDM using one specific application, the IEEE 802.11a standard. The application of some more general communications concepts such as the discrete Fourier transform (DFT), forward error correction coding (FEC), sub-carrier modulation techniques, and block interleaving will also be discussed within the context of their application to OFDM. Armed with this knowledge, we will then discuss OFDM in the broader context of fading channels.

A. OFDM BACKGROUND

The evolution of OFDM is an interesting and, at the same time, relevant topic. In this section, we will examine the concept of multi-carrier modulation, the orthogonality principal, and study the advantages and limitations of OFDM. This will lay the foundation upon which rest the remaining sections of this chapter.

1. Multi-carrier Modulation

As mentioned in the first chapter, a multi-carrier system is one that modulates data to be transmitted onto many different carrier frequencies. The classical multi-carrier system is the FDM system. FDM is a multiplexing technique whereby each channel carries a distinct, separate, signal. These signals are all transmitted simultaneously. It is worth noting at this point that OFDM may be considered both a multiplexing technique as well as a modulation type. It is a multiplexing technique in that it utilizes multiple carriers with simultaneous transmission as in classical FDM, however, in an OFDM system the individual sub-carriers each carry a portion of a single message distributed throughout. When viewed in the frequency domain, the channels have overlapping spectra and thus yield tremendous bandwidth savings as illustrated in Figure 1.

In order for carrier overlap to be possible without crosstalk among sub-carriers, the carriers must be orthogonal that is, they must be spaced at intervals of 1/T where T is the symbol duration for each sub-carrier. In the next section we discuss the orthogonality principal, as it is central to any discussion of OFDM.

More important to our understanding of OFDM at this point is why multiple-carrier systems are important and what they offer over other single-carrier systems. In order to achieve a fixed data rate R_b bits/second over a single carrier, modulated symbols must be transmitted at a much higher rate. This requires a reduction in

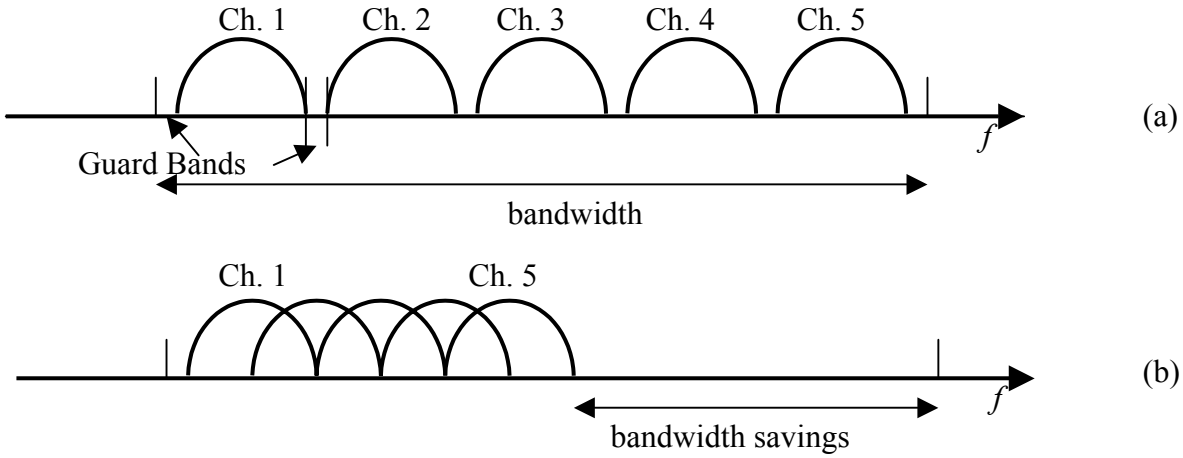

Figure 1. FDM (a) vs. OFDM (b)

symbol duration. The delay spread induced by multipath channels is now a greater percentage of the symbol duration, thus increasing the amount of ISI experienced by a high data rate single carrier system. Looked at another way, the time dispersion in such a case is greater than the symbol rate, which introduces ISI [1], and equalization techniques must be employed to overcome the ISI. It is well known that equalization significantly increases the complexity of a single-carrier system. In multi-carrier systems, such as OFDM, the data stream is transmitted in parallel over several low-rate sub-carriers. The lower data rates result in longer symbol duration for each sub-carrier and, for the same delay spread as we considered above, a smaller percentage of the symbol duration will be affected by ISI. Thus, complex equalization techniques are not required. Since OFDM uses the FFT algorithm to provide orthogonal cover to the sub-carriers, some may argue that the FFT's complexity makes up for the loss of equalization complexity, however, as

shown in [7], the complexity of the single carrier equalizer is ten times that of the FFT utilized in the OFDM system. Further, equalizer performance declines significantly when the delay spread exceeds that which the equalizer was designed to handle. Through the concept of the cyclic extension, OFDM better tolerates or adapts to delay spread variation.

As with any multi-carrier system, OFDM requires reliable synchronization. Since multi-carrier transmission systems transmit symbols over N_S parallel sub-carriers, resulting in longer symbol durations, the result is less sensitivity to timing errors [8]. In single-carrier systems, these so called timing jitters can introduce a significant amount of ISI. Thus, a major concern in single carrier systems is avoided with OFDM.

Multi-carrier systems also have the additional benefit of superior performance in frequency-selective fading channels or in the presence of narrowband interference. In single-carrier systems, a single fade can render the entire system unreliable, whereas in the multi-carrier system, the same single interference will only affect a few of the sub-carriers [7].

2. Orthogonality

The orthogonality principal is central to understanding the unique capabilities of OFDM. It is this precise mathematical relationship that allows the bandwidth savings due to carrier overlap previously discussed. Mathematically, orthogonality requires two vectors to be perpendicular, that is, the projection of one vector onto another, usually referred to as the "dot product," equals zero. This necessarily means that the two vectors are also linearly independent of one another. Communications theory, however, states that two signals are orthogonal if they are uncorrelated over a symbol interval. That is, they satisfy the following relationship [9]:

$$\int_0^T s_1(t)s_2(t)dt = 0 \tag{2.1}$$

where $s_1(t)$ and $s_2(t)$ are two signals we are attempting to correlate and T is the symbol duration.

The orthogonality of sub-carriers in an OFDM symbol can be illustrated a number of ways. In Figure 2 we see the waveform of four sub-carriers which together make up an OFDM signal. The waveforms are chosen to have equal amplitude and co-phase for illustration though in reality this is generally not the case. Notice that each waveform contains an integer number of cycles over the symbol duration, and the number of cycles per symbol duration of adjacent carriers differs by exactly one. That is, they are harmonically related. This behavior indicates that the time domain waveforms depicted here are orthogonal. In this example the frequencies are arbitrarily chosen to be 60, 120, 180, and 240 Hz with a symbol duration of T=1/60 depicted.

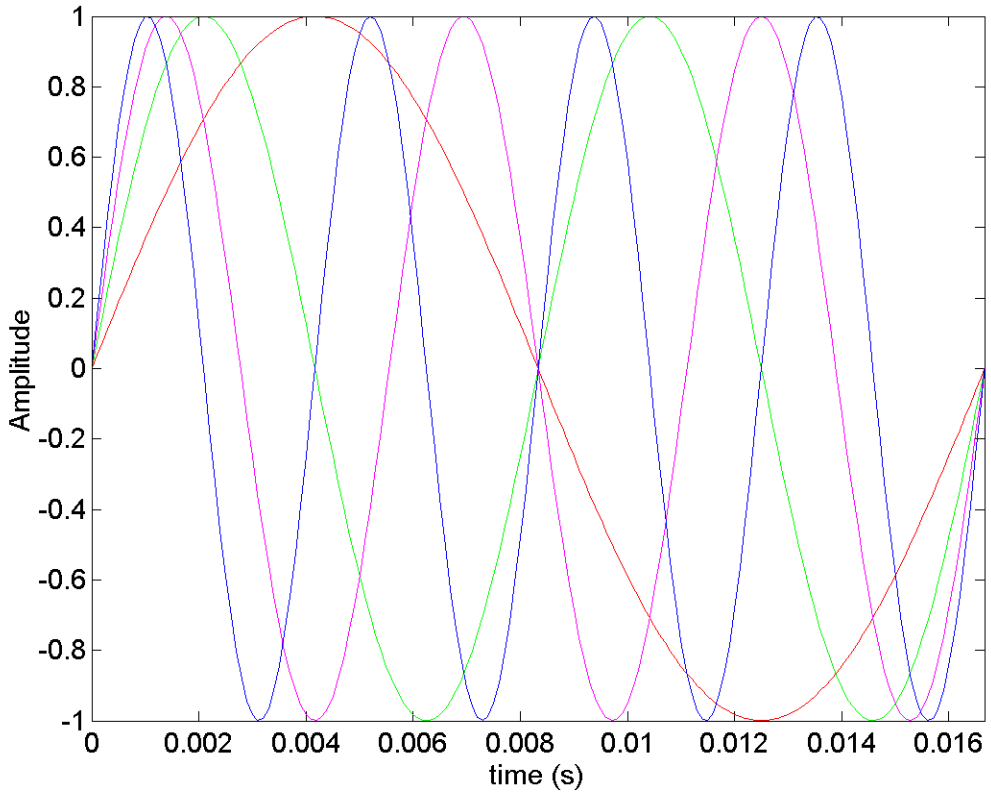

Figure 2. Orthogonal Sub-carriers

When viewed in the frequency domain, as in Figure 3, these sub-carriers clearly demonstrate the spectral overlap and bandwidth savings inherent in orthogonally spaced carriers. It can also be seen in Figure 3 that such orthogonal carriers are spaced in frequency by integer multiples of 1/T.

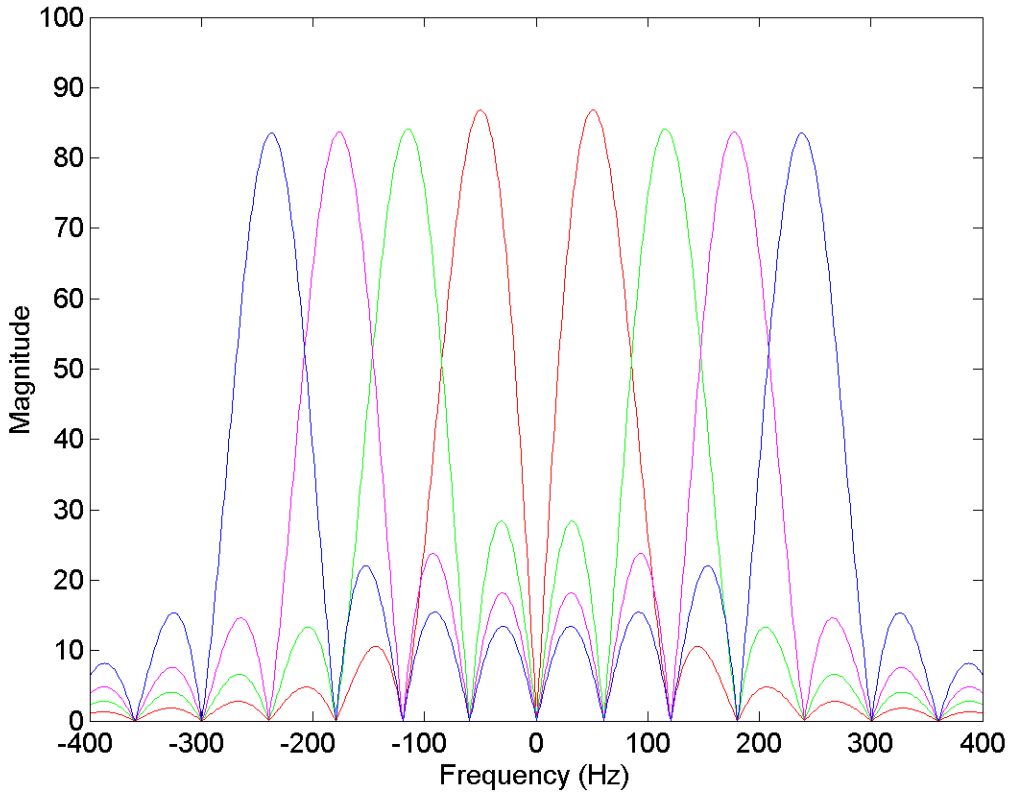

Figure 3. Orthogonally Spaced Carriers in Frequency Domain.

The orthogonality principle as it relates to OFDM is demonstrated analytically in [7]. If d_i represents complex QAM modulated symbols, N_s the number of sub-carriers in the OFDM symbol which begins at $t = t_s$, then the complex baseband OFDM symbol may be represented as:

$$s(t) = \sum_{i=0}^{N_s-1} d_i e^{j2\pi \frac{i}{T}(t-t_s)} \tag{2.2}$$

In the demodulation process the OFDM signal is translated to baseband and then integrated over a symbol interval in order to produce the desired sub-carrier data. For instance, if the demodulator were attempting to recover the jth sub-carrier, the result would be the complex QAM symbol on that carrier as in Equation (2.3):

$$\int_{t_s}^{t_s+T} e^{-j2\pi\frac{j}{T}(t-t_s)} \sum_{i=0}^{N_s-1} d_i e^{j2\pi\frac{i}{T}(t-t_s)} dt =$$

$$\sum_{i=0}^{N_s-1} d_i \int_{t_s}^{t_s+T} e^{j2\pi\frac{(i-j)}{T}(t-t_s)} dt = d_j T \tag{2.3}$$

The correlation of the jth sub-carrier with any other sub-carrier yields zero, thus demonstrating the orthogonality of the carriers.

3. Limitations

In the discussion up to this point, we have mentioned and elaborated on many of the advantages of employing OFDM by way of the discussion of multi-carrier modulation. In this section we examine some of the disadvantages of OFDM that must be considered carefully when an OFDM based system is in the design stage.

Virtually all modulation techniques involve the use of local oscillators to produce carriers at a desired frequency. There is, therefore, in such systems the potential for frequency offset. Frequency offset occurs when small errors in the local oscillator cause minor deviations in the frequency of the carrier. Such deviations have been minimized with some of today's newer crystal oscillators, however, frequency offset is a menacing and unavoidable fact of life in modern communications. Since such deviation can change the actual carrier frequency on any given sub-carrier and thereby run the risk of violating the orthogonality of the sub-carriers, it is a crucial factor in OFDM system design. Such frequency offset can result in inter-carrier interference (ICI). ICI can be minimized by using proper windowing techniques. In practical systems design, a small amount of ICI is tolerated, and the choice of the appropriate windowing technique is made based upon this minimum allowable ICI.

Another source degradation in the performance of any coherent communications system is phase noise. Phase noise is defined in [8] as the "zero mean random process of the deviation of the oscillator's phase from a purely periodic function at the average frequency." That is, just as frequency deviates, phase deviates in many of the less expensive local oscillators. Phase noise due to phase deviation can be introduced at the

intermediate stages of the modulation process such as that between RF and IF. In [8], it is shown that when the OFDM symbol rate is less than twice the phase noise bandwidth, performance degrades as the sub-carrier spacing (or symbol rate) decreases. If the OFDM symbol rate (or carrier spacing) increases to a point greater than twice the phase noise bandwidth, there is little degradation.

Probably the most significant disadvantage in an OFDM system is its peak-to-average power (PAP) ratio. Because OFDM uses N_s independently modulated sub-carriers, the power produced by coherently adding all of these sub-carriers is N_s times the average of each individual sub-carrier. The result of a large PAP is increased complexity of analog-to-digital and digital-to-analog conversion and reduced RF power amplifier efficiency [7]. There are generally three approaches to reducing PAP: signal distortion, such as clipping the signal, peak windowing, and peak cancellation; coding techniques which exclude OFDM symbols with very large PAP; and OFDM symbol scrambling. These techniques are discussed further in [7] but are beyond the scope of this study.

B. ANATOMY OF AN OFDM SIGNAL

Now we turn our attention to the generation of an OFDM signal. There are many standards that employ OFDM, depending on the application, and OFDM can be implemented in a number of different ways. Despite this, there are a few critical steps involved in generating an OFDM signal. Among the key concepts are the IFFT/FFT and cyclic extension. In addition to these key OFDM specific concerns, there are also the fundamental concerns in improving the performance of any communications system which influence the choice of modulation type, FEC coding, and block interleaving which must be covered.

In this section we begin by treating the use of the IFFT/FFT algorithms as part of generating the OFDM symbol, followed by the benefits of adding the cyclic extension to the symbols as a method of reducing ISI. After this we examine the types of sub-carrier modulation and error correction coding available to OFDM system designers.

1. The Fast Fourier Transform and Sub-carrier Generation

One of the many advantages of OFDM is that it is computationally efficient. The reason for this efficiency is tied to its use of the inverse fast Fourier transform (IFFT) to provide the orthogonal spacing of the OFDM sub-carriers on the transmit side. The equally efficient method of removing this spacing on the receive side is accomplished through the FFT. Let us examine the first principle, the IFFT, in the context of orthogonality. In order to understand the relationship between the IFFT and OFDM symbol generation, we first represent the transmitted bandpass signal after symbol mapping as:

$$x(t) = a_I(t)\cos(2\pi f_c t + \theta) - a_Q(t)\sin(2\pi f_c t + \theta) \tag{2.4}$$

where $a_I(t)$ represents the in-phase data signal, $a_Q(t)$ the quadrature data signal, f_c the carrier frequency, and θ some arbitrary phase. From Euler's identity we know this can also be written as:

$$x(t) = \mathrm{Re}\left\{ z(t)e^{-j(2\pi f_c t + \theta)} \right\} \tag{2.5}$$

where

$$z(t) = a_I(t) + ja_Q(t) \tag{2.6}$$

represents the complex envelope of $x(t)$. If we consider the signal in Equation (2.5) to be a reference carrier, we must now consider other sub-carriers shifted in frequency by Δf. The i[th] sub-carrier may be represented as:

$$x_i(t) = a_{I,i}(t)\cos(2\pi f_c t + 2\pi i\Delta f t + \theta_i) - a_{Q,i}(t)\sin(2\pi f_c t + 2\pi i\Delta f t + \theta_i) \tag{2.7}$$

or alternatively:

$$x_i(t) = \mathrm{Re}\left\{ z_i(t)e^{j(2\pi f_c t + 2\pi i\Delta f t + \theta_i)} \right\} = \mathrm{Re}\left\{ z_i(t)e^{j2\pi i\Delta f t}e^{j(2\pi f_c t + \theta_i)} \right\} \tag{2.8}$$

From (2.8) we can see that (2.5) and (2.8) differ only by $z_i(t)e^{j2\pi\Delta f t}$. Thus, we see that there is no new information, just a shift in the carrier frequency by the amount $i\Delta f$.

Since an OFDM signal is comprised of N_s orthogonal sub-carriers, we may represent the transmitted signal $y(t)$ as:

$$y(t) = \sum_{i=0}^{N_s-1} x_i(t) = \sum_{i=0}^{N_s-1} \mathrm{Re}\left\{ z_i(t) e^{j2\pi i \Delta f t} e^{j(2\pi f_c t + \theta_i)} \right\} \tag{2.9}$$

and the complex envelope of $y(t)$ is thus:

$$v(t) = \sum_{i=0}^{N_s-1} z_i(t) e^{j2\pi i \Delta f t} \tag{2.10}$$

If T is the symbol interval with N_s samples, the sampling rate is N_s/T, and the sampling interval is T/N_s. We can now define the k^{th} sample as:

$$v(k) = v\left(k\tfrac{T}{N_s}\right) = \sum_{i=0}^{N_s-1} z_i\left(k\tfrac{T}{N_s}\right) e^{j2\pi i \Delta f \left(k\frac{T}{N_s}\right)} \qquad for\, k = 0,1,2,...,N_s-1 \tag{2.11}$$

From our earlier discussions of orthogonality, we know that the spacing of the sub-carriers must be an integer multiple of 1/T. Thus,

$$\Delta f = \frac{1}{T} \qquad \therefore (\Delta f) T = 1 \tag{2.12}$$

Substituting (2.12) into (2.11), we obtain:

$$v(k) = \sum_{i=0}^{N_s-1} z(i) e^{j2\pi i \frac{k}{N_s}} \quad for\, k = 0,1,2,...,N_s-1 \tag{2.13}$$

where,

$$z(i) = z_i\left(i\tfrac{T}{N_s}\right) \tag{2.14}$$

is independent of k. Now the DFT and IDFT, respectively, are defined as:

$$\begin{aligned} X(k) &= \sum_{n=0}^{N-1} x(n) e^{-\frac{j2\pi kn}{N}} \\ x(n) &= \frac{1}{N} \sum_{k=0}^{N-1} X(k) e^{\frac{j2\pi kn}{N}} \end{aligned} \tag{2.15}$$

It is clear that $v(k)$ is merely the IDFT of $z(n)$ less the normalizing factor 1/N. Thus the IDFT can be used to generate a baseband signal with N_s orthogonal sub-carriers.

The DFT/IDFT may be more efficiently implemented by use of the FFT. The FFT/IFFT takes advantage of the regularity of operations involved in the computation of the IDFT. It is shown in [10] that direct computation of the DFT/IDFT requires approximately N^2 complex multiplications and N^2-N complex additions, where N equals the number of points in the DFT. With the FFT/IFFT these numbers are reduced to $(N/2)\log_2(N)$ complex multiplications and $N\log_2(N)$ complex additions. The speed improvement factor is increased from four in the case of N=4 to 204.8 in the case of N=1024.

Since the FFT is used to extract the sub-carriers on the receive side, it is clear that in addition to complexity and speed, the FFT/IFFT algorithms enable the system to separate carriers by use of baseband signal processing techniques as opposed to bandpass filtering which would otherwise significantly increase the complexity of the multi-carrier system.

The method of generating an OFDM symbol is demonstrated in the following example modified from [7]. If we wish to transmit four binary values {-1,1,-1,-1} over four sub-carriers, the result of the IDFT/IFFT computation as defined in Equation (2.15) is:

$$\frac{1}{4}\begin{bmatrix} 1 & 1 & 1 & 1 \\ 1 & j & -1 & -j \\ 1 & -1 & 1 & -1 \\ 1 & -j & -1 & j \end{bmatrix}\begin{bmatrix} -1 \\ 1 \\ -1 \\ -1 \end{bmatrix} = \frac{1}{4}\begin{bmatrix} -2 \\ 2j \\ -2 \\ -2j \end{bmatrix} \tag{2.16}$$

The left side of Equation (2.16) is the IDFT matrix where each column corresponds to a complex sub-carrier. The right side of the equation yields the four output samples that together make up one OFDM symbol.

2. Guard Time and Cyclic Extension

As previously discussed, one of the primary reasons for utilizing OFDM is the significant reduction in ISI otherwise caused by multipath delay spread through the use of multiple, low data-rate sub-carriers. The relative delay spread per sub-carrier is reduced compared to an equal data-rate single carrier system. In an OFDM system further steps are taken to reduce ISI through the addition of a guard time to each symbol. If the guard time chosen is sufficiently large relative to the expected delay spread induced by the channel, it prevents multiple delayed versions of symbols from interfering with one another. Though the guard time tends to eradicate any time domain interference, it is shown in [7] that this guard time must be a cyclic extension of the OFDM symbol in order to prevent frequency domain ICI and maintain orthogonality. So there are two considerations. To put it another way, in theory the guard time could be a "no signal" extension of the OFDM symbol, and that would be sufficient to eliminate time domain ISI. The result of such an extension of the OFDM symbol, however, is that the number of cycles per interval between any two arriving symbols is no longer an integer and orthogonality is compromised as in Figure 4. Thus, although ISI is decreased, ICI increases.

When the OFDM symbol is cyclically extended beyond the FFT interval for a time larger than the estimated delay spread, both the time domain consideration of ISI and the frequency domain ICI concern are remedied since the number of cycles between delayed version of the symbol in both the FFT interval and the entire OFDM symbol duration is still an integer as demonstrated in Figure 5.

As discussed above, the guard band must be larger than the anticipated delay spread for the cyclic extension to have any impact. As far as OFDM system design is concerned, the general rule for the choice of a guard interval ranges from at least twice to as many as four times the RMS delay spread that a system is designed to tolerate [7].

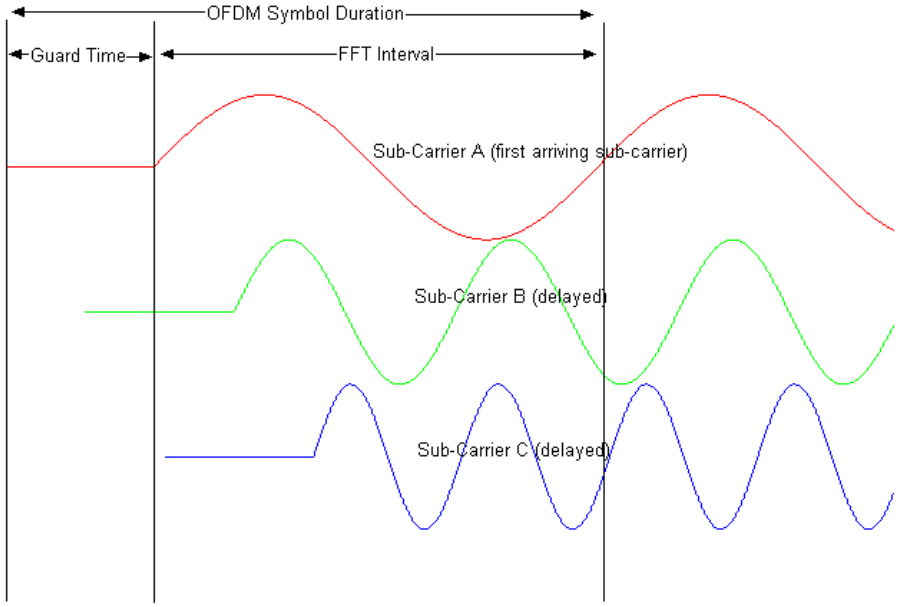

Figure 4. Effect of "no signal" Guard Time.

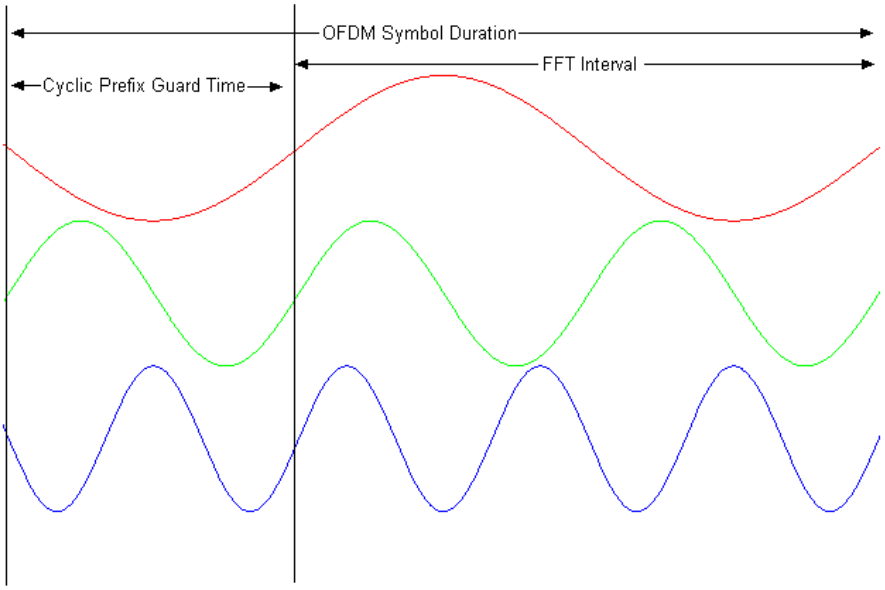

Figure 5. OFDM symbol with Cyclic Extension.

If a communications system employing OFDM can tolerate an RMS delay spread of 150 ns, for instance, then a reasonable value for the cyclic extension/guard time is be 600 ns. Since there are many factors which influence the sensitivity of the system to RMS delay spread, such as modulation format and error control coding, the delay spread dependent guard time will vary with on the techniques involved. For instance, higher order modulation techniques are more sensitive to ISI and ICI and the more robust the error control coding, the less sensitive a system is to ISI and ICI. Therefore, a system engineer may not anticipate as long of a guard time with BPSK or QPSK as he/she might with 16 or 64-QAM.

3. Sub-carrier Modulation

The nature of OFDM and the multi-carrier concept are such that any digital modulation technique may be used to impress data bits onto the sub-carriers. Within the context of OFDM, phase-shift keying (PSK) and quadrature amplitude modulation (QAM) are the most commonly seen modulation types. In general PSK is a modulation scheme in which the phase of a carrier is altered by the information bearing data bits. In binary PSK (BPSK) binary "1"s and "0"s induce 180 degree phase changes in the carrier. In the case of quadrature PSK (QPSK), also known as 4-PSK, each group of two bits (i.e., 11, 00, 01, 10) represents one of four possible carrier phases. That is, the phase of the carrier may be altered by 90, 180, 270 or it may remain at 0 degrees. Differential PSK techniques may also be applied whereby changes in the received data bits induce a relative phase change. Put another way, phase is altered based on where the phase is in its current state as opposed to bit patterns corresponding to absolute phases. QAM is a modulation scheme in which the information bearing bits modulate both the amplitude and the phase of the carrier. If the signal constellation is square, then QAM can be thought of as two independent amplitude modulated carriers in phase quadrature. Since this amounts to amplitude-shift keying (ASK) in two dimensions, QAM is sometimes referred to as QASK.

One measure of gauging how well a modulation technique performs is probability of bit error or BER (bit error ratio). Among the key advantages of BPSK and QPSK in

any communications system are their superior performance in the presence of noise. Since QAM techniques transmit more bits per symbol, the probability of an error occurring increases, and QAM does not perform as well in noise as BPSK or QPSK. The higher the order of the QAM constellation, the worse this performance degradation becomes. Since 4-QAM is equivalent to QPSK, the performance degradation occurs in QAM constellations above 4-QAM. It can be shown that the probability of bit error for BPSK and QPSK are the same and are given by:

$$P_b = Q\left(\sqrt{\frac{2E_b}{N_0}}\right) \tag{2.17}$$

where the ratio E_b/N_o is the signal-to-noise ratio per bit. For square QAM constellations, the probability of bit error is [2]:

$$P_b = \frac{1}{\log_2(M)} \frac{4(\sqrt{M}-1)}{\sqrt{M}} Q\left(\sqrt{\frac{3qE_b}{(M-1)N_0}}\right) \tag{2.18}$$

where q is the number of bits per symbol, M is the number of possible combinations of q bits, and $Q(.)$ is the Guassian integral function defined as:

$$Q(x) = \frac{1}{\sqrt{2\pi}} \int_x^\infty e^{-\frac{y^2}{2}} dy \tag{2.19}$$

The probability of bit error vs. signal-to-noise ratio per bit for BPSK, QPSK, 16-QAM, 64-QAM, and 256-QAM in additive white Gaussian noise (AWGN) is plotted in Figure 6.

Bandwidth efficiency is another measure of the performance of a digital modulation technique and may be defined as the ratio of the transmission bit rate to the minimum bandwidth required for a particular modulation scheme. Bandwidth efficiency is usually normalized to a 1 Hertz bandwidth and thus represents the maximum number of bits that can be transmitted for each Hertz of bandwidth [11]. Because of its ability to transmit so many bits over the same interval, QAM obtains much higher data rates for a significantly lower bandwidth requirement and is therefore bandwidth efficient. Bandwidth efficiency was critical to the successful adoption of QAM in OFDM and other

applications. The bandwidth efficiency of the various PSK and QAM modulations in bits per cycle is summarized in Table 1. As the table indicates, 64-QAM, for example, requires 1/6 as much bandwidth as BPSK for the same bit rate.

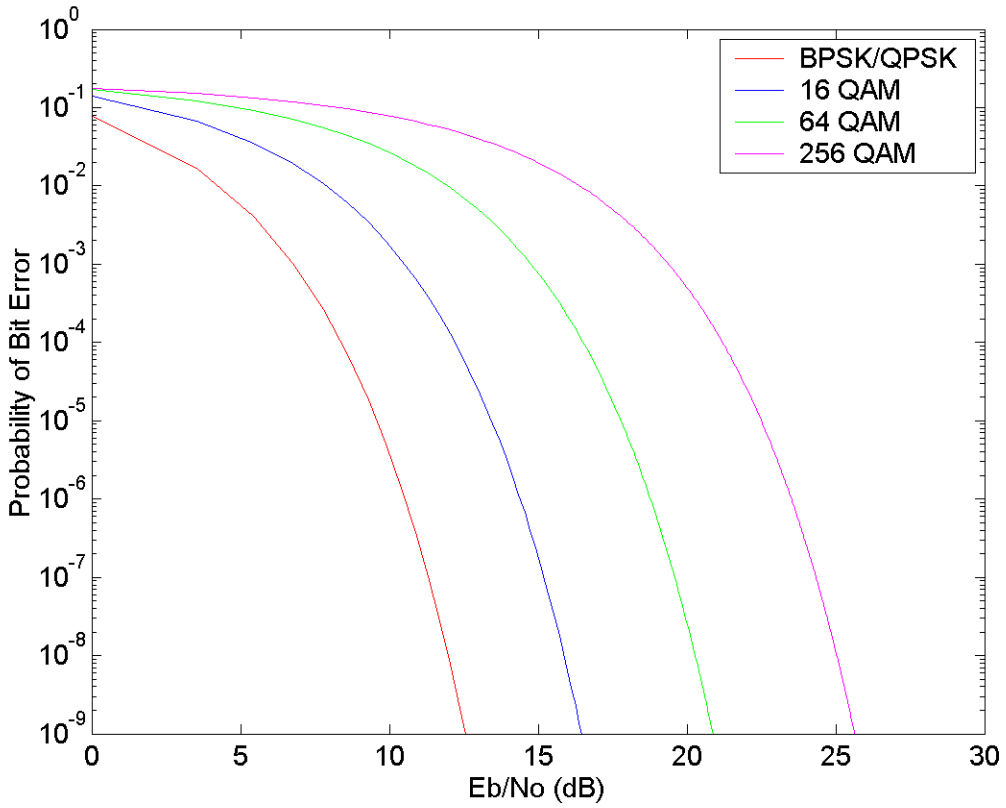

Figure 6. BPSK, QPSK, 16-QAM, 64-QAM, and 256-QAM in AWGN.

Modulation	**Bandwidth Efficiency**
BPSK	≤ 1 bits/s/Hz
QPSK	≤ 2 bits/s/Hz
16-QAM	≤ 4 bits/s/Hz
64-QAM	≤ 6 bits/s/Hz

Table 1. Bandwidth Efficiency [After Ref. 11]

The IEEE 802.11a standard has adopted PSK and QAM as the sub-carrier modulation techniques for use in conjunction with OFDM. Specifically, BPSK, QPSK, 16-QAM, and 64-QAM are specified. These techniques are chosen not only for their combination of excellent bit error performance and bandwidth efficiency but more importantly for the ease with which these configurations can be implemented. Since square QAM constellations may be divided into independent pulse amplitude modulated components as previously mentioned, the real and imaginary components of a symbol can be modulated separately by so called "I-Q" modulation techniques. By describing a constellation point in rectangular coordinate values, the symbol need only modulate the amplitude of the I (cosine) and Q (sine) channels. This greatly simplifies hardware implementation as, for example, by the IFFT as previously discussed. The bit to symbol mapping required for the four sub-carrier modulations adopted in the IEEE 802.11a standard is shown in Figure 7. The bits are allocated according to Gray-code configurations which reduce the likelihood of bit error. As data bits are fed directly into the symbol mapping stage of the modulation process, they are gathered together based on the value of q and assigned an in-phase and quadrature coordinate as required by the modulation type. If we let a stream of binary ones and zeros to be modulated be represented as a vector of bits $\mathbf{b}=[b_0, b_1, \ldots b_{k-1}]$, then the manner in which bits are mapped in 64-QAM (where $q = 6$) is illustrated by Table 2.

The signal constellations in Figure 7 are not normalized. It is worth mentioning here that in order to achieve the same average power for all mappings the constellations above must be multiplied by the normalization factors in Table 3.

Since the IEEE 802.11a standard specifies data rates up to 54 Mbps, the modulation type utilized depends on the data rate specified. Naturally, a higher data rate requires a higher order modulation such as 16 or 64-QAM. A summary of the relationship between data rate and modulation techniques in the IEEE standard is included in Section C of this chapter.

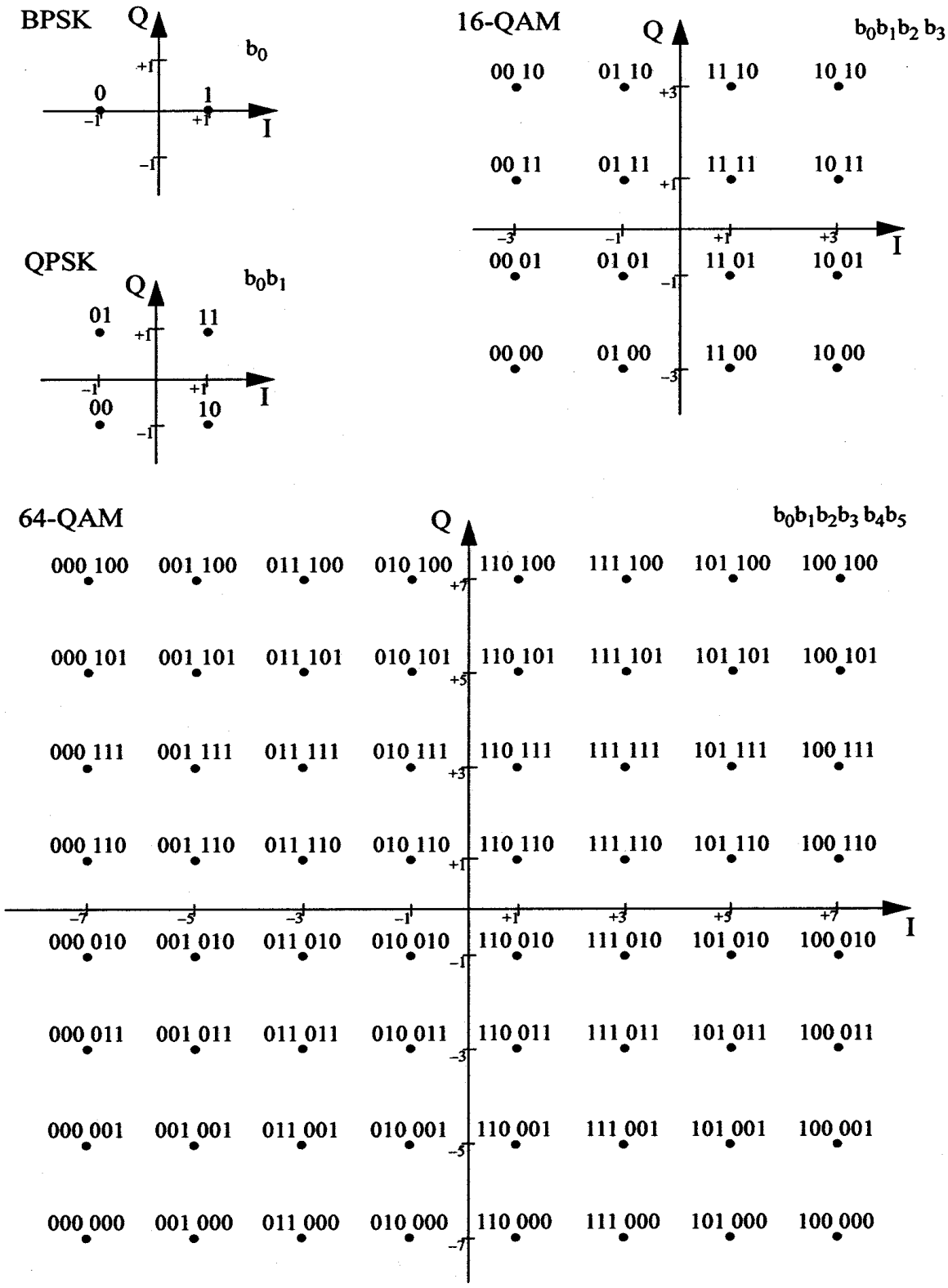

Figure 7. BPSK, QPSK, 16-QAM, and 64-QAM Constellation Bit Encoding [From Ref. 12]

Input bits (b_0 b_1 b_2)	**I_{out}**	**Input bits (b_3 b_4 b_5**	**Q_{out}**
000	-7	000	-7
001	-5	001	-5
011	-3	011	-3
010	-1	010	-1
110	1	110	1
111	3	111	3
101	5	101	5
100	7	100	7

Table 2. 64-QAM Encoding Table [From Ref. 12].

Modulation	**Normalization**
BPSK	1
QPSK	$\frac{1}{\sqrt{2}}$
16-QAM	$\frac{1}{\sqrt{10}}$
64-QAM	$\frac{1}{\sqrt{42}}$

Table 3. Modulation Dependent Normalization Factor [From Ref. 12].

4. Forward Error Correction Coding (FEC)

As explained in previous sections, the critical benefits of OFDM involve its performance in multi-path environments that result from breaking down the data and transmitting it over several sub-carriers. The addition of the cyclic extension is further used to combat ICI. However, in multipath channels, the sub-carriers will tend to arrive at the receiver with wildly varying amplitudes as discussed in chapter one. Even though the sub-carriers may be correctly detected, many of them may be lost due to deep fades; thus, the error probability will largely be determined by these few sub-carriers. For this reason, FEC coding is required to reduce the likelihood that these weaker sub-carriers will completely dominate overall system performance. Through the insertion of redundant bits into the data stream as defined by the coding rate r, errors due to these weaker sub-carriers may be corrected up to some limit determined by the code used. Thus, coding allows the overall link performance to be judged based on the average received power and not that of a few weak carriers [7]. Much can be said of error correction coding. In this section we will focus on the primary types of coding and their benefit, if any, in an OFDM system.

There are basically two types of FEC codes, convolutional and block codes. Briefly, convolutional codes utilize linear shift-registers to add redundancy into the entire data stream. Convolutional codes are defined by three parameters, n, k, and K, where n is the total number of coded bits, k is the number of input bits, and K is the constraint length of the code. The constraint length describes the number of k-tuple stages in the encoding shift-register [9]. The convolutional encoder, therefore, has memory and the output of the encoder depends on what is held in previous shift registers. The code rate r is defined as the ratio of information bits to coded bits, or k/n, and gives an indication of how much redundancy is added to the original data. The convolutional encoder is so named because it may be viewed as a discrete time convolution of the input signal with the impulse response of the encoder [13]. Block codes, unlike convolutional codes, are defined only by n and k. Block codes segment data into "blocks" of data rather than applying the code to the entire data stream as one code word as in convolutional codes [14]. When an FEC code is applied, the difference in SNR required (in dB) to achieve a

given probability of bit error P_b between the uncoded and coded cases defines the coding gain of a particular code.

There are also codes which combine modulation and encoding in one step. One such method, called trellis coded modulation (TCM) achieves the encoding redundancy and modulation without increasing bandwidth. At face value this seems like a good match for our bandwidth efficient OFDM based system, however [7] points out that TCM is not well suited for OFDM as the minimum Hamming distance (one metric used in determining a code's effectiveness) is limited for practical TCM systems. If a TCM symbol is attenuated, the result is the occurrence of one or more bit errors. Since in OFDM it is common for the data of several sub-carriers to be lost in a single deep fade, TCM is not a wise choice for OFDM. Further, TCM is designed for specific constellations and therefore would require separate coders and decoders for each modulation type. This inflexibility is not welcome in an OFDM system that can potentially be called upon to dynamically apply differing modulation types.

One final type of error correction coding which bears mentioning is concatenated codes. Concatenated codes serially combine two different codes, usually a block and a convolutional code, in order to obtain the best benefits of both. Most concatenated codes use a Reed-Solomon (RS) block code as the outer code and pass the output of the RS code to an inner encoder which is usually convolutional. The outer RS code has the benefit of potentially correcting a greater number of errors, where the inner convolutional encoder enables the use of "soft decision" decoding techniques which improve performance by allowing a greater degree of metric variation. With concatenated coding comes additional complexity, which is why they were not chosen for the IEEE 802.11a standard.

The performance of any FEC coding approach can be improved, especially in the presence of bursts, by interleaving. Interleaving may be thought of as a form of diversification as adjacent bits are re-ordered after they are encoded in order to give them sufficient spacing in either frequency or time. The result at the decoder is increased reliability in the error correction process through the randomization of errors. A common form of interleaving is so called block interleaving. The process of block interleaving

may be envisioned as an $n \times m$ matrix where the bits are fed into the matrix by columns and read out by rows in dedicated groups dependent upon the number of rows n and columns m. Interleaving is critical in any system and is equally important to utilize in an OFDM based system. The IEEE 802.11a standard calls for block interleaving with the block size corresponding to the number of bits in a single OFDM symbol N_{CBPS}. This depends on the modulation and coding involved. A summary of these values are given in Table 6 of the next section; however, the interleaving process in 802.11a is defined by two permutations. The first permutation is designed to ensure that adjacent bits are mapped onto non-adjacent sub-carriers [12]. The second involves guaranteeing that adjacent coded bits are mapped in an alternating fashion onto less and more significant bits of the constellation [12]. This second permutation avoids extended runs of poor reliability.

For its simplicity of design and the ability to employ highly efficient Viterbi decoding algorithms, the IEEE 802.11a standard calls for the use of convolutional encoding with variable rates. As with the sub-carrier modulation, the coding rates required are dictated by the data rates sought as well as the modulation type involved. 802.11a employs convolutional codes of rates $r = 1/2,\ 2/3,$ or $3/4$. The convolutional encoder employed by the 802.11a standard for the rate 1/2 code has a constraint length of seven $(K = 7)$; that is, six linear shift registers make up the memory components of the encoder as demonstrated in Figure 8. The generator polynomials utilized are the industry standard rate 1/2 generator polynomials $g_0 = 133_8$ $(1+D^2+D^3+D^5+D^6)$ and $g_1 = 171_8$ $(1+D+D^2+D^3+D^6)$ as demonstrated in Figure 8.

The higher data rates called for by the standard are derived from this encoder by employing "puncturing" techniques. Puncturing is a method of increasing the code rate by reducing the number of transmitted bits. This is accomplished by omitting some of the encoded bits in the transmitter and inserting "dummy" zeros into the decoder on the receive side in place of the omitted bits [12].

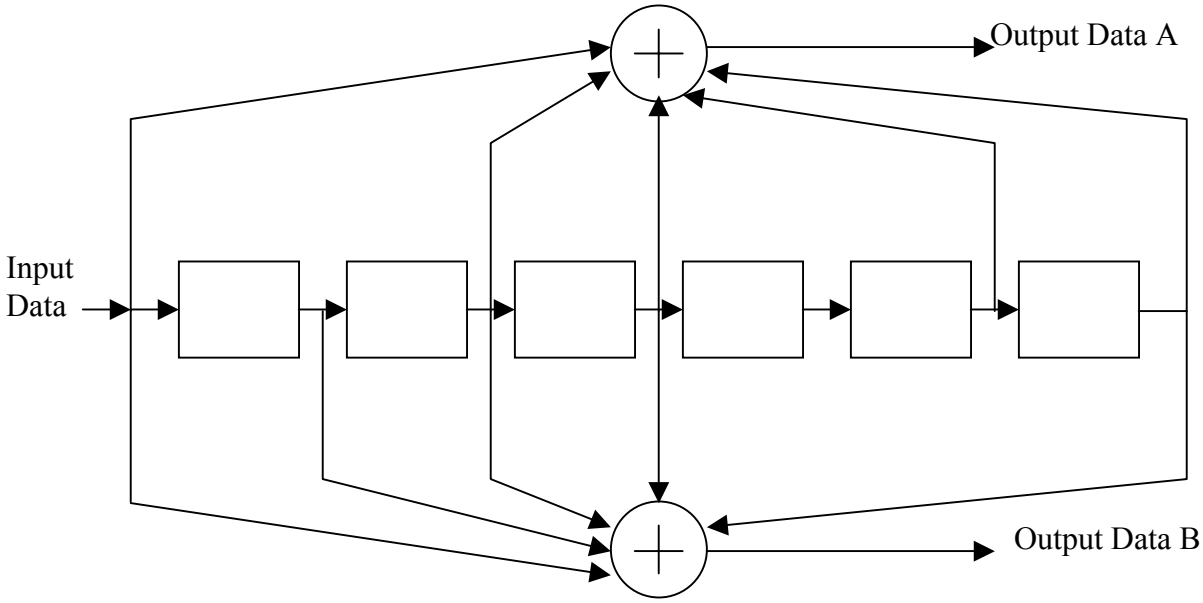

Figure 8. Convolutional Encoder (r=1/2, K=7).

The relationships between coding rate, data rate, and modulation will be revisited in the next section. In Chapter IV we will incorporate the use of convolutional encoding in our mathematical development when assessing the performance of OFDM in a Nakagami channel as this represents a more realistic scenario.

C. THE IEEE 802.11A STANDARD

In order to have a more coherent understanding of the process by which an OFDM symbol is generated, one of the many approaches to OFDM signal generation must be adopted in this study. As mentioned in Chapter I, DVB, DAB, ETSI HIPERLAN II, and IEEE 802.11a are some of the standards which employ OFDM. In this section we examine more closely the IEEE 802.11a standard and its method of implementation of OFDM. Specifically, we are interested in the transmitter and receiver and some of the major parameters of the OFDM PHY layer as specified in the IEEE standard. This section is intended merely to illustrate one possible implementation of OFDM and give the reader a better feel for some realistic values for the parameters previously discussed.

1. The OFDM Transmitter

According to the 802.11a standard, the process of transmitting an OFDM signal involves first encoding the raw data stream then interleaving and mapping the bits into PSK/QAM symbols. These symbols are used to generate a complex baseband signal by the IFFT, and the guard interval with the cyclic extension is added. Symbol wave shaping follows, whereby some form of windowing is applied to the symbol to smooth the transition from symbol to symbol and reduce the spectral side-lobes of the transmitted waveform. The I/Q modulation process impresses the symbols onto sine and cosine carriers through pulse amplitude modulation (PAM) of the separate channels. The channels are then summed and a single waveform emerges. This waveform is then translated into a higher frequency range (the 5 GHz band for 802.11a applications) for amplification and final transmission. This process is illustrated in Figure 9.

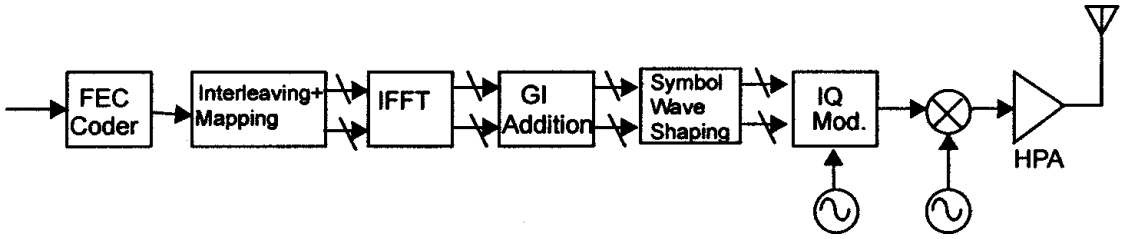

Figure 9. OFDM Transmitter Block Diagram [From Ref. 12]

2. The OFDM Receiver

The process of receiving and recovering the OFDM signal is essentially the reverse of the process whereby it is transmitted. With the exception of the presence of a low noise amplifier (LNA) to boost the signal while minimizing the amount of noise increased and the addition of automatic gain control (AGC), what is done on the transmit side is undone on the receive side. A block diagram of this process is shown in Figure 10.

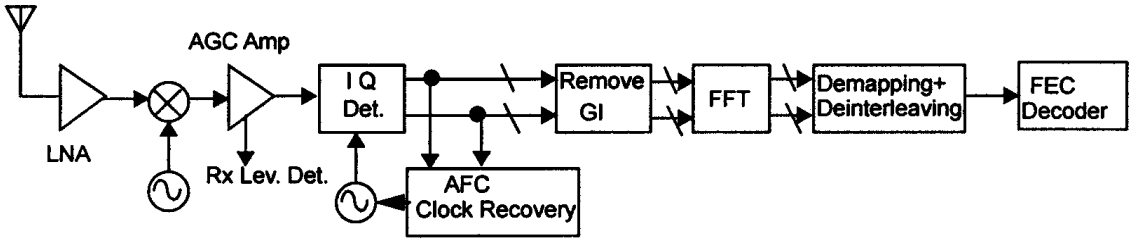

Figure 10. OFDM Receiver Block Diagram [From Ref. 12].

3. IEEE 802.11a OFDM Parameters

As previously mentioned, 802.11a calls for variable data rates, sub-carrier modulation, and FEC coding rates. Many of the key components in the standard such as

Information data rate	**6, 9, 12, 18, 24, 36, 48 and 54 Mbit/s (6, 12 and 24 Mbit/s are mandatory)**
Modulation	BPSK OFDM QPSK OFDM 16-QAM OFDM 64-QAM OFDM
Error correcting code	K = 7 (64 states) convolutional code
Coding rate	1/2, 2/3, 3/4
Number of subcarriers	52
OFDM symbol duration	4.0 μs
Guard interval	0.8 μs[a] (T_{GI})
Occupied bandwidth	16.6 MHz

Table 4. Major Parameters of the OFDM PHY [From Ref. 12]

modulation, error correction coding, symbol duration, and bandwidth are defined in Table 4. In Table 5, the relationships among the modulation, error correction coding, and bit rates are summarized.

Data rate (Mbits/s)	Modulation	Coding rate (R)	Coded bits per subcarrier (N_{BPSC})	Coded bits per OFDM symbol (N_{CBPS})	Data bits per OFDM symbol (N_{DBPS})
6	BPSK	1/2	1	48	24
9	BPSK	3/4	1	48	36
12	QPSK	1/2	2	96	48
18	QPSK	3/4	2	96	72
24	16-QAM	1/2	4	192	96
36	16-QAM	3/4	4	192	144
48	64-QAM	2/3	6	288	192
54	64-QAM	3/4	6	288	216

Table 5. Rate-Dependent Parameters [From Ref. 12].

Timing parameters are also clearly specified in the 802.11a standard. The most important of these OFDM parameters are summarized in Table 6.

Parameter	Value
N_{SD}: Number of data subcarriers	48
N_{SP}: Number of pilot subcarriers	4
N_{ST}: Number of subcarriers, total	52 ($N_{SD} + N_{SP}$)
Δ_F: Subcarrier frequency spacing	0.3125 MHz (=20 MHz/64)
T_{FFT}: IFFT/FFT period	3.2 μs ($1/\Delta_F$)
$T_{PREAMBLE}$: PLCP preamble duration	16 μs ($T_{SHORT} + T_{LONG}$)
T_{SIGNAL}: Duration of the SIGNAL BPSK-OFDM symbol	4.0 μs ($T_{GI} + T_{FFT}$)
T_{GI}: GI duration	0.8 μs ($T_{FFT}/4$)
T_{GI2}: Training symbol GI duration	1.6 μs ($T_{FFT}/2$)
T_{SYM}: Symbol interval	4 μs ($T_{GI} + T_{FFT}$)
T_{SHORT}: Short training sequence duration	8 μs ($10 \times T_{FFT}/4$)
T_{LONG}: Long training sequence duration	8 μs ($T_{GI2} + 2 \times T_{FFT}$)

Table 6. Timing-related Parameters [From Ref. 12].

From our previous discussions of suitable guard interval lengths, it is clear from table 6 that with an interval of $0.8\,\mu s$, the system is designed to handle anywhere from below 200 up to a 400 ns delay spread. One other fact from Table 6 is that not all 52 sub-carriers are utilized for data. For synchronization purposes, pilot tones occupy four of the 52 sub-carriers.

D. OFDM SUMMARY

We have seen throughout this chapter that the process of generating an OFDM symbol requires a great many considerations. Many of the methods involved in transmitting OFDM are analytically complex yet strive for simplicity of implementation. Concepts such as FEC coding, interleaving, and modulation are common to any communications system. The two most prominent features, however, in the OFDM system are the FFT/IFFT algorithms and the unique use of the cyclic extension to provide a guard interval to combat ICI and ISI. Now that we have discussed the principles involved in the generation of OFDM signals, we can begin to discuss the transmission of such a signal over some electronically hostile channels. These channels are usually fading channels whose effects on the received envelope of the signal can be significant. In the next chapter, we will address some of the key elements in transmitting an OFDM signal through one such channel model, the Nakagami.

III. PERFORMANCE ANALYSIS

Now that we posses a fundamental understanding of OFDM and how it is generated, we move on to an assessment of OFDM's performance in fading channels. In this chapter we first explore the Nakagami channel as a statistical model in section III.A. This includes an examination of the probability density function (PDF) of the Nakagami-m distribution and some general comments as to its application to this study. Section III.B consists of an analysis of the modulation techniques utilized in the IEEE 802.11a application of OFDM in the presence of Nakagami-m distributed fading. Each modulation technique will be independently evaluated and the probability of bit error analytically derived. In section III.C we will pool all of these concepts together and analyze an OFDM system as it might ordinarily be applied in a WLAN environment. The metric for performance analysis in this chapter and in subsequent chapters will be the bit error ratio (BER) versus average SNR per bit $\left(E_b / N_0\right)$ as this is the accepted standard for evaluation of digital communications systems. Finally, the chapter concludes with a review of our findings in section III.D and a preview of Chapter IV.

A. THE NAKAGAMI CHANNEL MODEL

As discussed in section I.A.2, the choice of the Nakagami-m distribution as the statistical channel model for this thesis is made largely for two reasons. The first is that the Nakagami channel model is purported to be the best statistical match for actual data measured under field conditions in the presence of fading. This means that whatever conclusions we reach will arguably be all the more accurate. The second reason for this choice is that the Nakagami model is more general than many others such as the Rayleigh or Ricean model. This enables us to evaluate multiple degrees of fading simply by adjusting certain model parameters, thus providing a greater breadth of application. For instance, the Rayleigh distribution is most commonly employed when the channel impulse response is modeled as a zero mean Gaussian process. It often is used to describe situations in which no line-of-sight (LOS) is available and there are numerous multi-path components. The Ricean distribution, on the other hand, is generally utilized when a zero mean Gaussian process is no longer applicable or when LOS exists but there remain some multipath components due to secondary reflections. The Nakagami may be

used to model both of these conditions and as such is capable of modeling fading conditions that are either more or less severe than Rayleigh fading [1].

In this section we will briefly examine the Nakagami distribution followed by a short discussion of channel fading characteristics. The purpose is to lay the foundation for later sections in which the performance of OFDM is analyzed. As we will discover, the effect of the Nakagami channel on system performance amounts to a serious degradation of performance requiring a remedy which will be treated in Chapter IV.

1. The Nakagami-m Distribution

The Nakagami-m distribution, which is a function of two parameters, is given by [1]:

$$p_R(r) = \frac{2}{\Gamma(m)}\left(\frac{m}{\Omega}\right)^m r^{2m-1} e^{-\frac{mr^2}{\Omega}} \tag{3.1}$$

where Ω is defined as

$$\Omega = E[R^2] \tag{3.2}$$

$\Gamma(m)$ is the Gamma function defined as

$$\Gamma(m) = \int_0^\infty t^{m-1} e^{-t} dt \qquad m > 0 \tag{3.3}$$

and the parameter m , the fading figure, is defined as the ratio of moments,

$$m = \frac{\Omega^2}{E[(R^2 - \Omega)^2]}, \qquad m \geq \frac{1}{2} \tag{3.4}$$

It can be shown that when $m = 1$, the Nakagami PDF reduces to the Rayleigh PDF given by

$$p_R(r) = \frac{r}{\sigma^2} e^{-\frac{r^2}{2\sigma^2}}, \qquad r \geq 0 \tag{3.5}$$

This is why we consider the Rayleigh distribution to be a special case of the Nakagami PDF. In Figure 11 the Nakagami-m PDF is illustrated graphically as a function of R for various values of m with $\Omega = 1$.

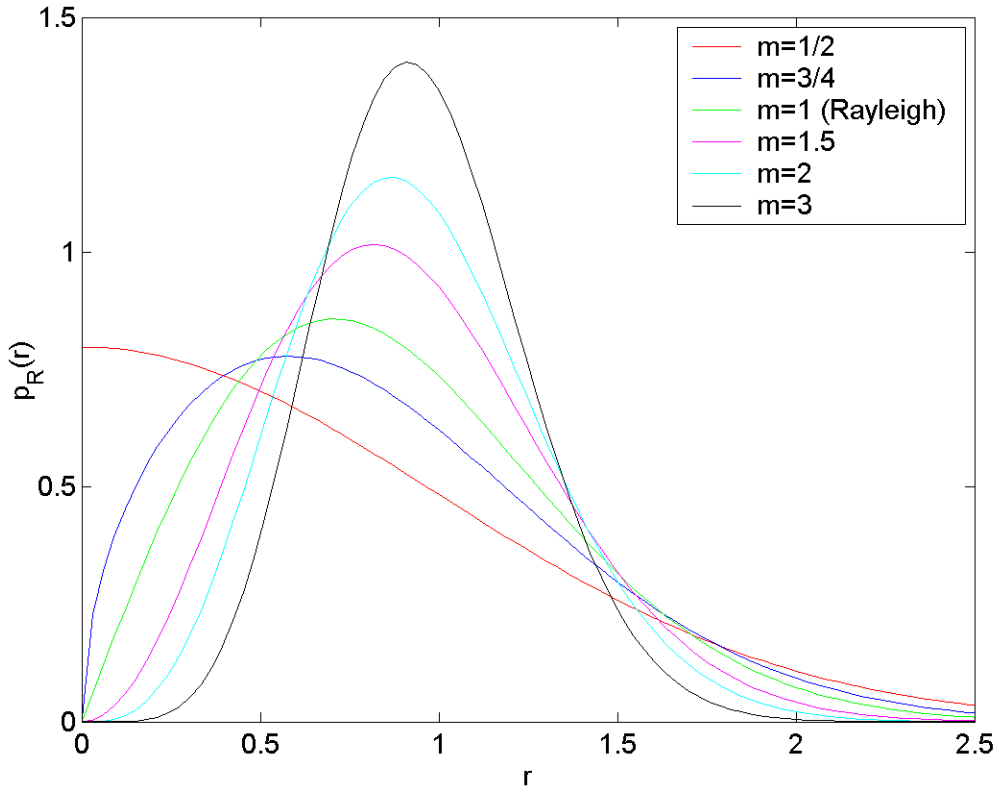

Figure 11. The Nakagami PDF for $\Omega = 1$.

As seen in Figure 11, the PDF roll-off for the Nakagami distribution is more rapid for larger values of m. For $m \leq 1$, the Nakagami PDF is useful in obtaining results which emulate fading conditions in which LOS communication is not available (Rayleigh fading). For values of $m > 1$, the Nakagami PDF more closely models fading environments in which LOS communications are possible (Ricean fading). It is this variability that gives the Nakagami distribution its added value.

2. The Channel

Before we tackle the performance of OFDM in frequency-selective, slowly fading channels, we must first say a few words about how we will contend with the not so

friendly nature of frequency-selective channels in our pending analysis. A frequency-selective channel is one in which the received signal contains multiple delayed versions of the transmitted signal. As previously discussed, these multipath components cause ISI which results in what is often called a BER floor or irreducible BER floor. In other words, at some point, the probability of bit error for digital modulation in frequency-selective channels will reach a minimum value after which there is no performance improvement even at high SNR [2]. It is no trivial matter to attempt to evaluate the performance of any modulation technique in this type of channel under such conditions. As a result, if the channel can somehow be treated as though it were frequency-nonselective (flat), simpler, more straightforward, and analytically plausible methods can be utilized in our analysis.

As discussed in section I.A.3, a frequency-selective channel may also be described in terms of bandwidth. That is, a frequency-selective channel is one in which the channel coherence bandwidth is less than the bandwidth of the transmitted signal. This bandwidth-oriented definition is useful at this point. We have already demonstrated that in OFDM, high data rate transmissions are divided up into N_s low data rate sub-carriers transmitted in parallel. As a result, the bandwidth of each data sub-carrier is $1/N_s$ smaller than the system bandwidth. This changes the relationship between coherence bandwidth of the channel (which remains constant) and the bandwidth of the OFDM sub-carrier. The sub-carrier signal bandwidth is now sufficiently small relative to the channel coherence bandwidth to be considered flat. Furthermore, since OFDM is utilized in large part to mitigate if not completely eliminate the effects of multipath delay through the use of its guard interval and cyclic extension, we may assume a situation in which our channel is now flat. Therefore, if we treat each sub-carrier independently we can justify the use of a frequency-nonselective, slowly fading channel model for the performance analysis.

B. MODULATION ANALYSIS

In this section we will begin our analysis of OFDM's performance in Nakagami fading channels. We begin by analyzing the four possible sub-carrier modulation

techniques specified in the IEEE 802.11a standard: BPSK, QPSK, 16-QAM, and 64-QAM. The same technique will be applied to all modulation types in that our approach to performance evaluation will be from the standpoint of evaluating a single sub-carrier experiencing frequency-nonselective, slow fading as discussed in section III.A.2 above.

1. BPSK/QPSK in Nakagami Fading

In section II.B.3 we saw that the performance of BPSK and QPSK in AWGN are the same and are given in Equation (2.17), restated here as:

$$P_b = Q\left(\sqrt{\frac{2E_b}{N_0}}\right) \tag{3.6}$$

Since we did not show the derivation of Equation (3.6), as it is readily available in the literature, we must clarify one point before continuing. The probability of bit error expressed in Equation (3.6) is a conditional probability based on a fixed attenuation factor $\alpha = 1$ and is derived from an evaluation of the decision variables in a binary communications system as in [1]. In general, we have $\alpha^2(E_b / N_0) = \gamma_b$, and Equation (3.6) can be rewritten as:

$$P_b(\gamma_b) = Q\left(\sqrt{2\gamma_b}\right) \tag{3.7}$$

where α is the aforementioned attenuation factor that describes the variations in the received signal amplitude and γ_b is a more generalized expression for signal to noise ratio per bit.

If we are to incorporate into our study the effects of Nakagami fading, we must now remove the dependence of Equation (3.7) on α and allow for the randomness of the received signal envelope. In other words, we model α as a random variable. More specifically for this study, we must account for the fact that α is statistically modelled by the Nakagami-m distribution.

In order to obtain the probability of bit error when α is random, we must average the conditional probability of bit error over the probability density function of γ_b as described in [1]. This amounts to evaluating the integral

$$P_b = \int_0^{\infty} P_b(\gamma_b)\, p(\gamma_b)\, d\gamma_b \tag{3.8}$$

where $p(\gamma_b)$ is the probability density function of γ_b when α is a random variable. This is the technique we will employ for all sub-carrier modulation types to be considered in this chapter.

Since we have the expression for $P_b(\gamma_b)$ given in Equation (3.7), all that remains in order to evaluate Equation (3.8) is to obtain an expression for $p(\gamma_b)$. To obtain this expression we recall that since α follows the Nakagami-m distribution, the PDF of α can be obtained from Equation (3.1) as,

$$p_{\alpha}(\alpha) = \frac{2}{\Gamma(m)}\left(\frac{m}{\Omega}\right)^{m} \alpha^{2m-1} e^{-\left(\frac{m\alpha^2}{\Omega}\right)} \qquad \alpha \geq 0 \tag{3.9}$$

It is clear that at this point we must obtain the PDF of γ_b from the PDF of α given in Equation (3.9) from:

$$p_{\gamma_b}(\gamma_b) = \frac{1}{\left|d\gamma_b / d\alpha\right|} p_{\alpha}(\alpha)\Big|_{\alpha = f^{-1}(\gamma_b)} \tag{3.10}$$

Since we know that

$$\gamma_b = \alpha^2 \left(\frac{E_b}{N_o}\right) \tag{3.11}$$

then,

$$\alpha = \sqrt{\gamma_b \frac{N_0}{E_b}} \tag{3.12}$$

Next, we obtain the differential term,

$$\frac{d\gamma_b}{d\alpha} = 2\alpha \frac{E_b}{N_0} = 2\sqrt{\gamma_b \frac{E_b}{N_0}} \tag{3.13}$$

When we substitute Equations (3.12) and (3.13) into (3.10), we obtain

$$p_{\gamma_b}(\gamma_b) = \frac{1}{2\sqrt{\gamma_b \frac{E_b}{N_0}}} \frac{2}{\Gamma(m)} \left(\frac{m}{\Omega}\right)^m \left(\sqrt{\gamma_b \frac{N_0}{E_b}}\right)^{2m-1} e^{-\frac{m\left(\gamma_b \frac{N_0}{E_b}\right)}{\Omega}} = \frac{m^m}{\Gamma(m)} \frac{{\gamma_b}^{m-1}}{\Omega^m \left(\frac{E_b}{N_0}\right)^m} \mathrm{e}^{-\frac{m\gamma_b}{\frac{E_b \Omega}{N_0}}} \quad (3.14)$$

We can further simplify this expression by defining a new term $\bar{\gamma}_b$, the average signal-to-noise ratio per bit as

$$\bar{\gamma}_b = E\left[\alpha^2\right] \frac{E_b}{N_0} \quad (3.15)$$

Since $\Omega = E\left[\alpha^2\right] = 1$ we obtain,

$$p_{\gamma_b}(\gamma_b) = \frac{m^m}{\Gamma(m) \bar{\gamma}_b^{\,m}} {\gamma_b}^{m-1} e^{-\frac{m\gamma_b}{\bar{\gamma}_b}} \quad (3.16)$$

which is the PDF we seek.

We are now poised to obtain an expression for the probability of bit error for a single BPSK modulated OFDM sub-carrier that encounters Nakagami-m distributed fading. As indicated above, we do this by substituting Equations (3.7) and (3.16) into Equation (3.8)

$$P_{b_{BPSK/QPSK}} = \int_0^\infty Q\left(\sqrt{2\gamma_b}\right) \frac{m^m}{\Gamma(m)\left(\bar{\gamma}_b\right)^m} {\gamma_b}^{m-1} e^{-\frac{m\gamma_b}{\bar{\gamma}_b}} d\gamma_b \quad (3.17)$$

It is no trivial matter to obtain an analytical solution for such an integration, however, with the help of some mathematical tables we can compare Equation (3.17) to the following mathematical equality

$$\frac{a^b}{\Gamma(b)} \int_0^\infty e^{-at} t^{b-1} Q\left(\sqrt{ct}\right) dt = \sqrt{\frac{\psi}{1+\psi}} \frac{\Gamma\left(b+\frac{1}{2}\right)}{2\sqrt{\pi}\,\Gamma(b+1)(1+\psi)^b} {}_2F_1\left(1, b+\tfrac{1}{2}; b+1; \frac{1}{1+\psi}\right) \quad (3.18)$$

where ${}_2F_1$ is called Gauss' hypergeometric function and is defined as

$${}_2F_1\left(1, b+\tfrac{1}{2}; b+1; z\right) = \sum_{k=0}^{\infty} \frac{\left(b+\frac{1}{2}\right)_k z^k}{(b+1)_k} \quad (3.19)$$

with

$$z = \frac{1}{1+\psi} \tag{3.20}$$

and

$$\begin{aligned} (r)_k &= \frac{\Gamma(r+k)}{\Gamma(r)} = r(r+1)\cdots(r+k-1) \\ (r)_0 &= 1 \end{aligned} \tag{3.21}$$

Equation (3.21) is known as Pochhammer's Symbol, and we can rewrite Equation (3.21) as

$$\frac{\Gamma(r+k)}{\Gamma(r)} = \prod_{n=0}^{k-1}(r+n) \tag{3.22}$$

If we now compare variables from the integral in Equation (3.17) to those of Equation (3.18), and set $b = m$, $a = m/\overline{\gamma}_b$, $c = 2$, $t = \gamma_b$, and $\psi = c/2a = \overline{\gamma}_b / m$, Equation (3.17) is now in a form suitable for analytical resolution as given in (3.18). Thus, we obtain

$$P_{b_{BPSK/QPSK}} = \sqrt{\frac{\overline{\gamma}_b}{m+\overline{\gamma}_b}}\frac{\Gamma\left(m+\frac{1}{2}\right)}{2\sqrt{\pi}\,\Gamma(m+1)\left(1+\frac{\overline{\gamma}_b}{m}\right)^m}\left(\sum_{k=0}^{\infty}\frac{\left(m+\frac{1}{2}\right)_k\left(\frac{1}{1+\frac{\overline{\gamma}_b}{m}}\right)^k}{(m+1)_k}\right) \tag{3.23}$$

By substituting Equations (3.21) and (3.22) into (3.23), we obtain the more computationally efficient expression

$$P_{b_{BPSK/QPSK}} = \sqrt{\frac{\overline{\gamma}_b}{m+\overline{\gamma}_b}}\frac{\Gamma\left(m+\frac{1}{2}\right)}{2\sqrt{\pi}\,\Gamma(m+1)\left(1+\frac{\overline{\gamma}_b}{m}\right)^m}\left(1+\sum_{k=1}^{\infty}\frac{\prod_{n=0}^{k-1}\left(m+\frac{1}{2}+n\right)\left(\frac{1}{1+\frac{\overline{\gamma}_b}{m}}\right)^k}{\prod_{n=0}^{k-1}(m+1+n)}\right) \tag{3.24}$$

In so doing we have obtained an expression for the probability of bit error for a single BPSK/QPSK modulated OFDM sub-carrier under the conditions that the sub-carrier by itself experiences flat, slow Nakagami-m fading.

For $\Omega = 1$ the term $\overline{\gamma}_b$ reduces to $\overline{\gamma}_b = E_b / N_0$, and we can plot Equation (3.24) in terms of the more familiar average signal-to-noise ratio per bit E_b / N_0.

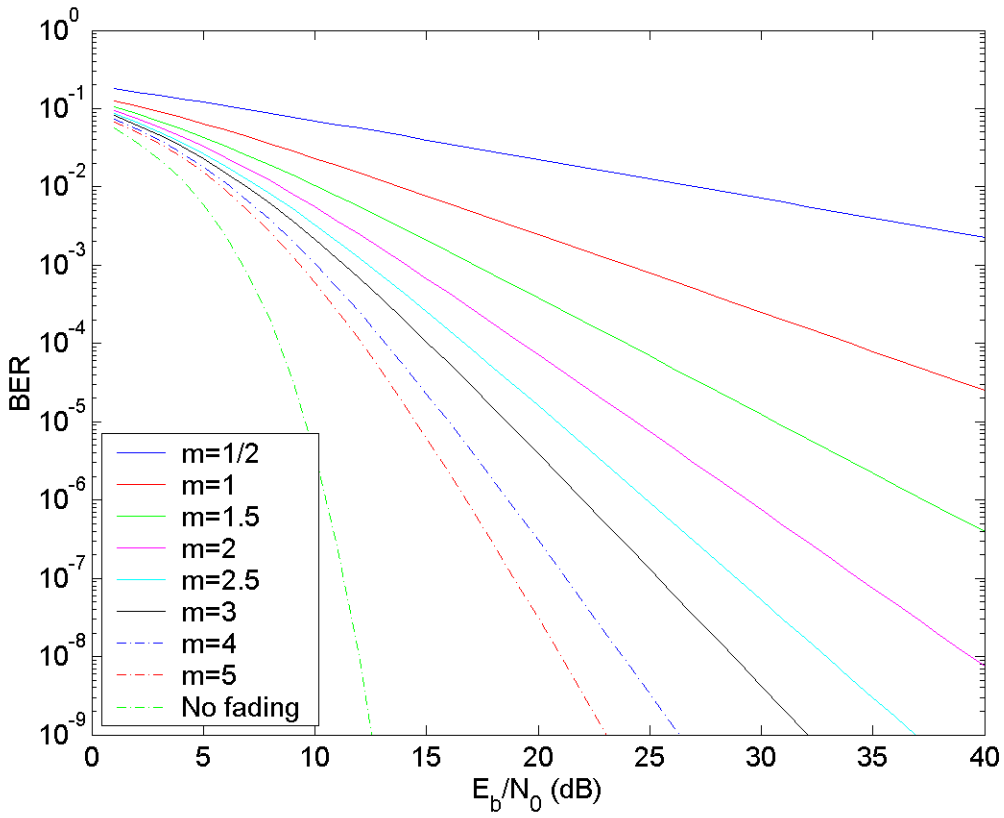

Figure 12. BPSK/QPSK in Nakagami Fading

Figure 12 is plotted for multiple values of the fading figure m. As previously discussed, the value of $m = 1$ corresponds to Rayleigh fading. Values of $m > 1$ indicate better fading conditions than Rayleigh and usually indicate LOS is available between outstation and access point. It is clear from Figure 12 that higher values of m indicate less severe fading conditions. If we let $m \to \infty$ there is no fading and the performance is as indicated in Figure 6 for BPSK and QPSK in AWGN. For values of $m < 1$ fading conditions are much more severe than that of the Rayleigh case and there is a corresponding reduction in performance as indicated by Figure 12. For example, for the case of $m = 1/2$, to achieve a probability of bit error on the order of 10^{-3}, that is, one error out of every 1,000 bits transmitted, the system requires over 40 dB of received

average signal-to-noise ratio (per bit). Clearly, this is not optimal. Once again referring to Figure 12, if we were to attempt to achieve a BER of 10^{-5}, as many modern communications systems require, the required SNR would be enormous and on the order of 70-80 dB. Obviously, conditions that allow a higher value of m are favorable.

Looking at Equation (3.24) more closely, we notice that for values of $\overline{\gamma}_b / m > 3$ the first term in the summation dominates. Therefore, a close approximation to Equation (3.24) can be made by setting

$$\left(1 + \sum_{k=1}^{\infty} \frac{\prod_{n=0}^{k-1} \left(m + \frac{1}{2} + n\right) \left(\frac{1}{1 + \frac{\overline{\gamma}_b}{m}} \right)^k}{\prod_{n=0}^{k-1} \left(m + 1 + n\right)} \right) \approx 1 \quad for \frac{\overline{\gamma}_b}{m} > 3 \tag{3.25}$$

With this substitution in Equation (3.24), a more analytically appealing expression for the probability of bit error is obtained:

$$P_{b_{BPSK/QPSK}} \approx \sqrt{\frac{\overline{\gamma}_b}{m + \overline{\gamma}_b}} \frac{\Gamma\left(m + \frac{1}{2}\right)}{2\sqrt{\pi}\,\Gamma\left(m+1\right)\left(1 + \frac{\overline{\gamma}_b}{m}\right)^m} \tag{3.26}$$

Equations (3.26) and (3.24) are plotted in Figure 13 for $m = 5$. From Figure 13 we see that this approximation is fairly tight for $\overline{\gamma}_b = 12$ dB, which implies that the approximation is accurate for $\overline{\gamma}_b > 3.17m$

2. 16 and 64-QAM in Nakagami Fading

To obtain data rates between 24 and 54 Mbps, 802.11a uses the bandwidth efficient M-ary QAM. Since we already have one generalized expression for the BER of QAM in the presence of AWGN as a function of M, given by Equation (2.18) as

$$P_b = \frac{1}{\log_2(M)} \frac{4(\sqrt{M} - 1)}{\sqrt{M}} Q\left(\sqrt{\frac{3qE_b}{(M-1)N_0}} \right) \tag{3.27}$$

where

$$q = \log_2(M) \tag{3.28}$$

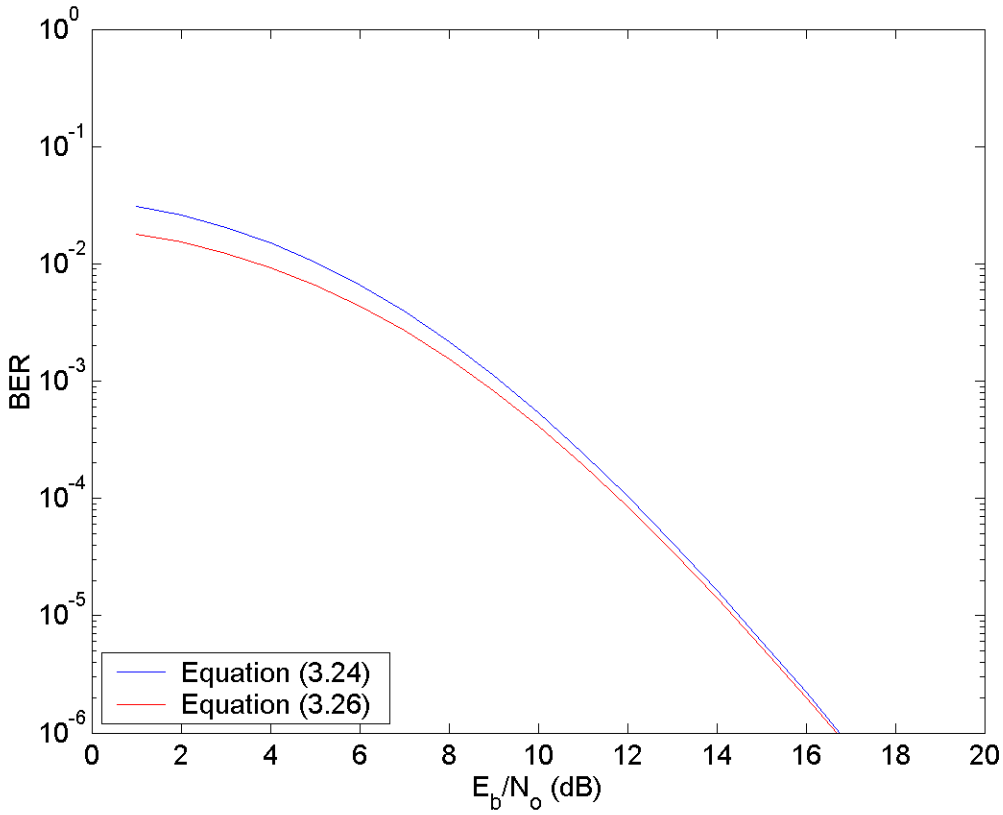

Figure 13. Comparison of Equations (3.24) and (3.26)

we may treat any square QAM constellation in the same manner, according to the same equations. We simply use the value of M corresponding to the desired QAM level. The manner in which we obtain the BER of QAM in Nakagami-m fading channels is the same as in the previous section for BPSK/QPSK.

Before proceeding, some rearranging of Equation (3.27) is in order to make the notation consistent. By making use of the relationship in Equation (3.28) and again making the statement that Equation (3.27) is conditioned on a fixed attenuation factor α, we substitute $\gamma_b = \alpha^2 \left(E_b / N_0 \right)$ into (3.27) and obtain

$$P_b = \frac{4\left(\sqrt{M}-1\right)}{q\sqrt{M}} Q\left(\sqrt{\frac{3q\gamma_b}{M-1}} \right) \tag{3.29}$$

Once again, to obtain the BER in Nakagami fading, we must average the non-fading probability of bit error for square QAM constellations over the Nakagami statistics by evaluating the integral in Equation (3.8):

$$P_{b_{QAM}} = \int_0^{\infty} \frac{4\left(\sqrt{M}-1\right)}{q\sqrt{M}} Q\left(\sqrt{\frac{3q\gamma_b}{M-1}}\right) \frac{m^m}{\Gamma(m)\bar{\gamma}_b{}^m} \gamma_b^{m-1} e^{-\frac{m\gamma_b}{\bar{\gamma}_b}} d\gamma_b \tag{3.30}$$

Again, we make use of the mathematical relationship in Equation (3.18) to obtain an analytical solution for this rather complicated integral by making the following substitutions from Equation (3.18) into Equation (3.30)

$$\begin{aligned} c &= \frac{3q}{M-1} \\ a &= \frac{m}{\bar{\gamma}_b} \\ t &= \gamma_b \\ b &= m \\ \psi &= \frac{c}{2a} = \frac{\frac{3q}{M-1}}{\frac{2m}{\bar{\gamma}_b}} = \frac{3}{2}\frac{q\bar{\gamma}_b}{(M-1)m} \end{aligned} \tag{3.31}$$

Since Equation (3.30) contains the scaling factor,

$$\frac{4\left(\sqrt{M}-1\right)}{q\sqrt{M}} \tag{3.32}$$

we add another factor, call it d, to Equation (3.18), where

$$d = \frac{4\left(\sqrt{M}-1\right)}{q\sqrt{M}} \tag{3.33}$$

Since d is a constant term it is not a function of the variable of integration γ_b and can be moved outside of the integration. We now have an integral which resembles that of Equation (3.18) once we multiply both sides of the equation by d. This does not change the value of the equation. We can now update (3.18) to reflect these changes

$$\frac{da^b}{\Gamma(b)}\int_0^\infty e^{-at}t^{b-1}Q\left(\sqrt{ct}\right)dt = d\sqrt{\frac{\psi}{1+\psi}}\frac{\Gamma\left(b+\frac{1}{2}\right)}{2\sqrt{\pi}\Gamma(b+1)(1+\psi)^b}\,{}_2F_1\left(1,b+\tfrac{1}{2};b+1;\frac{1}{1+\psi}\right) \quad (3.34)$$

We are now ready to use Equation (3.34) to solve the problem at hand. From (3.34), (3.30) has the solution

$$P_{b_{QAM}} = d\sqrt{\frac{\psi}{1+\psi}}\frac{\Gamma\left(b+\frac{1}{2}\right)}{2\sqrt{\pi}\Gamma(b+1)(1+\psi)^b}\,{}_2F_1 \quad (3.35)$$

After making appropriate substitutions from Equation (3.31) and noting that only the term ψ changes in ${}_2F_1$ from the BPSK/QPSK case, we obtain the final result

$$P_{b_{QAM}} = \frac{4\left(\sqrt{M}-1\right)}{q\sqrt{M}}\sqrt{\frac{3q\bar{\gamma}_b}{(M-1)2m+3q\bar{\gamma}_b}}\frac{\Gamma\left(m+\frac{1}{2}\right)}{2\sqrt{\pi}\Gamma(m+1)\left(1+\frac{3q\bar{\gamma}_b}{(M-1)2m}\right)^m} \times\left[1+\sum_{k=1}^{\infty}\frac{\prod_{n=0}^{k-1}\left(m+\frac{1}{2}+n\right)\left(\frac{(M-1)2m}{(M-1)2m+3q\bar{\gamma}_b}\right)^k}{\prod_{n=0}^{k-1}(m+1+n)}\right] \quad (3.36)$$

Thus, Equation (3.36) represents an expression for the performance of square constellation QAM in Nakagami-m fading.

As with BPSK/QPSK, we obtain a plot of $P_{b_{QAM}}$ (BER) vs. E_b/N_0 by letting $\bar{\gamma}_b = E_b/N_0$ under the condition that $\Omega = 1$. In Figures 14 and 15, Equation (3.36) is plotted for 16-QAM ($M=16$, $q=4$) and 64-QAM ($M=64$, $q=6$), respectively, for a full range of values of m.

Just as for BPSK/QPSK we can simplify Equation (3.36) by noting the dominance of the first term in the summation and substituting Equation (3.25) into (3.36) resulting in

$$P_{b_{QAM}} \approx \sqrt{\frac{3q\bar{\gamma}_b}{(M-1)2m+3q\bar{\gamma}_b}}\frac{4\left(\sqrt{M}-1\right)\Gamma\left(m+\frac{1}{2}\right)}{2q\sqrt{M\pi}\Gamma(m+1)\left(1+\frac{3q\bar{\gamma}_b}{(M-1)2m}\right)^m} \quad (3.37)$$

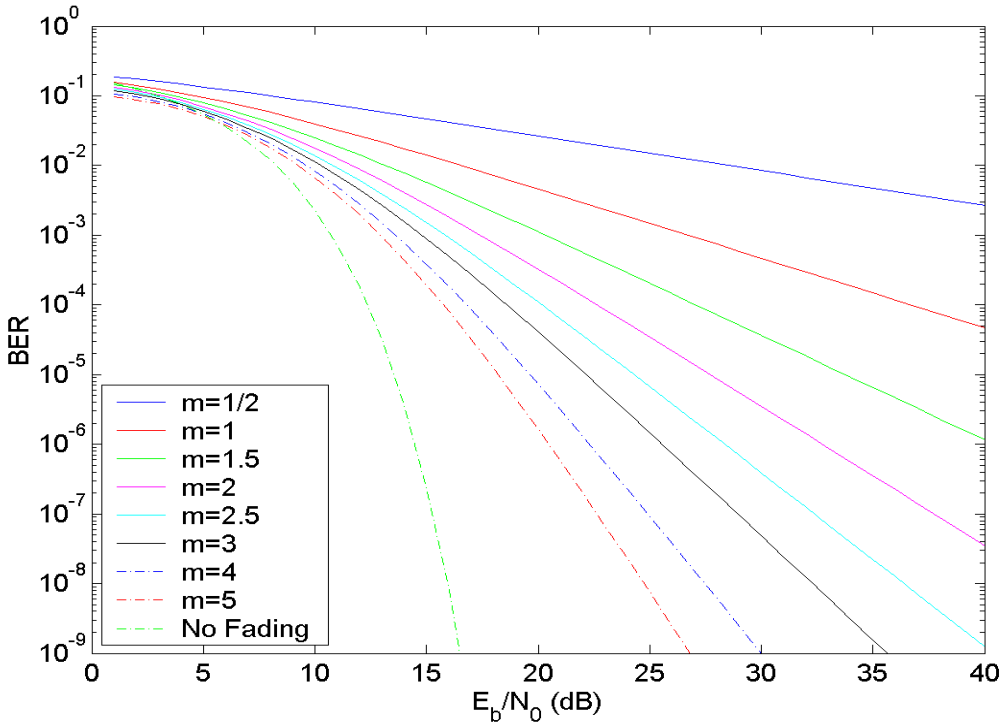

Figure 14. 16-QAM in Nakagami Fading

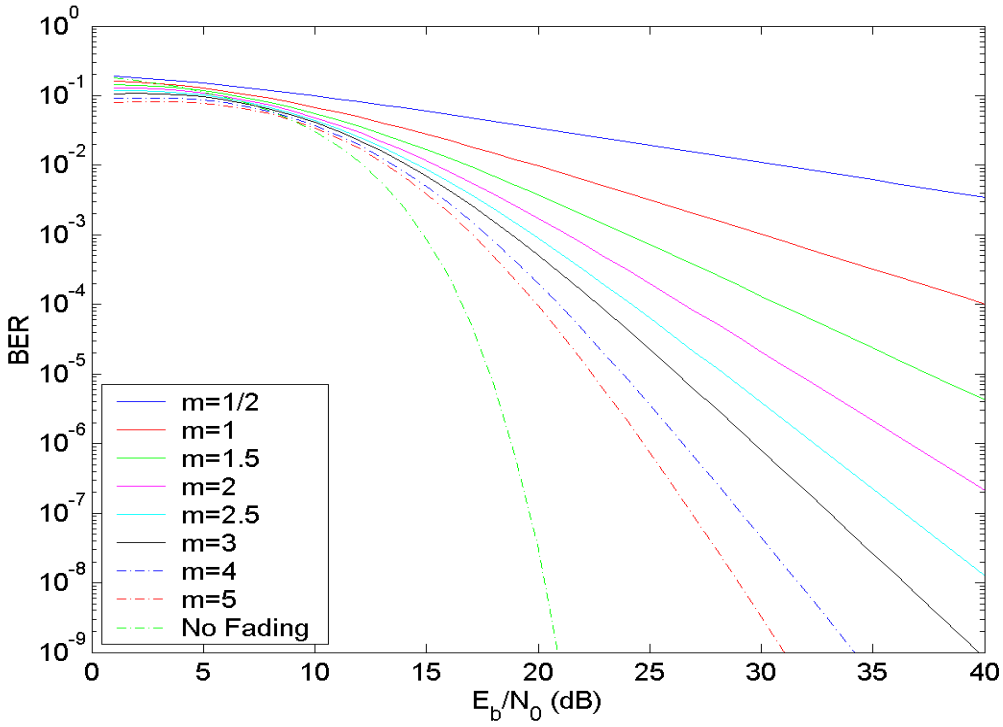

Figure 15. 64-QAM in Nakagami Fading

What we see in both Figures 14 and 15 indicates the same general trend of improved performance for higher values of m. However, at low m, performance is significantly degraded.

In looking back at Figures 12, 14, and 15 we can verify by inspection that our results agree with the notion that BPSK and QPSK have superior performance to M-QAM. As mentioned earlier, however, this improvement comes at considerable cost to bandwidth and data rate. The design engineer must balance these requirements. By way of comparison, we overlay the results of Figures 12, 14, and 15 for the case of $m = 1$ to view their performance relative to each other in Figure 16.

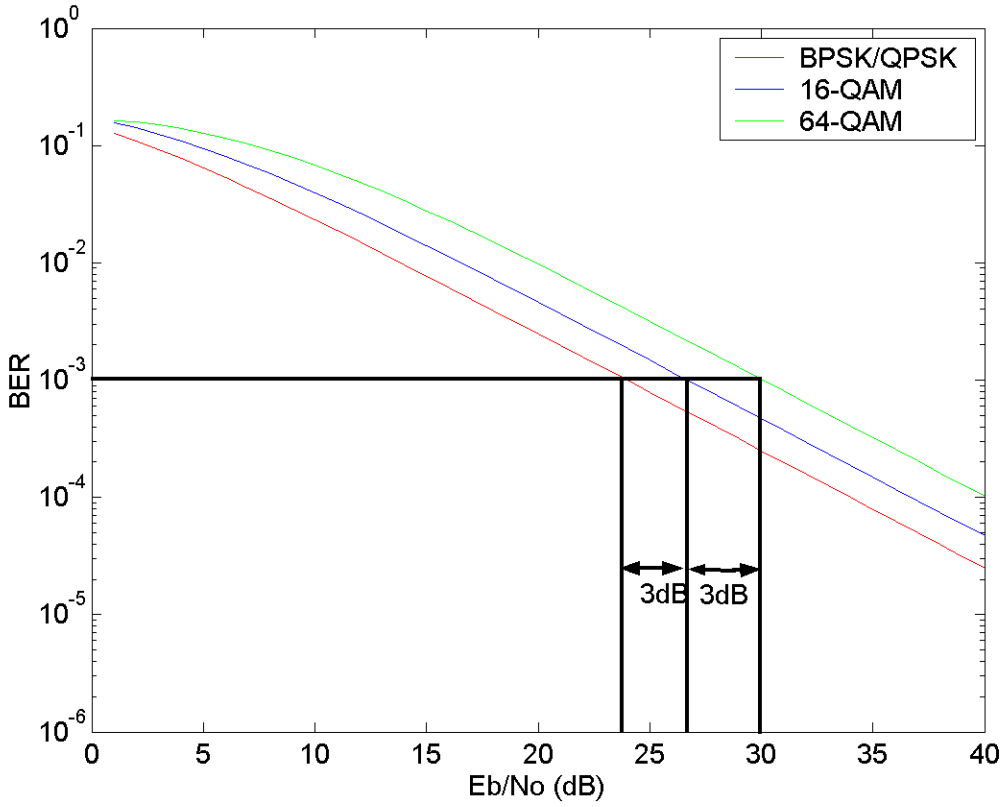

Figure 16. All Modulations in Nakagami Fading for m=1

In Figure 16, we see that the performance trends are as expected. That is, BPSK outperforms 16-QAM which outperforms 64-QAM. For instance, as indicated in Figure 16, 16-QAM requires a received SNR that is 3 dB greater than that of BPSK and QPSK

in order to achieve the same BER of 10^{-3} for $m = 1$. This also holds true for 16 and 64 - QAM.

C. OFDM SYSTEM PERFORMANCE

Now that we have assessed the performance of BPSK, QPSK, 16 and 64-QAM in Nakagami-m fading, we are ready to view the entire OFDM transmission as a whole. All we have done to this point is to consider the performance of particular modulation techniques in Nakagami-m fading. Since our findings to this point treat individual sub-carriers experiencing the same values for the fading factor m, we must now consider all sub-carriers that would actually be transmitted in parallel in an OFDM system. Here again we will model our approach after the IEEE 802.11a standard which calls for 48 data sub-carriers.

So how then do we approach obtaining a probability of bit error for a system of 48 sub-carriers when in reality they will each likely encounter independent fading? We will not stray from the Nakagami-m model in our approach to resolving this issue. The potential benefits of conducting the analysis with Nakagami-m fading are evident and have been sufficiently covered in prior sections. Our approach to this issue is quite simple and straightforward in theory. Since the Nakagami-m distribution is a function of m and Ω, we can fix $\Omega = 1$ as we have in previous cases and randomly assign values of m to each sub-carrier. We can then evaluate the solutions given in Equations (3.23) and (3.36) 48 times, each time with a different value for m. Once this has been accomplished, we can then average our results. This should provide us with an indication of the overall OFDM transmission performance in Nakagami-m fading incorporating all 48 data sub-carriers.

The question that begs an answer then is, how will we assign values for m? As mentioned above, the assignment must be random to properly emulate the unpredictable nature of communication in ever changing environments. At the same time we must choose a distribution that best replicates the degree of fading an OFDM transmission would likely encounter when employed in a WLAN environment. In other words, we must have some realistic values for mean and standard deviation in the case of a Gaussian

distribution, or end points in the case of a uniform distribution, for instance. There are any number of random distributions we can use.

As we consider the appropriate distribution, we must consider the environment in which we are operating. Since the beginning we have assumed we are treating a WLAN application of OFDM which is the standard for the PHY and MAC layers of the OSI model for data rates up to 54 Mbps, the IEEE 802.11a standard. This being the case, we must then suppose that we are transmitting from a laptop computer in a building where our distance to the access point, for example, is short and we must also allow for LOS and non-LOS transmission since both are plausible. The outstation, or laptop computer, may be in the same room as or around the corner from the receiving terminal. In this case then, we must assume the values of m are equally probable. These requirements naturally point us to a uniform distribution of m since the uniform random variable is used to model situations in which all values within an interval are equally likely to occur [15]. The uniform distribution is a simple one and has a PDF given by

$$f_X(x) = \begin{cases} \dfrac{1}{b-a} & a \le x \le b \\ 0 & x < a \quad and \quad x > b \end{cases} \tag{3.38}$$

The uniform distribution is shown graphically in Figure 17.

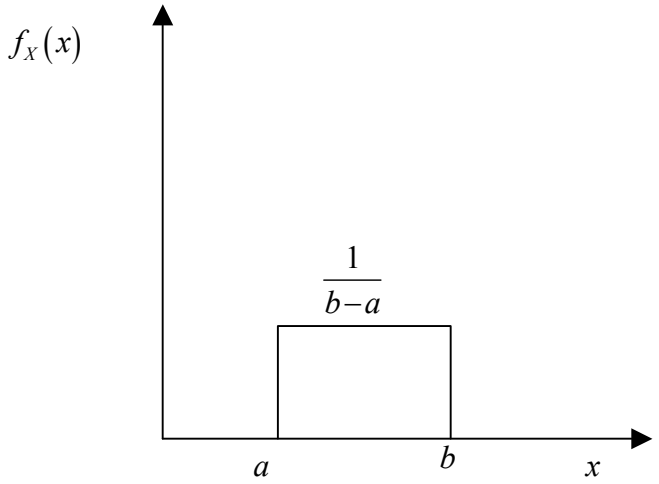

Figure 17. Uniform Random Variable PDF

If we utilize the uniform distribution in our simulations, what then are to be our equivalents of a and b in Figure 17? From our discussions in section III.A.1, it is clear that we must range values of m somewhere between one half and five. To go any higher than $m = 5$ would be to simulate a situation in which there is very little fading. Recall that as the the value of $m \to \infty$, we approach a non-fading AWGN channel performance. Further, since $m > 0$ as stated in Equation (3.3), $1/2$ seems a logical point of departure for situations of more severe fading.

We will see in coming sections that the choice of end points in the distribution is a critical element in the performance of the OFDM system of sub-carriers. In section III.C.1. we will evaluate BPSK and QPSK modulation as described above. After briefly commenting on the results, we will then take up 16 and 64-QAM in section III.C.2. Throughout, we will vary the end points and discuss their effect.

1. BPSK/QPSK Modulated OFDM

In this section we will examine the performance of a BPSK/QPSK modulated OFDM transmission in Nakagami-m fading, only this time we will allow for 48 data sub-carriers experiencing independent Nakagami-m fading. As discussed above, this requires the evaluation of Equation (3.23) 48 times. In each case m is assigned randomly from a uniform distribution. In this first simulation we allow the fading figure to vary between $1/2$ and 5 to see the full range of potential types of fading encountered by the composite 48 sub-carriers. In Figure 18 we plot the results for BPSK/QPSK.

For some perspective, in Figure 19 we plot the results of our evaluation given by Figure 18 against the two endpoints in the uniform distribution. The results are interesting. What we find is that although m is allowed to vary from $1/2$ to five, it appears that the negative effects of the lower fading figure dominate the overall OFDM system performance. We see in Figure 19 that for low values of E_b / N_0, the performance trend for the average of all 48 sub-carriers appears to be near the midpoint between $m = 1/2$ and $m = 5$. However, as the SNR per bit increases, the average BER decreases and at a point near 26 dB, settles out somewhere between $m = 1/2$ and $m = 1$. The more

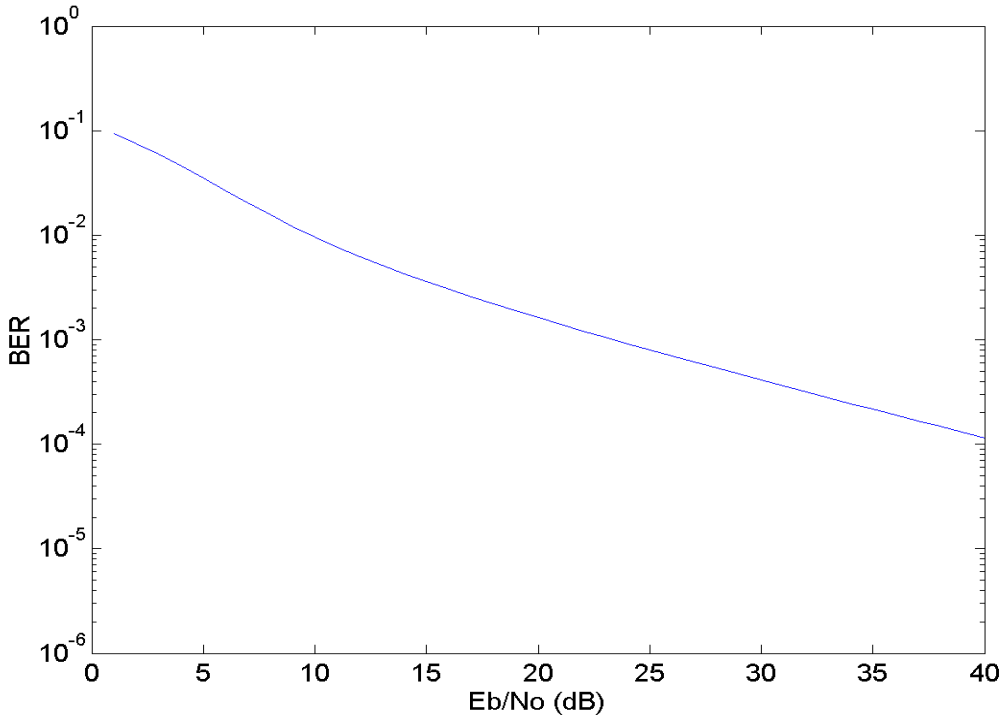

Figure 18. BPSK/QPSK Modulated OFDM $1/2 \le m \le 5$

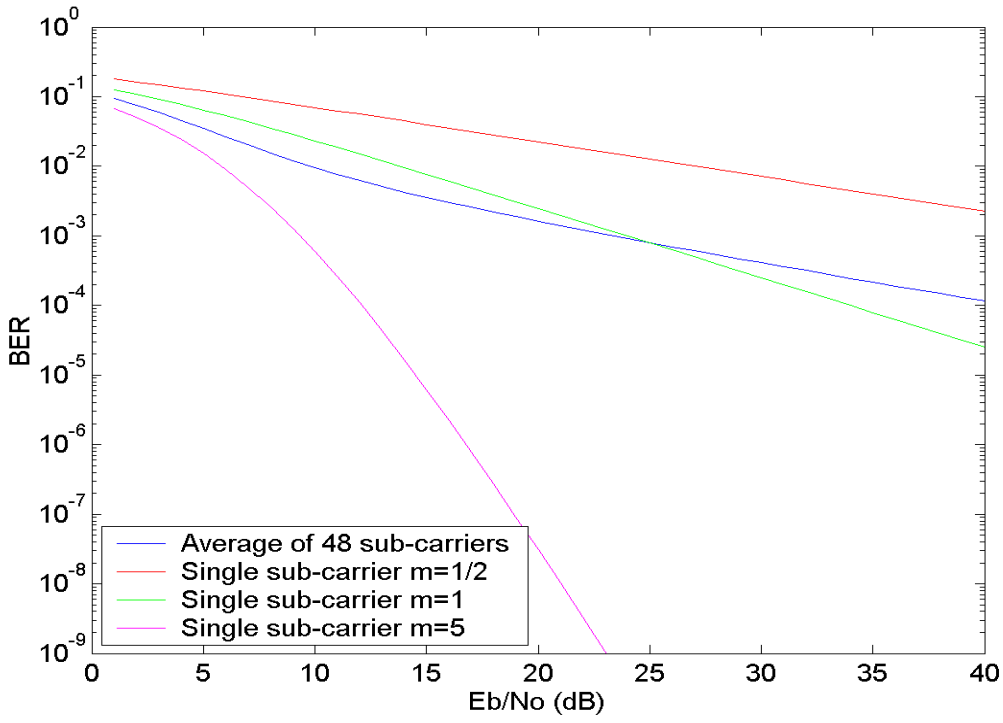

Figure 19. BPSK/QPSK average for 48 sub-carriers $1/2 \le m \le 5$

severe fading is dominating at higher SNR. It is interesting to note that the resulting composite signal is fairly well approximated by $m = 1$, a Rayleigh channel.

Let us narrow the scope of the fading figure a bit to see what happens. If we improve fading conditions by restricting the range of m to now allow conditions more favorable than Rayleigh, that is $1 \le m \le 5$, we can observe what happens to the average over 48 sub-carriers in Figure 20.

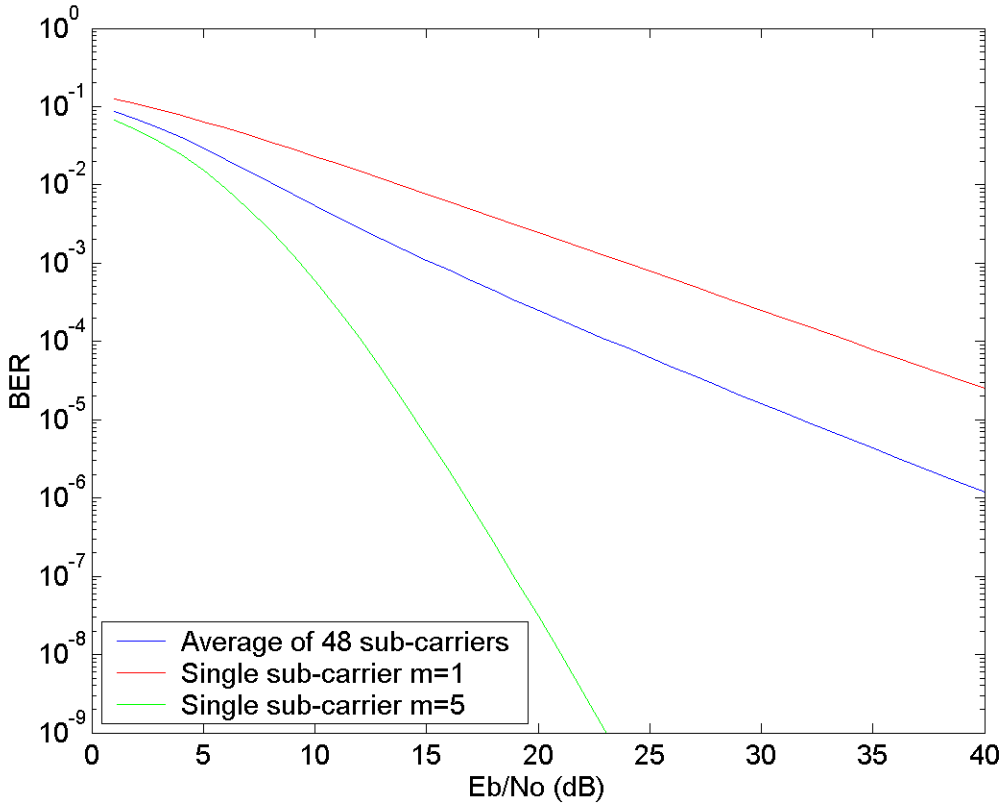

Figure 20. BPSK/QPSK average for 48 sub-carriers $1 \le m \le 5$

Figure 20 appears to exhibit a behavior similar to that of Figure 19; at low SNR the average appears to closely split the difference between the two boundaries. At high SNR, the average tends toward the higher value, or the condition of more severe fading. As a matter of fact, although not pictured here, we find this trend continues as we restrict m all the way down to $4 \le m \le 5$.

It is the degree of domination of the $m = 1/2$ term, however, as given in Figure 19 that is noteworthy. To demonstrate just how dominant the high fading term (low m) is,

we examine two more situations. In the first case (Figure 21), we allow m to range between $1/2 \le m \le 10$ and in the second (Figure 22) $1/2 \le m \le 50$. What we see is very little change in the performance of the overall system, despite the more favorable limits on the fading.

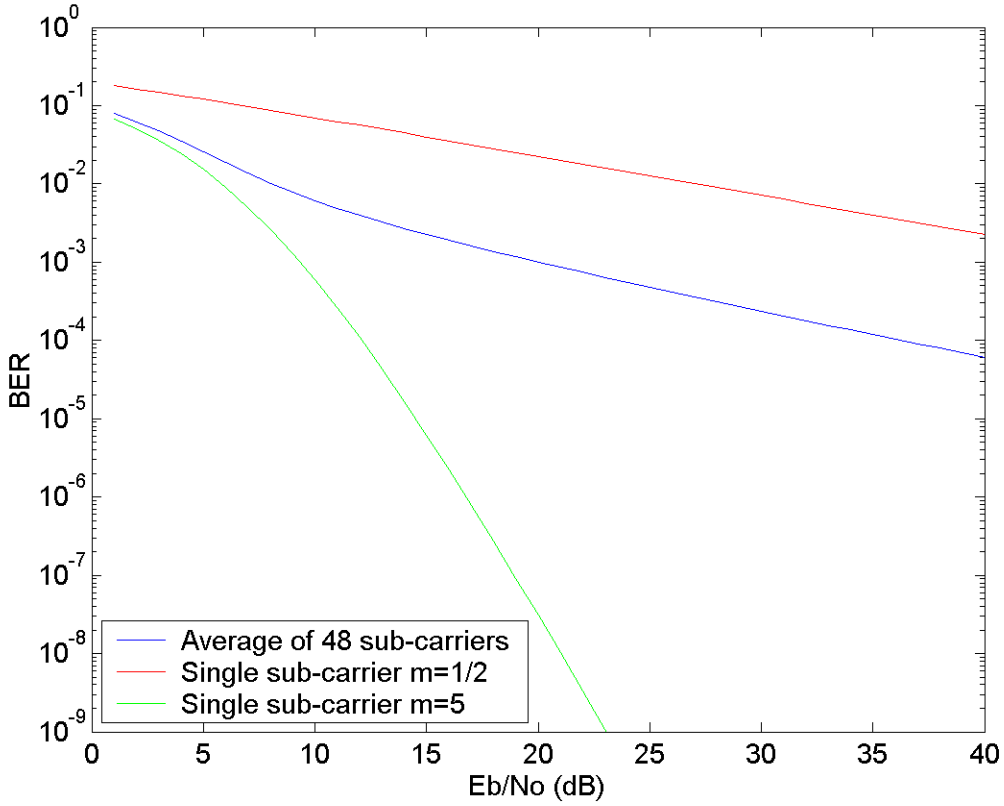

Figure 21. BPSK/QPSK average for 48 sub-carriers $1/2 \le m \le 10$

After numerous trials, it appears that the only appreciable difference in performance among the 48 sub-carrier averages is due to the random nature of the assignment of m as we might expect, however, the general results are the same. Only at very low SNR does the more favorable fading condition seem to have any effect. The dominance of the low fading figure is significant no matter how high we allow m to go. Furthermore, during the analysis it was discovered that the number of sub-carriers made little difference in overall OFDM average performance once the number of sub-carriers exceeded 30. A range of sub-carrier values was tested between four and 480, and the performance trend reached a steady state as in Figure 19 at around 30 sub-carriers. In

other words, there is no appreciable change in average performance for 30 or more sub-carriers.

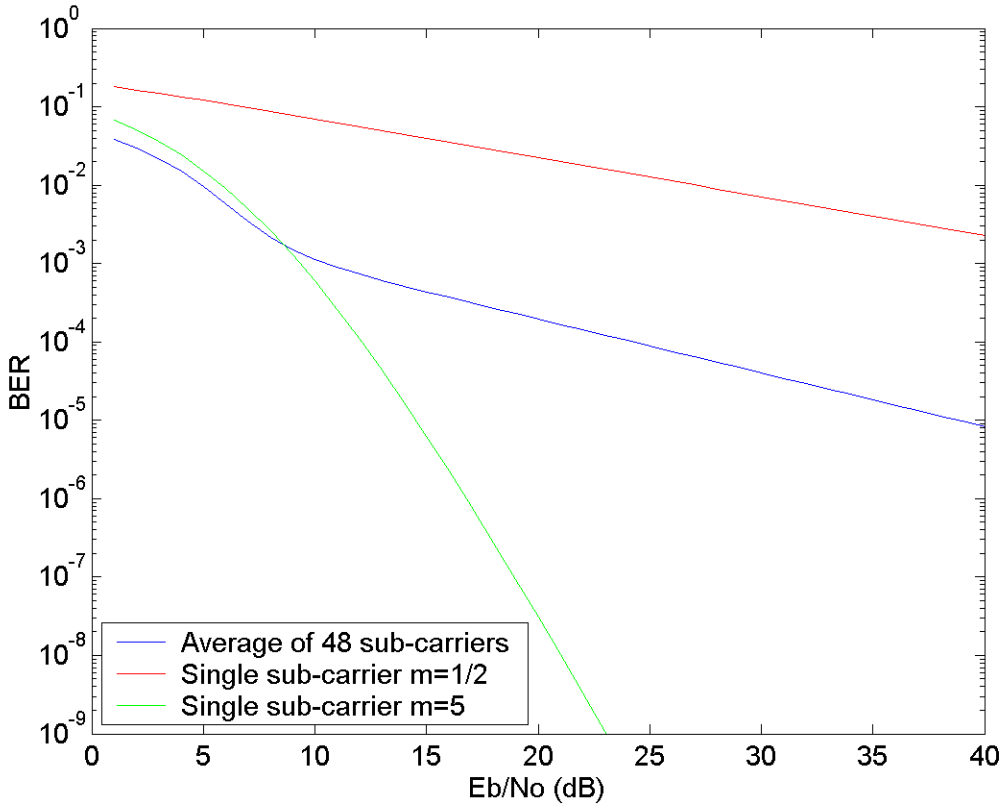

Figure 22. BPSK/QPSK average for 48 sub-carriers $1/2 \le m \le 50$

2. 16 and 64-QAM Modulated OFDM

In this section we consider the case of the higher order modulation techniques of 16 and 64-QAM. We follow an approach similar to that for BPSK/QPSK. That is, we begin with the random distribution of m between values of $1/2 \le m \le 5$ for each sub-carrier. As with the BPSK case, P_b is evaluated 48 times for random m, only this time Equation (3.36) is evaluated instead. We plot the results for 16-QAM in Figure 23. Again, Figure 23 appears to demonstrate the same sort of results we found with BPSK/QPSK, and this is predictable as the only thing changing is based on the difference between BPSK/QPSK and 16-QAM performance in AWGN. So the task at hand now becomes simply a matter of plotting the results of 16-QAM in Nakagami fading as we drastically increase the range of m.

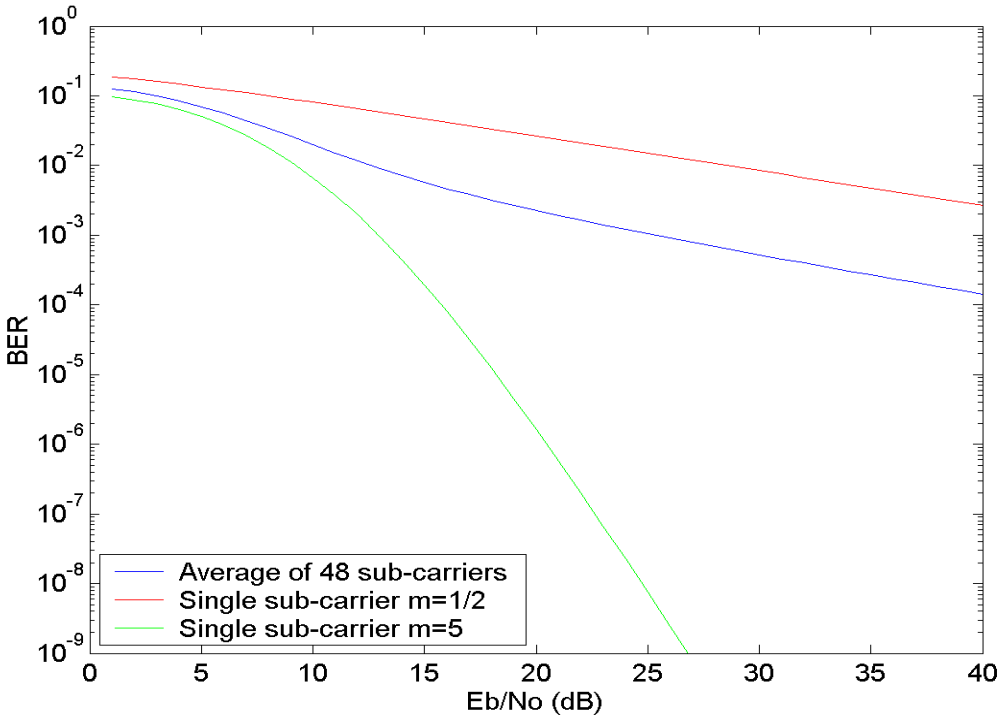

Figure 23. 16-QAM average for 48 sub-carriers $1/2 \le m \le 5$

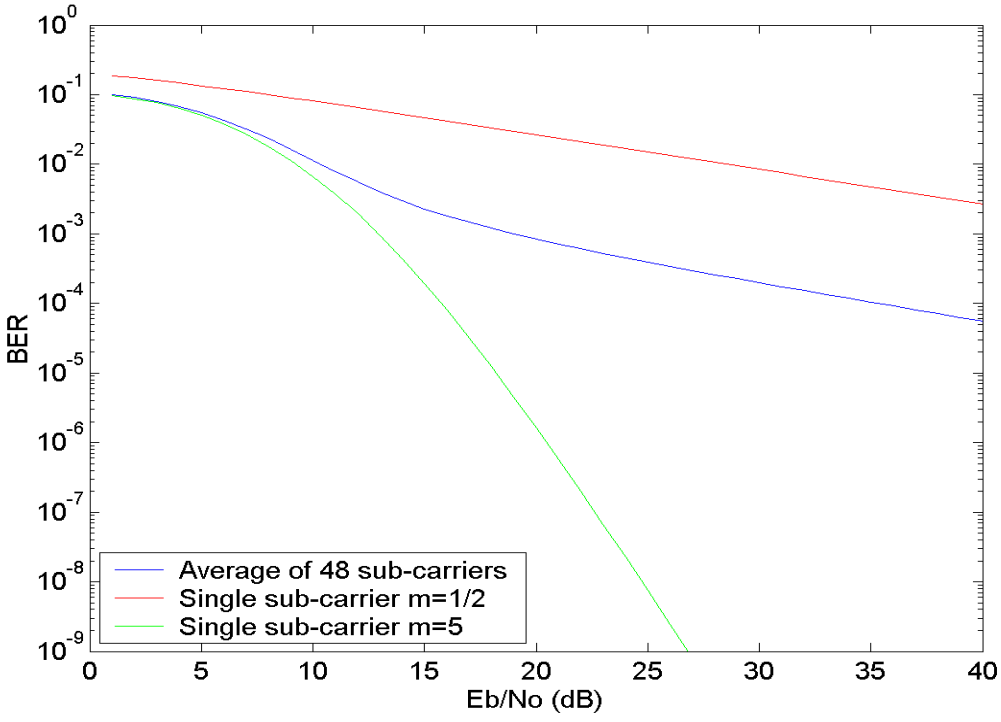

Figure 24. 16-QAM average for 48 sub-carriers $1/2 \le m \le 10$

It bears mentioning here that we are allowing m to vary from $1/2$ up to very high values because even though we know that $m = 50$, for instance, is not realistic, it does give us some indication of exactly how dominant the higher fading values (lower fading figures) are.

Once more we plot the results of 16-QAM modulated OFDM. As we did in the previous section we plot the results for the condition $1/2 \le m \le 50$.

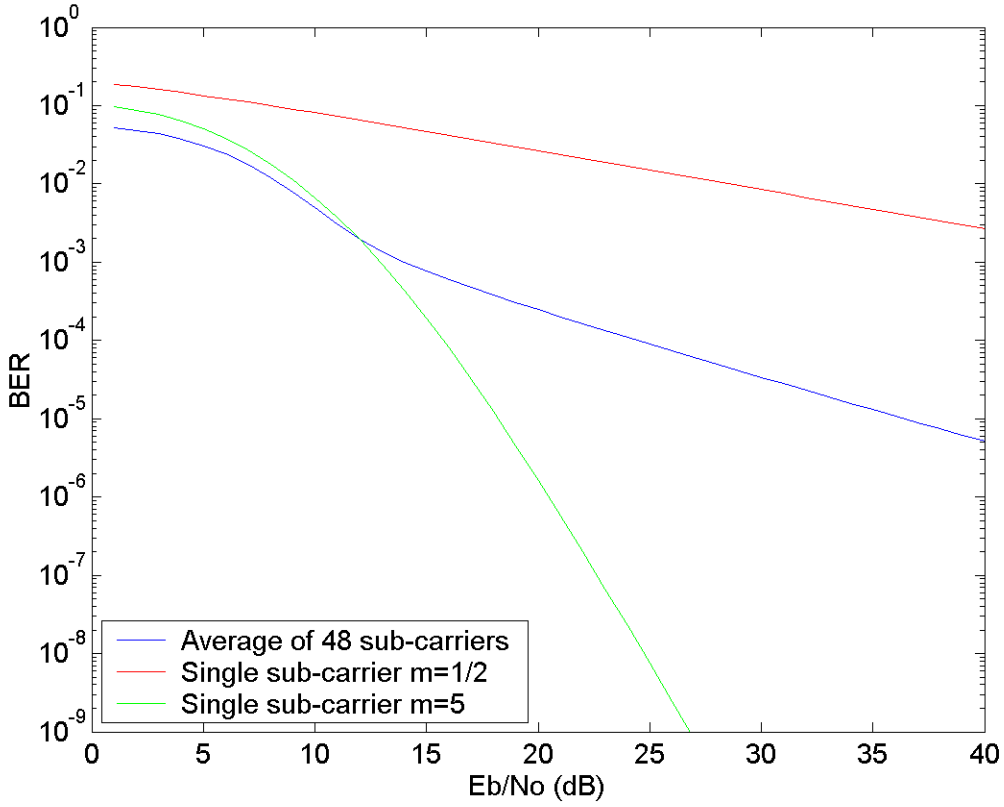

Figure 25. 16-QAM average for 48 sub-carriers $1/2 \le m \le 50$

Finally, we turn our attention to the case of 64-QAM modulated OFDM. When the same analysis is performed for $M = 64$, we obtain the results shown in Figures 26-28. These results are comparable to those obtained for BPSK/QPSK and 16-QAM. Naturally, the curves reflect a slight degradation in performance relative to BPSK/QSPK and 16-QAM since we know 64-QAM does not perform as well (see Figure 6) for the same E_b / N_0.

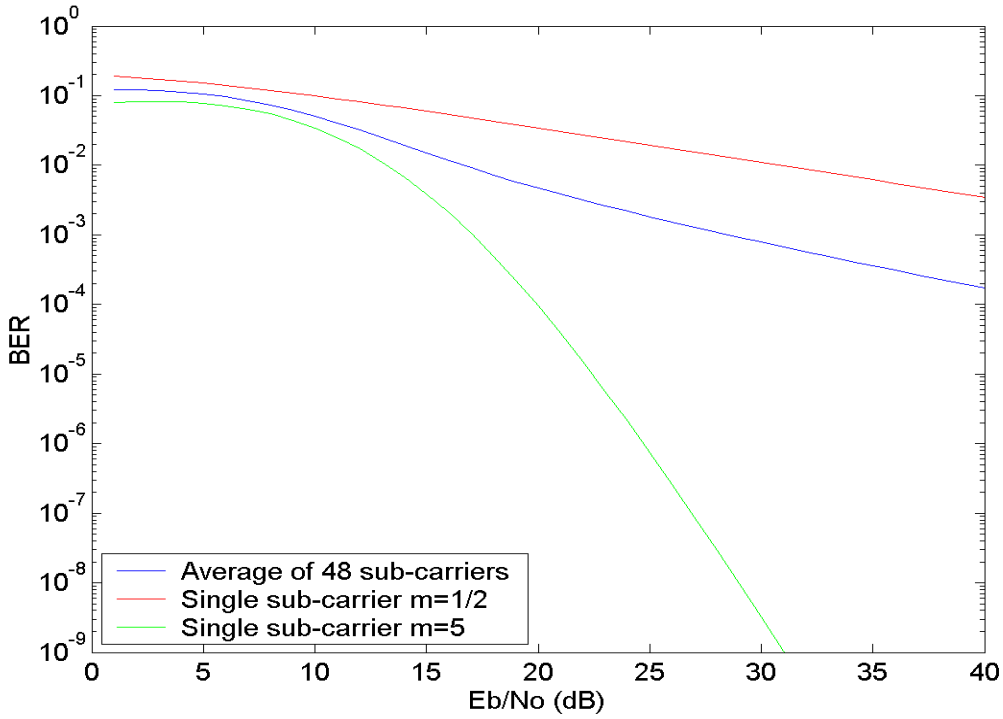

Figure 26. 64-QAM average for 48 sub-carriers $1/2 \le m \le 5$

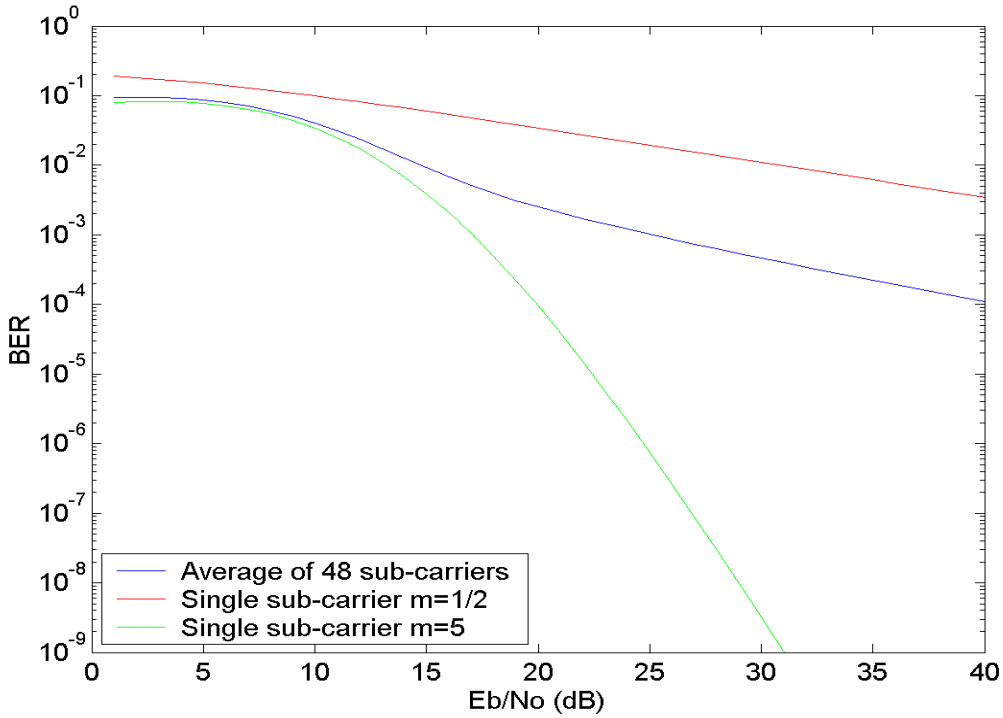

Figure 27. 64-QAM average for 48 sub-carriers $1/2 \le m \le 10$

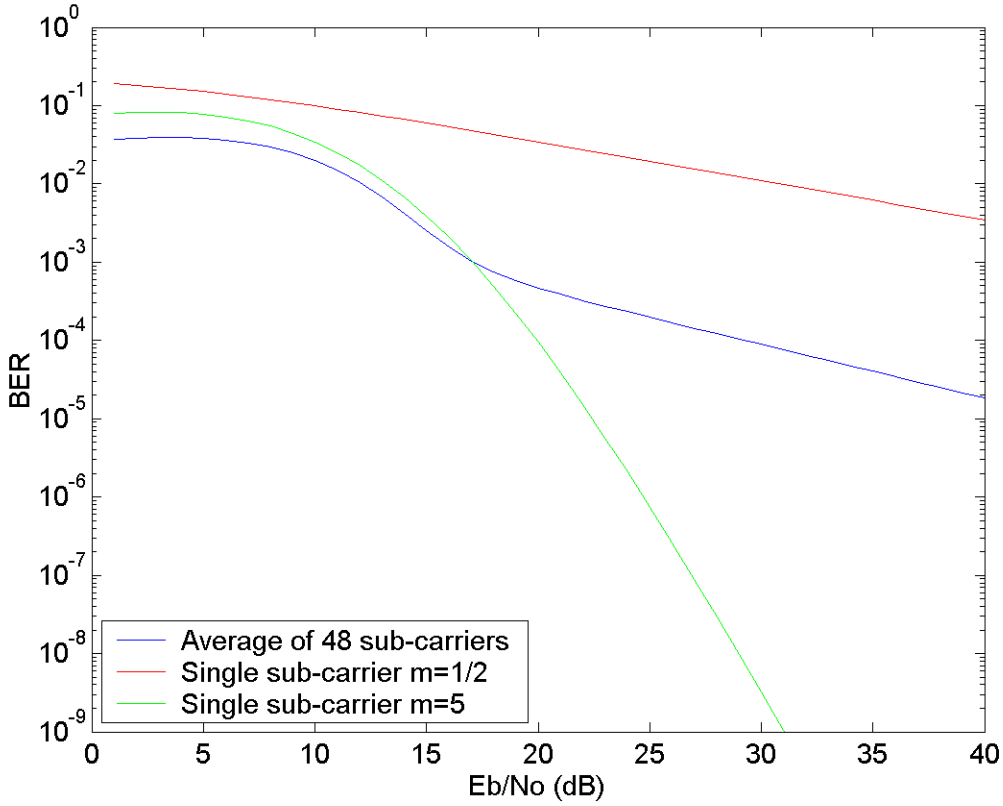

Figure 28. 64-QAM average for 48 sub-carriers $1/2 \le m \le 50$

D. PERFORMANCE SUMMARY

In this chapter we have accomplished a great many things. We began with a discussion of the Nakagami-m distribution and how it fits into our analysis of OFDM in fading channels. Next, we obtained the performance of four modulation types in the aforementioned Nakagami fading analytically. We plotted these results and learned of the severity of performance degradation brought about by Nakagami fading when m is small. Finally, we simulated an IEEE 802.11a compliant OFDM transmission by utilizing the results of the sub-carrier modulation schemes. We assigned random values of the fading figure, a key variable in the Nakagami distribution, to each data sub-carrier and averaged the performance. What we noticed is that the performance is dominated by the smaller values of m indicating more severe fading conditions.

It is clear from many, if not all, of the plots in this chapter, that the performance is not acceptable. In some cases the values of SNR required to achieve a given bit rate are well beyond what might be expected of any communication system. How then do we improve on this? We do this by adding convolutional FEC coding. As discussed in Chapter II.B.4, the addition of convolutional encoding techniques should significantly improve the performance of the sub-carrier modulations and the system as a whole. This is the subject of Chapter IV.

THIS PAGE INTENTIONALLY LEFT BLANK

IV. PERFORMANCE WITH FEC CODING

In Chapter III we observed the effects of Nakagami-m fading on various modulation types and on the OFDM system as a whole. We also noted that degradation in performance is significant for lower values of the fading figure (m) since small values of m dominate overall system performance at moderately high SNR. Though these results are interesting and form the foundation of our analysis, they are by no means complete. Most modern communications systems overcome such poor performance in fading environments by incorporating FEC coding. As discussed in Chapter II, by adding redundancy into the bit stream FEC coding improves the likelihood that a bit will be correctly identified on the receiving end. There are primarily two types of error correction codes, block and convolutional codes.

Since the beginning of this thesis we have used the IEEE 802.11a standard as our framework for studying OFDM. This standard specifies, as indicated in Chapter II.B.4, that constraint length seven $(K = 7)$ convolutional codes shall be utilized in order to achieve performance improvement. The standard further specifies the code rates that will be used for the various types of modulation and desired data rates. The generator polynomials are specified, as is the use of puncturing to achieve higher code rates. So there is little guess-work for us when considering what types of FEC codes to use in our analysis.

Recall that the process of FEC coding requires the encoding of information bits at the transmitter followed by decoding at the receiver. The manner in which a convolutional code is decoded is a key factor in determining overall performance. A computationally efficient, easily realizable algorithm used for the optimum decoding of convolutional codes is called the Viterbi algorithm. The Viterbi algorithm, which will not be discussed in detail in this thesis, develops a metric that enables the decoder to estimate quantitatively the most probable match of the received bits to an actual transmitted bit sequence. This is often referred to as maximum-likelihood sequence estimation (MLSE) [1]. More information on the Viterbi algorithm can be found in a number of publications on FEC coding such as [1], [9], and [14].

In the process of decoding, two different types of "decisions" can be made as to the nature of the received bits. A "hard decision" can be made in which a received bit is demodulated as being either a binary one or zero. This determination is then sent to the Viterbi decoding algorithm for decoding of the actual information bits. A "soft decision" may also be made in which the decoder allows for varying degrees of certainty that a received bit is a one or a zero. This quantization enables the decoder to classify a received bit as a "strong" binary one or zero or marginally declaring the bit a binary one or zero. This approach improves the ability of the decoder to accurately estimate a received bit's identity.

Since the type of "decision" made by the decoder defines the performance of the decoding process, our approach to analyzing OFDM's performance in Nakagami-m fading must be separated into two categories, hard and soft decision Viterbi decoding. In this chapter we will re-examine the analytical expressions obtained in Chapter III with the addition of FEC coding. The chapter is divided into three sections. Section A briefly discusses FEC coding in general. Some of the trade-offs involved in employing FEC coding are discussed. Section B incorporates FEC coding into the OFDM system that utilizes hard decision Viterbi decoding. Finally, section C addresses the case of soft decision Viterbi decoding for BPSK and QPSK.

Since the maximum achievable data rates are tied to the FEC code rate, sections B and C are further divided into sub-sections based on the modulation type and desired data rate. We will see in this chapter how dramatically the addition of FEC coding improves the performance over the uncoded cases explored in Chapter III. This will give us a better idea of what to expect from an IEEE 802.11a-compliant OFDM based system for the fading conditions specified in this thesis.

A. FEC CODING (GENERAL)

Before discussing the performance improvements brought about by FEC coding, a few words about coding are required to give future discussions some context. The topic of error correction coding is broad. Since the context in which we apply FEC coding is OFDM and IEEE 802.11a, we are forced to assume that the reader possesses a

rudimentary knowledge of FEC coding. In this section we cover only the fundamental trade-offs in employing FEC codes.

The addition of FEC coding to a communications system can have many benefits. It may improve the system in terms of better bit error performance, lower power requirements, higher achievable data-rates, or increased capacity. To illustrate these points, let us examine a typical plot of an uncoded modulation vs. a coded modulation as in [9]. In Figure 29, uncoded BPSK is plotted along with coded BPSK in AWGN.

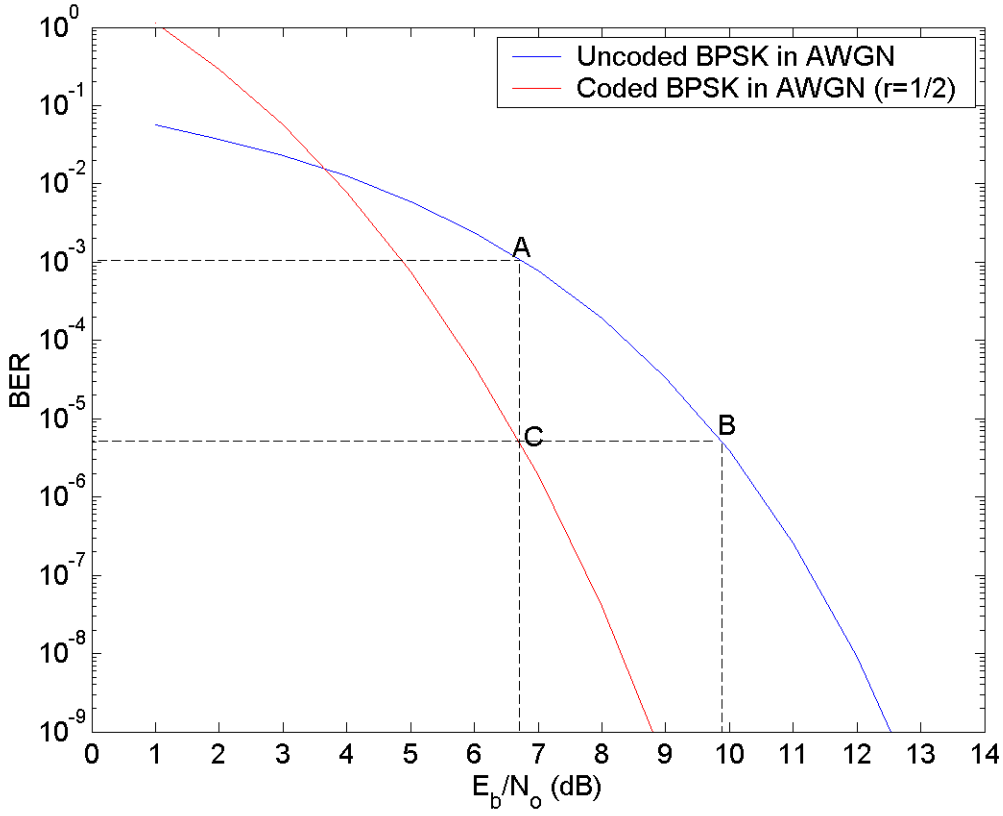

Figure 29. Uncoded vs. Hard Decision Decoded BPSK ($r = 1/2$, $K = 7$) in AWGN

Imagine a scenario in which a communications system is designed to operate at point A, that is, a received SNR per bit of 6.75 dB achieves a BER on the order of 10^{-3}, or one bit out of every 1,000 is in error. What if the application of this communications system necessitated better error performance, such as 5×10^{-6}? In the absence of error correction coding, the system engineer would be required to move the operating point along the

uncoded curve to point B. Suppose, however, that this system is power limited and can only achieve a maximum of 7 dB at the receiver. In this case operating at point B is out of the SNR limit. As an alternative to operating at point B, the use of FEC coding enables the engineer to operate at point C on the coded curve, achieving the desired bit error performance for the same SNR. Thus, we see that FEC coding improves the BER.

Likewise we can imagine a scenario in which a system is designed to operate at point B (SNR per bit about 10dB with a BER of 5×10^{-6}). Suppose that constantly employing the system at this SNR causes occasional hardware failure but the BER is optimal. In order to reduce the average SNR per bit in the system (to around 7dB suppose) the design engineer is required to move the system operating point to a point near A. As seen in Figure 29, this achieves the objective but sacrifices BER. Instead of taking this approach the designer can, after employing FEC coding, choose to operate the system at point C, where he/she can work within power limitations while still maintaining optimal performance. This demonstrates the utility of FEC coding in lowering power requirements.

In terms of data rate, let us assume again that our system is operating at point B. Without FEC coding, if the engineer wishes to increase maximum achievable data rates he must again change the operating point of the system to point A since data rate and SNR per bit are inversely proportional according to [9]

$$\frac{E_b}{N_0} = \frac{P_r}{N_0 R} \tag{4.1}$$

Increased data rate is achieved at significant cost to BER performance. If the system instead operates at point C, the data rate at points A and C are the same, yet the use of FEC coding enables the system to achieve these higher data rates while maintaining the satisfactory BER performance originally desired in operating at point B.

Capacity is also improved by the use of error correction coding as is the case in code-division multiple access (CDMA), a multiple access technique used in cellular communications. Since each user of a given frequency spectrum in each cell is a potential source of interference to other users in the same and neighboring cells, the performance of any user is degraded by the increased number of users per cell. From this

we see that capacity, or the number of users per cell, increases as SNR per bit decreases. Therefore, just as in Equation (4.1), reducing the SNR required causes an increase in the maximum number of users sustained in the CDMA system [9].

As with any design there is a cost involved in using FEC coding. Since the coding adds redundancy to the original data stream, it logically follows that the price paid in employing FEC codes is the need for increased bandwidth. This bandwidth expansion is a function of the code rate. For example, it is well known that the null-to-null bandwidth required for BPSK modulation is twice the data rate ($W_{n-n} = 2R$). If an FEC code produces two coded bits for every one data bit ($k = 1, n = 2, r = k/n = 1/2$), then the bandwidth expansion for BPSK is $1/r = 1/0.5 = 2$. In other words, we require twice as much bandwidth to encode our transmission. This is where the benefits of higher code rates are helpful. In terms of data rate, we now require a bandwidth of $4R$ to encode BPSK at the rate of 1/2. Though this is a concern in bandwidth-limited applications, the potential benefits of FEC codes to BER performance in most applications significantly outweigh the bandwidth price tag.

As discussed in the previous paragraph, the higher the code rate, the less severe the bandwidth expansion. However, since a higher code rate adds less redundancy to the original data, it naturally follows that higher code rates will not improve performance as well as the lower code rates. Therefore, we expect to see more profound performance improvement for lower code rates in the pending analysis. Here again we are faced with the classic engineering trade-off.

At this point it is beneficial to future analysis to develop the relationship between uncoded and coded bit energy. From Equation (4.1) we know that the average transmitted power is the product of average bit energy E_b and bit rate R_b

$$P = E_b R_b \tag{4.2}$$

Furthermore, since transmitted power is that same whether coded or uncoded bits are transmitted we obtain the relationship between coded and uncoded bit energy,

$$
\begin{aligned}
P &= E_b R_b = E_{b_c} R_{b_c} \\
E_b R_b &= E_{b_c} R_{b_c} \\
E_{b_c} &= \frac{R_b}{R_{b_c}} E_b = r E_b
\end{aligned}
\tag{4.3}
$$

where E_{b_c} is the average coded bit energy, R_{b_c} is the coded bit rate and r is the code rate.

In this chapter we will concern ourselves with the first of these coding trade-offs, the improvement in BER over the uncoded case for a given SNR per bit, often referred to as "coding gain" as discussed in Chapter II.B.4. We will not be concerned with matters of bandwidth expansion as it is of little importance in a performance analysis. We leave the balancing of these factors to the system designers. As we move now to analytically developing the benefits of coding in our OFDM system with Nakagami-m fading, our results will be given and analyzed in the context of this BER performance improvement.

B. HARD DECISION DECODING

As previously indicated, hard decision decoding (HDD) is a process in which the received signal is examined and a "hard decision" made as to whether the signal represents a binary one or zero. When the output of a binary symmetric channel is used as the decoder input, the demodulator is said to be a hard decision demodulator. In the decoding process, a trellis is constructed that maps out all possible "paths" a received sequence can take through the decoder. The received sequence is compared to all possible encoder outputs and the path through the trellis with the lowest overall metric is determined to be the closest match to the original transmitted sequence. The metric assigned in HDD is the minimum Hamming distance between the possible outputs of the encoding process and the received sequence. Recall that the Hamming weight of a sequence is the number of binary ones in the sequence and the Hamming distance between two sequences is the difference of their Hamming weights. In the analysis of HDD, the all-zero path through the trellis is assumed to be the transmitted sequence. Since convolutional codes are linear, this assumption simplifies the mathematics involved in deriving a probability of information bit error and means that any binary ones received represent bit errors.

In this section we will apply HDD to the expressions obtained in Chapter III and analyze how HDD improves the performance of OFDM in frequency-selective, slow, Nakagami-m fading channels. The methods for arriving at the error performance of a modulation technique when HDD is employed are complicated and involved. In the interests of brevity and relevance to this thesis, we will not develop all of the equations as this derivation is readily available in the literature. The reader can consult any one of a number of references such as [1] and [14]. In the sub-sections that follow we will examine the modulation types individually at the code rates specified in the IEEE 802.11a standard.

1. BPSK/QPSK with HDD (6,9,12, and 18 Mbps)

For data rates of six and 12 Mbps, the IEEE 802.11a standard calls for BPSK and QPSK modulation, respectively, with convolutional coding at the rate $r = 1/2$. For nine and 18 Mbps, the standard requires BPSK and QPSK, respectively, at a code rate $r = 3/4$ as indicated in Table 5 of Chapter II. In this section we revisit the equations obtained in section III.B.1 for uncoded BPSK and QPSK.

The probability of bit error with HDD cannot be precisely obtained. Therefore, an upper bound on the probability of information bit error is often used in assessing the performance of HDD. This represents a "worst-case scenario" for performance and is given by [1]

$$P_b < \frac{1}{k} \sum_{d=d_{free}}^{\infty} B_d P_d \tag{4.4}$$

where B_d represents the sum of all possible bit errors that can occur when the all-zero code word is transmitted and a path of weight d is selected; P_d is the probability that the decoder will select a code word that is a Hamming distance d from the correct code word; k is the number of information bits; and d_{free} represents the minimum Hamming distance between all pairs of complete convolutional code words [14].

The coefficients in B_d have been determined by computerized searches of large numbers of convolutional codes in order to obtain optimal coding performance for a

given constraint length and code rate. The values of B_d for the constraint length seven $(K = 7)$ code specified in the 802.11a standard are listed in Table 7 by code rate. These values therefore are fixed and will be used in our analysis. It is generally accepted that the first five terms in Equation (4.4) dominate; therefore, Equation (4.4) can be rewritten

$$P_b < \frac{1}{k} \sum_{d=d_{free}}^{d_{free}+4} B_d P_d \tag{4.5}$$

As a result, Table 7 lists only the first five values of B_d, beginning with $B_{d_{free}}$, for the generators used in 802.11a.

Rate	d_{free}	$B_{d_{free}}$	$B_{d_{free}+1}$	$B_{d_{free}+2}$	$B_{d_{free}+3}$	$B_{d_{free}+4}$
1/2	10	36	0	211	0	1404
2/3	6	1	81	402	1487	6793
3/4	5	21	252	1903	11995	72115

Table 7. Weight Structure of the Best Convolutional Codes [After Ref. 16]

Determining P_d is different for hard and soft decision decoding. For HDD, since each decoded bit is demodulated prior to decoding, the probability that a length d path will differ from the correct path in i positions is

$$\Pr(i) = p^i (1-p)^{d-i} \tag{4.6}$$

where p is the channel transition probability. The number of ways in which a length d path can differ in i positions from the correct path is given by

$$\frac{d!}{i!(d-i)!} = \binom{d}{i} \tag{4.7}$$

If d is odd, the all-zero path will be correctly selected if the number of errors in the received sequence is less than $(d+1)/2$; otherwise, the incorrect path is selected [1]. Therefore, for HDD and d odd, the probability of selecting a code word that is a Hamming distance d from the correct codeword is given by

$$P_d = \sum_{i=\frac{d+1}{2}}^{d} \binom{d}{i} p^i (1-p)^{d-i} \tag{4.8}$$

If d is even, if the number of errors is greater than $d/2$, then the incorrect path is chosen. If the number of errors equals $d/2$, then a tie between the two metrics results. This may be settled by randomly choosing one of the paths. In this case, an error occurs half of the time. Hence, the probability of selecting the incorrect path when d is even is given by [1]

$$P_d = \frac{1}{2}\binom{d}{\frac{d}{2}} p^{\frac{d}{2}} (1-p)^{\frac{d}{2}} + \sum_{i=\frac{d}{2}+1}^{d} \binom{d}{i} p^i (1-p)^{d-i} \tag{4.9}$$

We have not yet explained the term p. In the above equations, p is the probability of bit error for the channel. The value of p is a function of coded channel SNR E_{b_c}/N_0. For instance, the channel transition probability for BPSK in AWGN as indicated in Equation (2.17) is

$$p = Q\left(\sqrt{\frac{2E_{b_c}}{N_0}}\right) \tag{4.10}$$

Since from Equation (4.3) we know that $E_{b_c} = rE_b$, we simply replace E_{b_c} in Equation (4.10) with rE_b and obtain

$$p = Q\left(\sqrt{\frac{2rE_b}{N_0}}\right) \tag{4.11}$$

We see that the channel transition probability is nothing more than the uncoded probability of bit error in AWGN with a minor modification to allow for the code rate r. What this means in the context of our analysis is the channel transition probability can be obtained simply by replacing the portion of Equation (3.17) that represents the uncoded

bit error probability for BPSK/QPSK with that of Equation (4.11) and re-evaluate the integral in its new form

$$p_{BPSK/QPSK} = \int_0^\infty Q\left(\sqrt{2r\gamma_b}\right) \frac{m^m}{\Gamma(m)\left(\overline{\gamma}_b\right)^m} \gamma_b{}^{m-1} e^{-\frac{m\gamma_b}{\overline{\gamma}_b}} d\gamma_b \tag{4.12}$$

noting that as before $\gamma_b = \alpha^2 (E_b / N_0)$ with $\alpha = 1$.

In the same manner as in Chapter III, we obtain an analytic solution for Equation (4.12) by noting the mathematical relationships given in Equations (3.18) through (3.22) and setting $c = 2r$, $a = m/\overline{\gamma}_b$, $b = m$, $t = \gamma_b$, and $\psi = c/2a = r\overline{\gamma}_b / m$. The result of these substitutions yields

$$p_{BPSK/QPSK} = \sqrt{\frac{r\overline{\gamma}_b}{m + r\overline{\gamma}_b}} \frac{\Gamma\left(m+\frac{1}{2}\right)}{2\sqrt{\pi}\,\Gamma(m+1)\left(1+\frac{r\overline{\gamma}_b}{m}\right)^m} \left(1 + \sum_{k=1}^{\infty} \frac{\prod_{n=0}^{k-1}\left(m+\frac{1}{2}+n\right)\left(\frac{1}{1+\frac{r\overline{\gamma}_b}{m}}\right)^k}{\prod_{n=0}^{k-1}(m+1+n)} \right) \tag{4.13}$$

Now all of the pieces of the puzzle are known. Thus, for BPSK and QPSK in Nakagami-m fading with hard decision Viterbi decoding we evaluate Equation (4.5) using the coefficients for B_d given in Table 7, by substituting Equation (4.13) into Equations (4.8) or (4.9) depending on the value of d, and in turn substituting Equation (4.8) or (4.9) into Equation (4.5). The results of this analysis are plotted in Figure 30 for the usual range of the fading figure m for a convolutional code rate $r = 1/2$. Recall that as stated earlier, this accounts for the IEEE 802.11a target data rates of six Mbps for BPSK and 12 Mbps for QPSK.

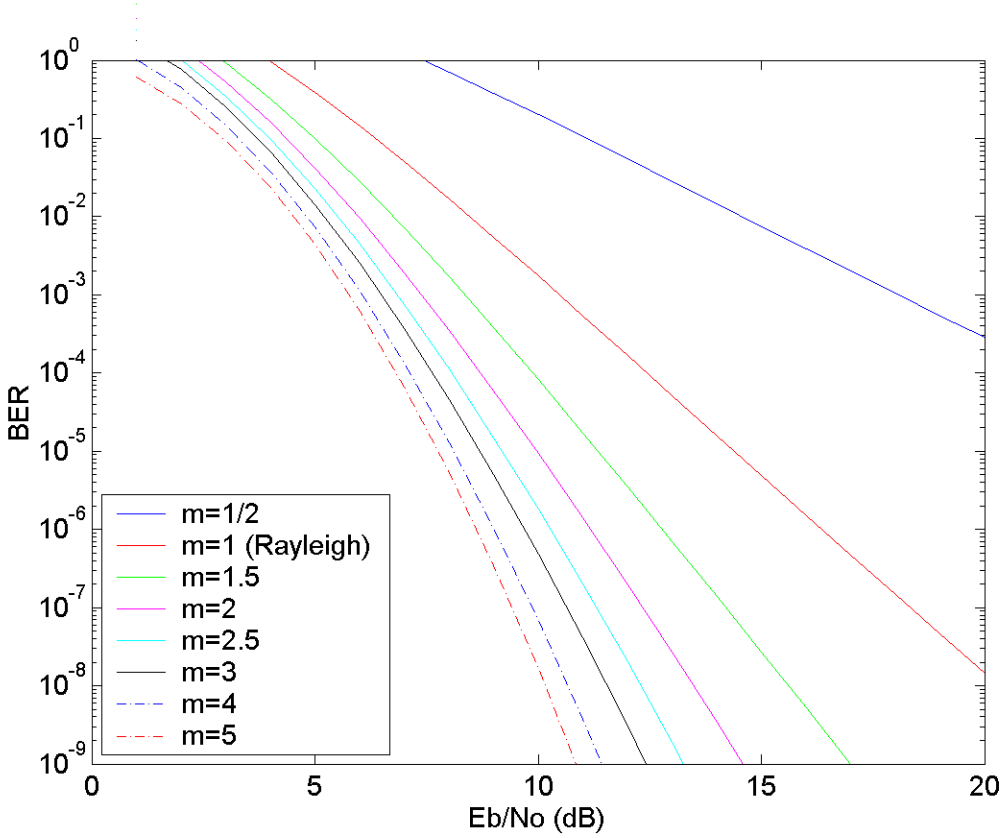

Figure 30. BPSK/QPSK in Nakagami-m Fading with HDD for $r = 1/2$

Although not shown here, it is interesting to note that the approximation for Equation (3.24) obtained in Equation (3.26) can no longer be used. Though the approximation remains valid even with the addition of the code rate as in Equation (4.12), the results obtained for P_b become unreliable after substituting Equations (4.8) or (4.9) and (4.13) into Equation (4.5). Hence, hereafter the full expression for the channel transition probability will be utilized in our analysis.

In order to gain some perspective on the performance improvement obtained in Figure 30, we expand the dB-axis and overlay some integer values of the uncoded results obtained in Chapter III for BPSK/QPSK in Figure 31. From Figure 31 we can see that error correction coding provides remarkable improvement over the uncoded performance. Also from Figure 31 we note that the benefits of FEC coding are realized beginning at very low values of SNR per bit and improve dramatically with lower BER relative to the uncoded case. At extremely low values of SNR and very high BER (the top left corner of

the figure), FEC coding actually results in poorer performance than the uncoded case. In reality however, a practical communications system requires a much lower BER and will not likely operate at such low values of E_b / N_0.

As shown in Figure 29, the performance improvement obtained for HDD with BPSK/QPSK in AWGN only ranges from as little as one dB at $P_b = 10^{-3}$ to four dB at $P_b = 10^{-9}$.

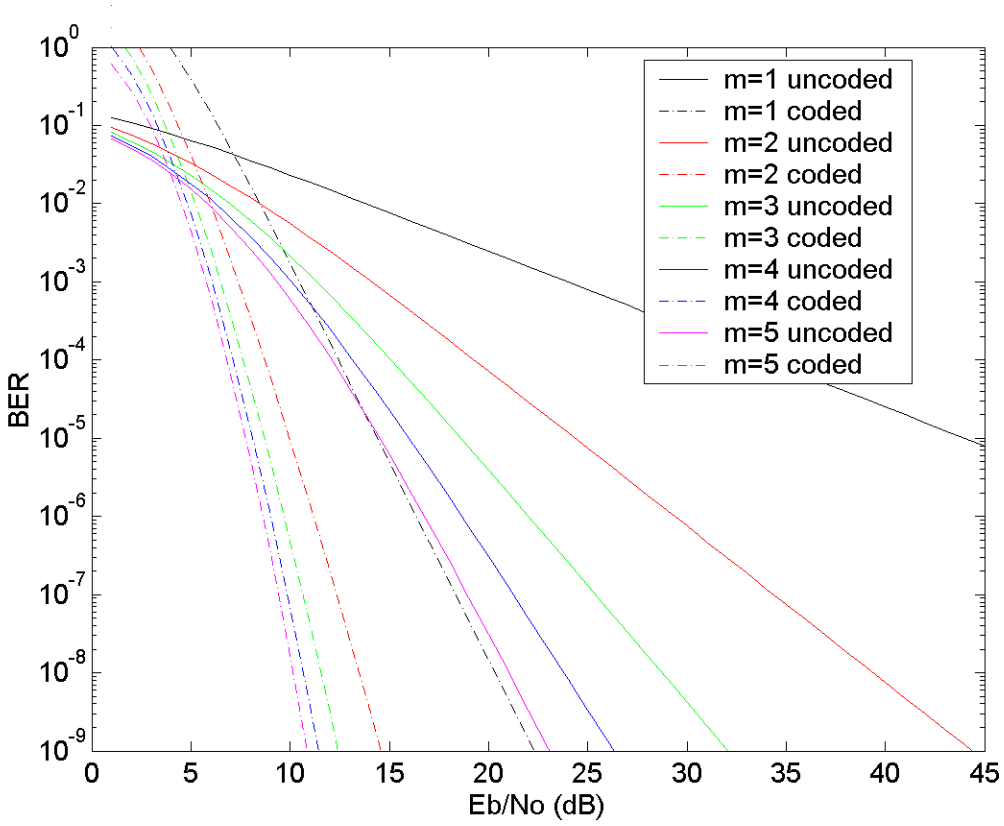

Figure 31. Uncoded vs. HDD BPSK/QPSK in Nakagami-m fading for $r = 1/2$

Although it is true that the presence of fading degrades performance much more severely than AWGN alone does, the relative improvement brought about by the FEC coding under fading conditions is greater than for the AWGN channel. In Figure 32 we illustrate the range of coding gain obtained with HDD and BPSK/QPSK. As we can see, the coding gain is greater for lower values of m. At the same time, the least coding gain is

realized at higher values of m. This is to be expected since under these circumstances, fading conditions are more favorable.

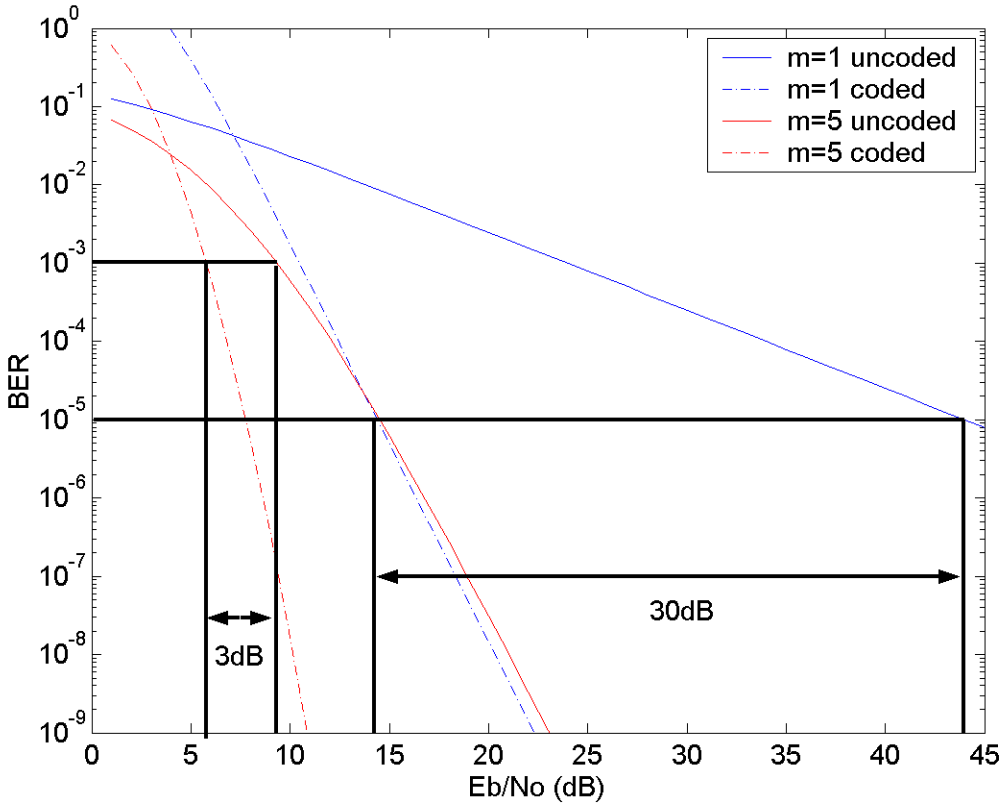

Figure 32. Range of Coding Gain for HDD BPSK/QPSK $r = 1/2$

A typical range of BER that would be acceptable for WLAN applications is indicated in Figure 32. A BER of 10^{-3} represents the low end of acceptable performance in a WLAN. Since smaller values of SNR and higher values of BER yield the lowest coding gain, we see that the FEC coding provides at least three dB of coding gain under these fading conditions. For the best case coding gain we choose the high end of required WLAN performance at BER 10^{-5} for small values of the fading figure. Here we see that an improvement of as much as 30 dB can be obtained for the Rayleigh fading case of $m = 1$. This is even more pronounced for $m = 1/2$.

Just as we did in Chapter III, we now turn our attention to the desired outcome of this thesis, that is, the analysis of OFDM under fading conditions. Since the performance

curves obtained in Figures 30-32 represent a single BPSK/QPSK modulated sub-carrier, we must account for the fact that all 48 sub-carriers in an OFDM system will encounter independent Nakagami-m distributed fading. As in Chapter III, we model m as a uniform random variable between $1/2 \le m \le 5$ and assign each of the 48 sub-carriers its own fading figure randomly. The average over all 48 sub-carriers represents the performance of BPSK/QPSK modulated OFDM in Nakagami-m fading with HDD and is plotted in Figure 33.

To demonstrate the coding gain obtained for OFDM, we choose a reference BER of 10^{-4} and overlay the uncoded OFDM results obtained in Chapter III. We see from Figure 33 that at 10^{-4} an average coding gain of approximately 23 dB is obtained. Furthermore, we see more clearly in Figure 33 that the benefit of coding for this code rate and sub-carrier modulation type begins at the crossover point near BER=10^{-2} and $E_b / N_0 \approx 10$ dB. This is the point at which coding gain becomes positive. In terms of

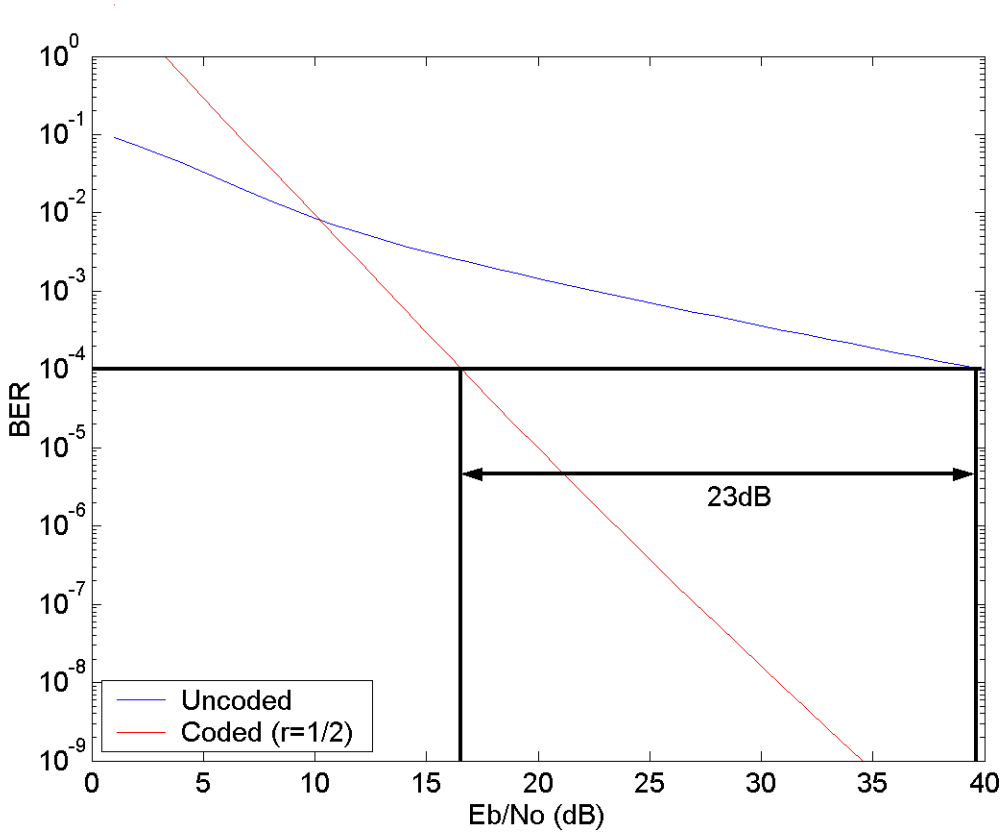

Figure 33. BPSK/QPSK Modulated OFDM in Nakagami-m Fading w/ HDD $r = 1/2$

absolute performance at BER=10^{-4}, we see from Figure 33 that the composite OFDM system requires a received average SNR per bit of 17 dB.

Now we perform the same analysis for $r = 3/4$ to obtain the performance curves for nine Mbps BPSK modulated OFDM and 18 Mbps QPSK modulated OFDM as specified in the 802.11a standard. The results of this analysis for a single sub-carrier are given in Figure 34 for the usual range of m.

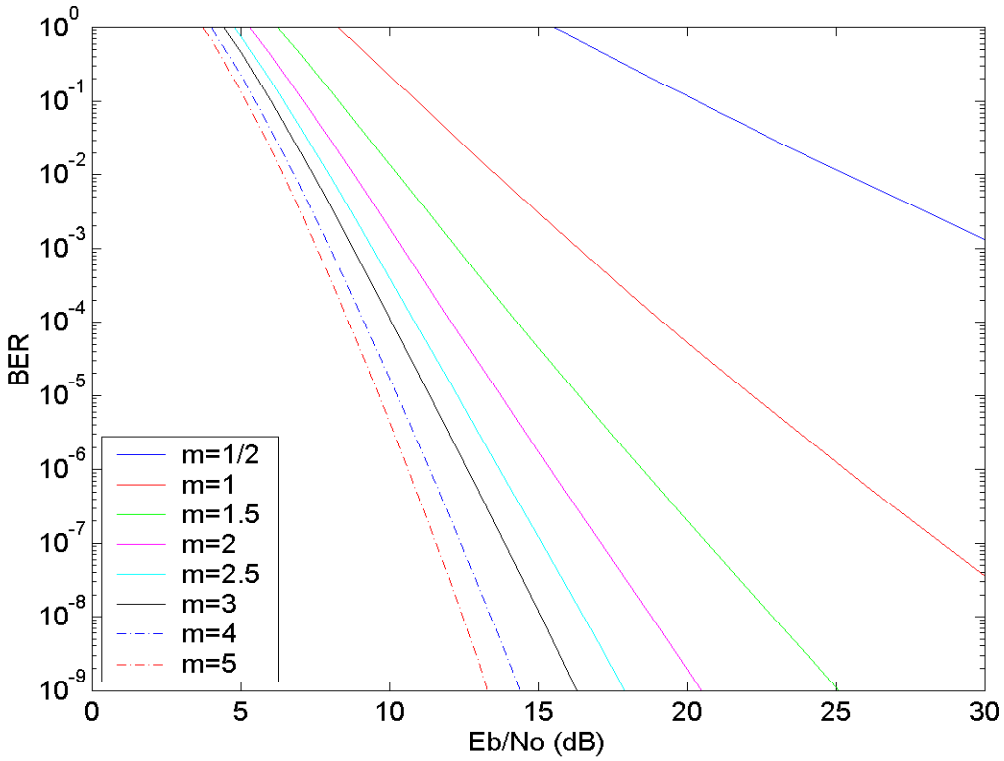

Figure 34. BPSK/QPSK in Nakagami-m Fading with HDD for $r = 3/4$

Comparing Figures 30 and 34, we notice that although the modulation remains the same, the curves are shifted slightly to the right. This represents a slight disadvantage in performance brought about by the change from $r = 1/2$ to $r = 3/4$. As discussed in section IV.A, this result is expected since the higher code rate corresponds to less redundancy added to the transmitted bit stream. The advantage, however, is higher achievable data rates and less bandwidth expansion since the higher code rate results in shorter channel bit duration relative to $r = 1/2$.

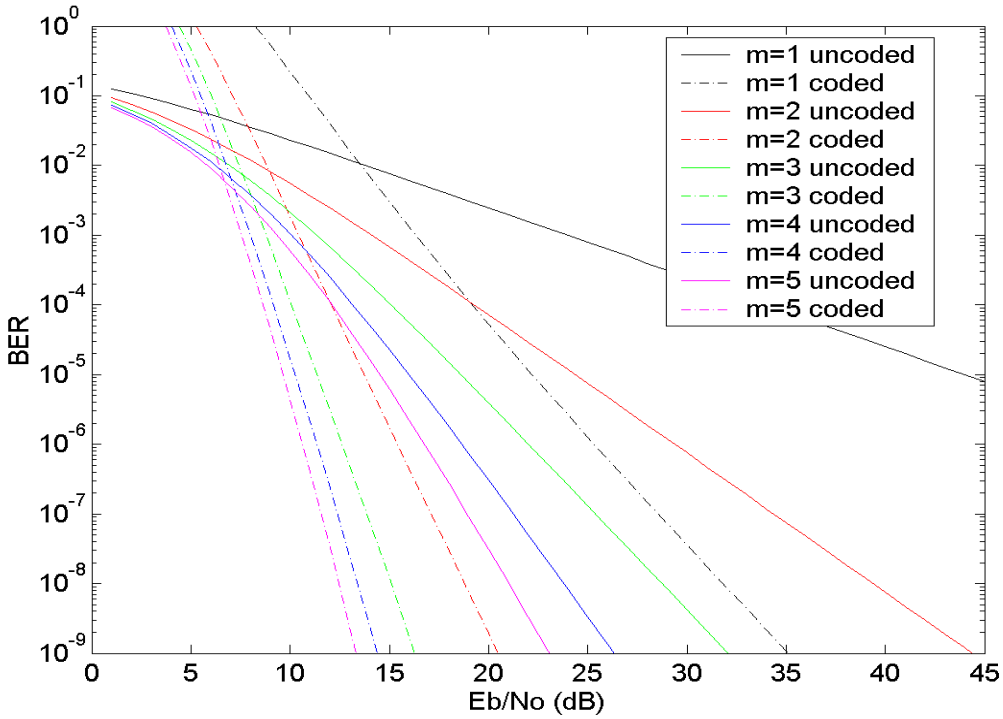

Figure 35. Uncoded vs. HDD BPSK/QPSK in Nakagami-m fading for $r = 3/4$

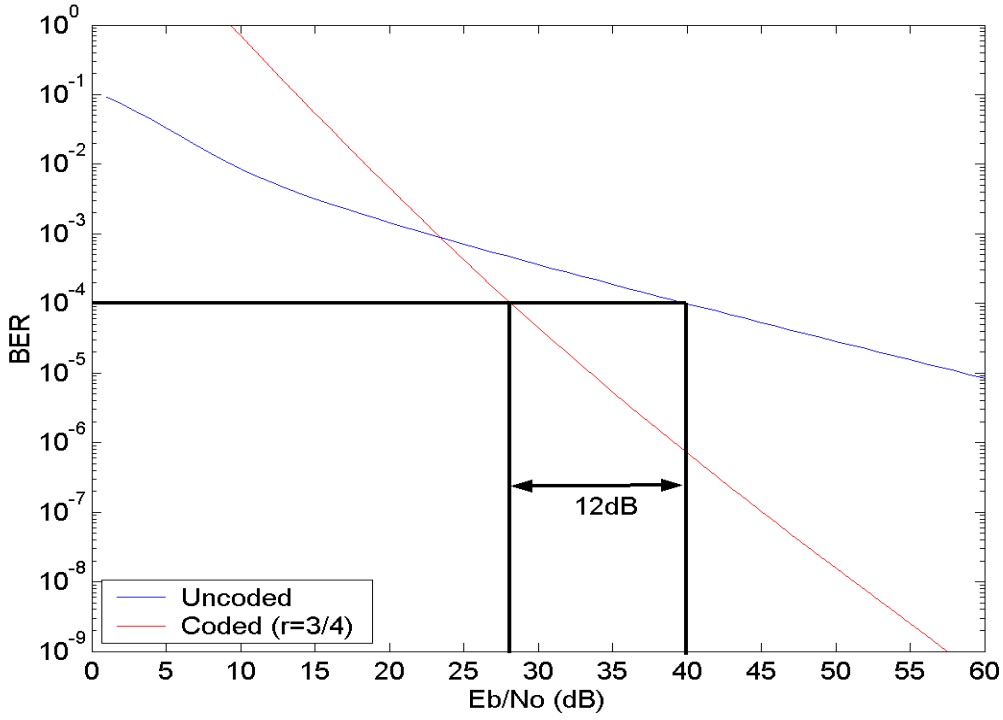

Figure 36. BPSK/QPSK Modulated OFDM in Nakagami-m Fading w/ HDD $r = 3/4$

In Figure 35 we overlay the uncoded BPSK/QPSK results onto those in Figure 34 to see the performance improvement of HDD for this code rate.

Just as for $r = 1/2$, when m is randomly assigned to all 48 sub-carriers and averaged, the performance of BPSK/QPSK modulated OFDM for $r = 3/4$ convolutional coding is obtained as in Figure 36. Here again we see the overall performance of $r = 3/4$ code is poorer than for $r = 1/2$. Hence, coding gain is less significant but still quite remarkable. Figure 36 also demonstrates that the advantages of adding FEC coding for this code rate begin at the point of positive coding gain near $E_b / N_0 \approx 23$ dB and BER near 10^{-3}. Prior to this point, the best performance is obtained by the uncoded BPSK/QPSK OFDM curve. Figure 36 also indicates that 28 dB of average SNR per bit is required at BER=10^{-4}.

2. 16-QAM with HDD (24 and 36 Mbps)

To achieve data rates of 24 and 36 Mbps, the IEEE 802.11a standard requires 16-QAM with convolutional coding at rates $r = 1/2$ and $r = 3/4$, respectively. In this section we perform the analysis on this modulation and code rate combination in the same manner as we did for BPSK/QPSK with HDD in the previous section. Although achievable data rates are higher and bandwidth efficiency greater, we learned earlier that QAM performance is inferior to that of BPSK and QPSK. It follows then that we expect our analysis in this section will reveal poorer performance than for BPSK or QPSK as we develop the analytical expressions for QAM.

From discussions in the previous section, we know that forming the channel transition probability for M-QAM in Nakagami-m fading begins with the probability of bit error in AWGN with an added factor accounting for code rate as follows:

$$P_b = \frac{4\left(\sqrt{M}-1\right)}{q\sqrt{M}} Q\left(\sqrt{\frac{3qr\gamma_b}{M-1}}\right) \tag{4.14}$$

Using Equation (4.14), we now evaluate

$$p_{QAM} = \int_0^{\infty} \frac{4\left(\sqrt{M}-1\right)}{q\sqrt{M}} Q\left(\sqrt{\frac{3qr\gamma_b}{M-1}}\right) \frac{m^m}{\Gamma(m)\bar{\gamma}_b{}^m} \gamma_b^{m-1} e^{-\frac{m\gamma_b}{\bar{\gamma}_b}} d\gamma_b \tag{4.15}$$

Given the mathematical relationship in Equation (3.18), we make the following substitutions

$$\begin{aligned} c &= \frac{3qr}{M-1} \\ a &= \frac{m}{\bar{\gamma}_b} \\ t &= \gamma_b \\ b &= m \\ \psi &= \frac{c}{2a} = \frac{\frac{3qr}{M-1}}{\frac{2m}{\bar{\gamma}_b}} = \frac{3}{2}\frac{qr\bar{\gamma}_b}{(M-1)m} \end{aligned} \tag{4.16}$$

to obtain

$$\begin{aligned} p_{QAM} = {} & \frac{4\left(\sqrt{M}-1\right)}{q\sqrt{M}} \sqrt{\frac{3qr\bar{\gamma}_b}{2(M-1)m+3qr\bar{\gamma}_b}} \frac{\Gamma\left(m+\frac{1}{2}\right)}{2\sqrt{\pi}\Gamma(m+1)\left(1+\frac{3qr\bar{\gamma}_b}{2(M-1)m}\right)^m} \\ & \times \left[1+\sum_{k=1}^{\infty} \frac{\prod_{n=0}^{k-1}\left(m+\frac{1}{2}+n\right)\left(\frac{2(M-1)m}{2(M-1)m+3qr\bar{\gamma}_b}\right)^k}{\prod_{n=0}^{k-1}(m+1+n)}\right] \end{aligned} \tag{4.17}$$

which represents the channel transition probability. Finally, substituting Equation (4.17) into Equation (4.8) for d odd or Equation (4.9) for d even, and taking the results for P_d into Equation (4.5), we obtain the performance of M-QAM in Nakagami-m fading with HDD. The results of this analysis for 16-QAM at 24 Mbps ($r = 1/2$) are plotted in Figure 37. In Figure 38, the results of this analysis are compared to the uncoded analysis performed in section III.B.2 to see how much savings HDD has enabled.

Now that we know how a single 16-QAM sub-carrier experiencing frequency-nonselective, slow Nakagami-m fading with HDD behaves, let us turn our attention to the OFDM system to account for all 48 sub-carriers and the frequency-selectivity of

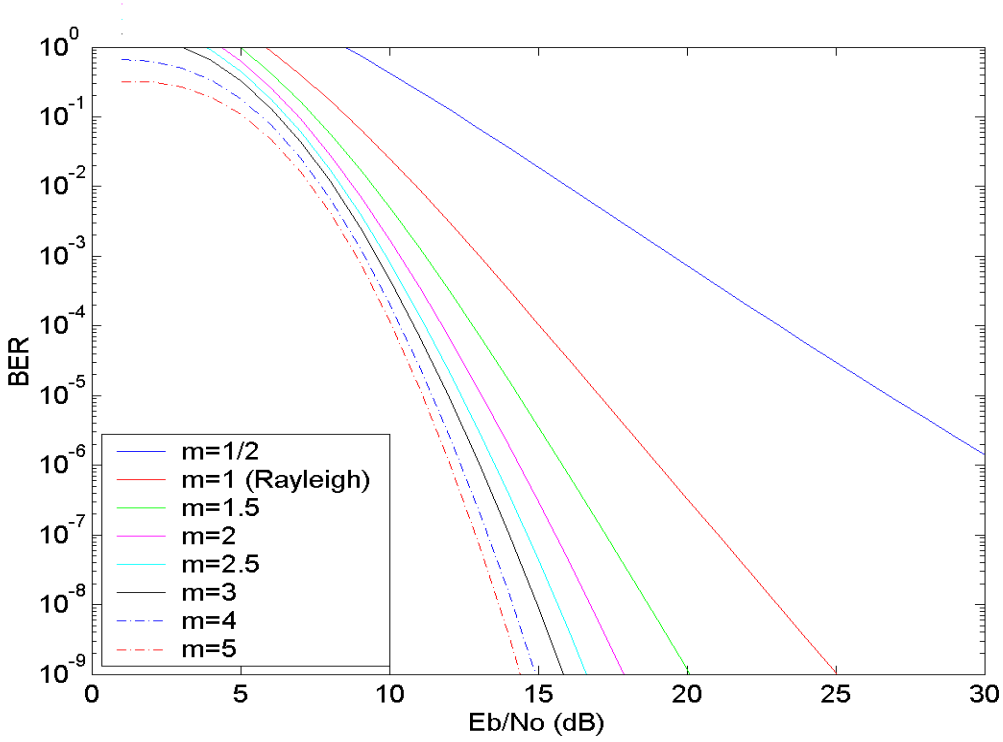

Figure 37. 16-QAM in Nakagami-m Fading with HDD for $r = 1/2$

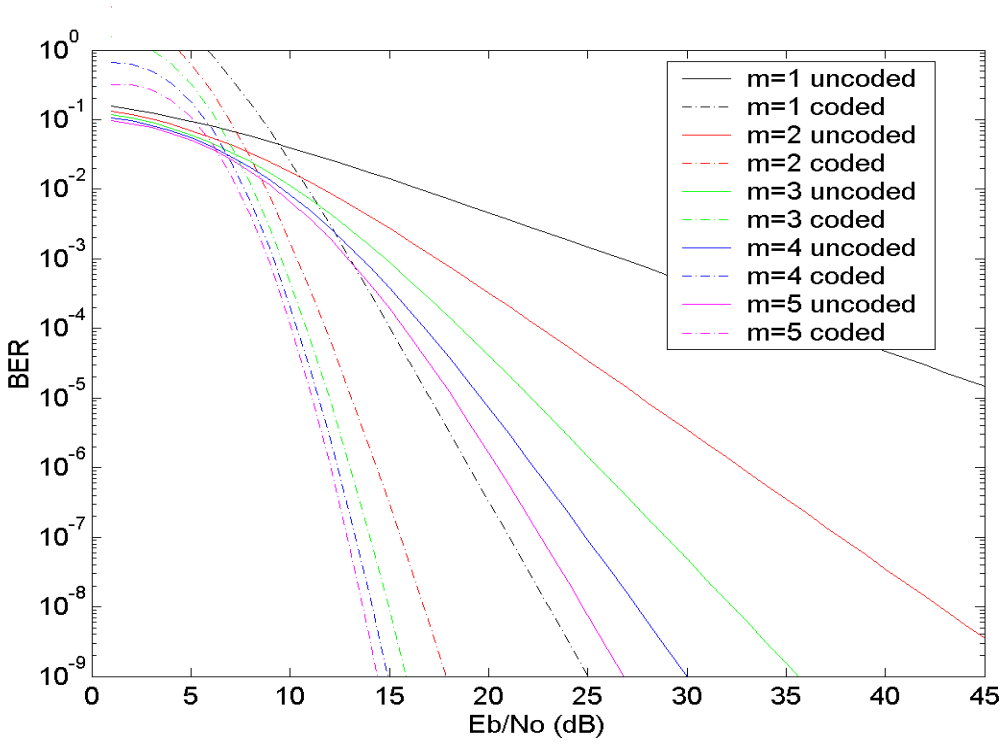

Figure 38. Uncoded vs. HDD 16-QAM in Nakagami-m fading for $r = 1/2$

the fading the entire system encounters. When the analysis performed above is computed for 48 sub-carriers with each one experiencing a randomly distributed fading figure and averaged, we obtain the results given in Figure 39.

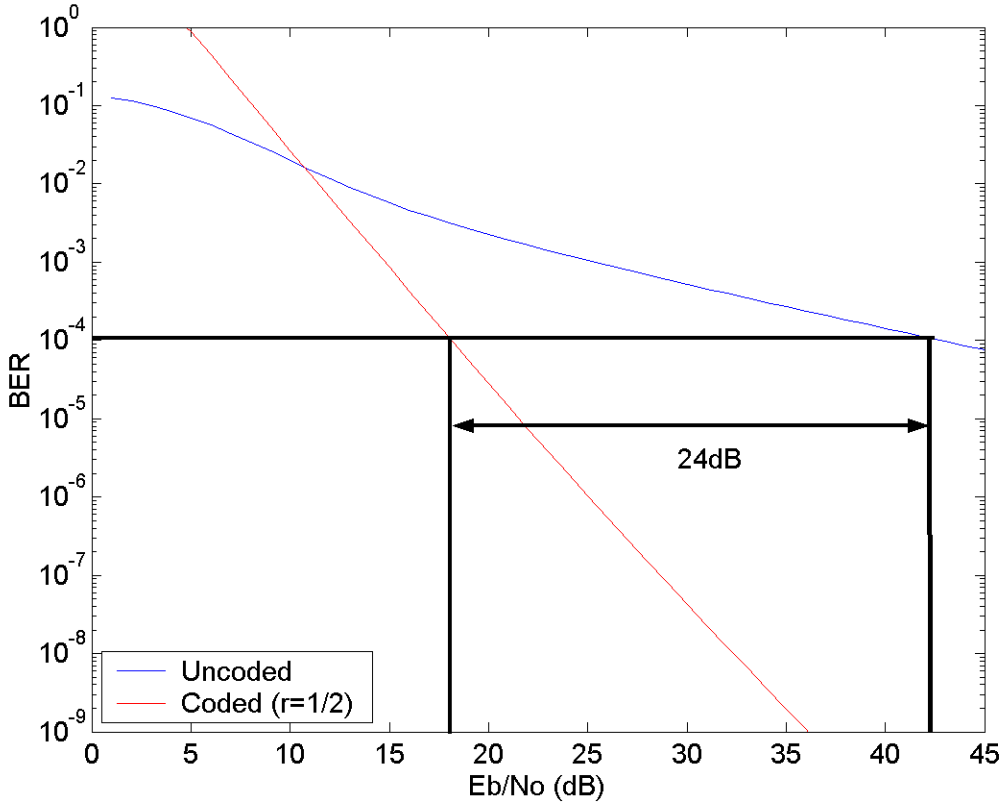

Figure 39. 16-QAM Modulated OFDM in Nakagami-m Fading w/ HDD $r = 1/2$

In this case, we see that for a nominal BER of 10^{-4}, we obtain a coding gain over the uncoded 16-QAM modulated OFDM of approximately 24 dB. The cross-over point on this graph where the positive coding gain begins lies just above a BER of 10^{-2} and $E_b / N_0 \approx 11\,\text{dB}$. This relatively small value of SNR and high BER are generally not the typical operating point for a digital communications system. Thus, the addition of FEC coding in this example benefits the performance almost immediately as was the case in BPSK. In terms of absolute performance at BER=10^{-4}, an SNR of 28 dB is required.

Likewise, the same analysis is performed for the 36 Mbps data rates with $r = 3/4$ and the appropriate coefficients for B_d according to Table 7 ($r = 3/4$). The results of 16-QAM at 36 Mbps are plotted in Figure 40.

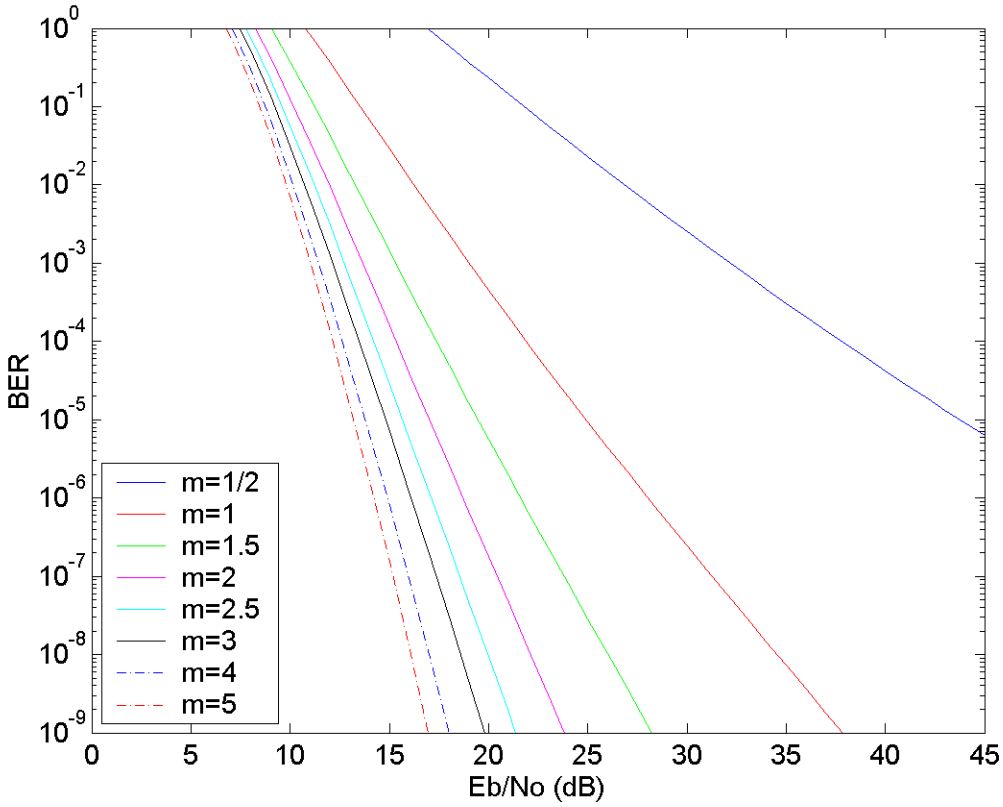

Figure 40. 16-QAM in Nakagami-m Fading with HDD for $r = 3/4$

We overlay the uncoded results of 16-QAM in Nakagami-m fading and view the performance improvement due to HDD in Figure 41. As before, the coding gain is far greater for smaller values of m.

In the final part of our 16-QAM performance analysis we plot the results of 16-QAM OFDM at 36 Mbps for all 48 sub-carriers in Figure 42. Here we observe the cross-over point moving slightly down and to the right on the graph as we expect. The point at which the coding gain becomes positive is near BER=10^{-3} and $E_b / N_0 \approx 24$ dB. The coding gain at 10^{-4} is approximately 13 dB. In absolute terms, at BER=10^{-4}, we require an average SNR per bit of 30 dB.

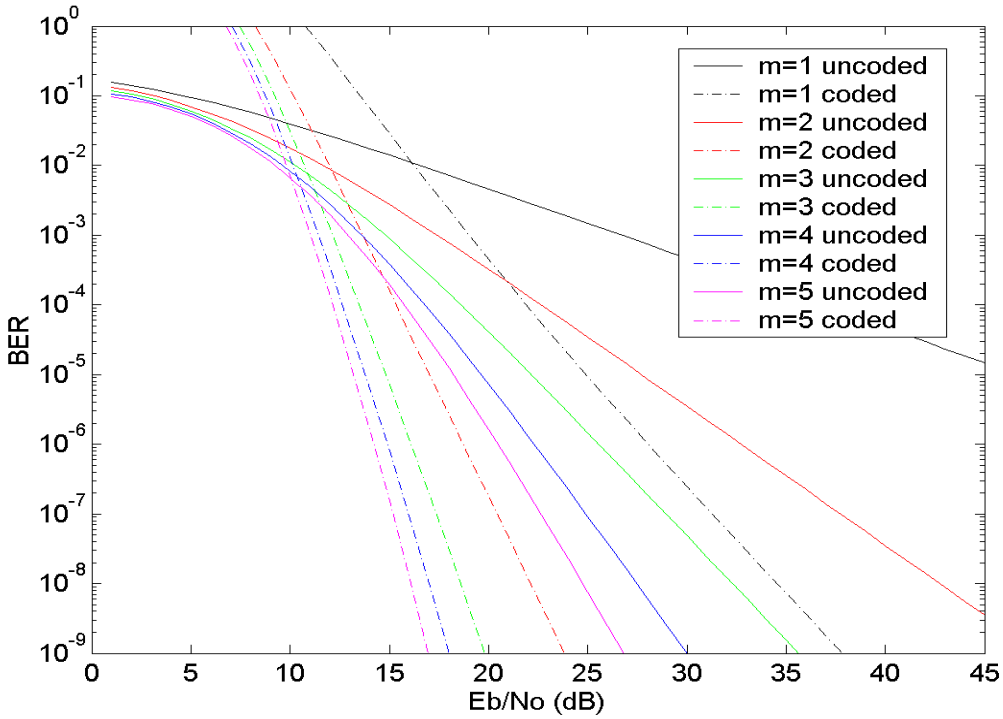

Figure 41. Uncoded vs. HDD 16-QAM in Nakagami-m fading for $r = 3/4$

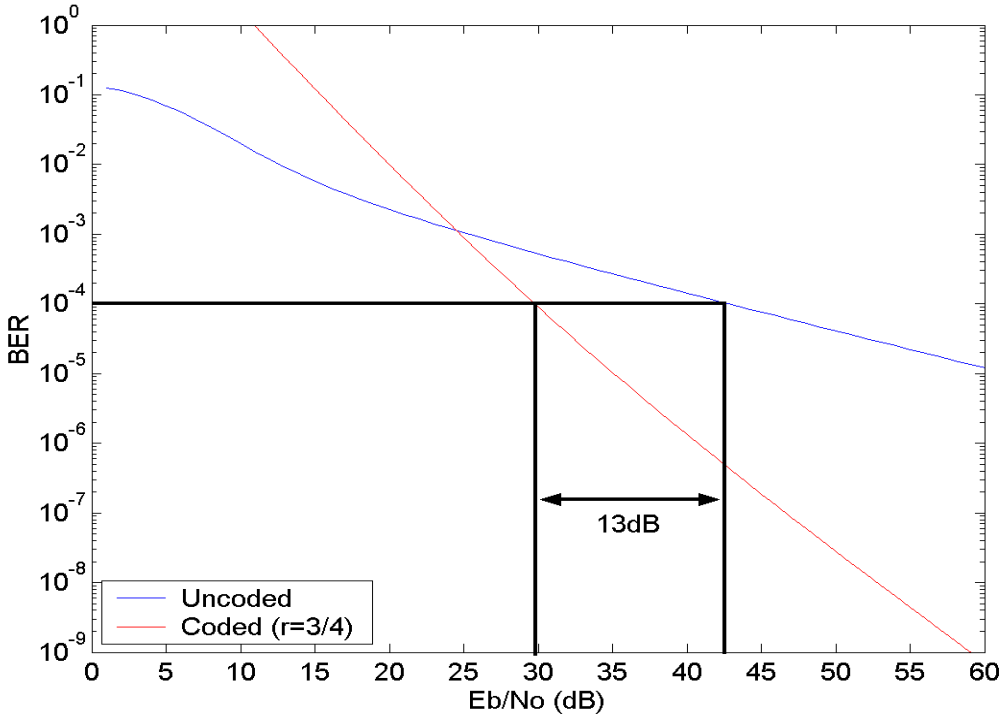

Figure 42. 16-QAM Modulated OFDM in Nakagami-m Fading w/ HDD $r = 3/4$

3. 64-QAM with HDD (48 and 54 Mbps)

The equations describing the performance analysis of 64-QAM in HDD are the same as those developed in the previous section since they were developed for the general case of square constellation M-QAM. Therefore, our analysis of 64-QAM modulated OFDM with HDD in Nakagami-m fading proceeds in the same manner as 16-QAM, from Equations (4.5), (4.8) or (4.9), and (4.17) for $M = 64$ and $q = 6$. This time, however, we note that the code rate is $r = 2/3$ vice $r = 1/2$ as with previous sub-carrier modulation types and the coefficients for B_d in Equation (4.5) are taken from Table 7 at this code rate. Figure 43 is a plot of this performance for a single sub-carrier for the usual range of m as a function of average SNR per bit $\overline{\gamma}_b$.

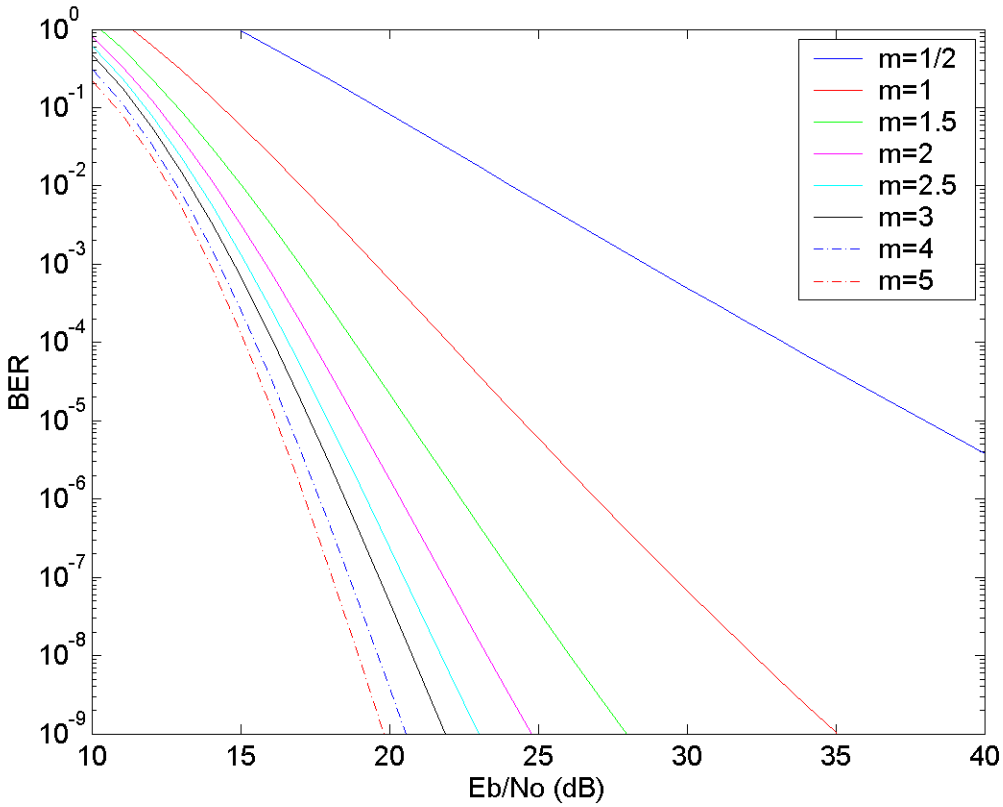

Figure 43. 64-QAM in Nakagami-m Fading with HDD for $r = 2/3$

As with previous analyses, we plot the performance curves obtained in Figure 43 against those of the uncoded results obtained in section III.B.2 for 64-QAM to show the range of possible coding gain. This comparison is made in Figure 44.

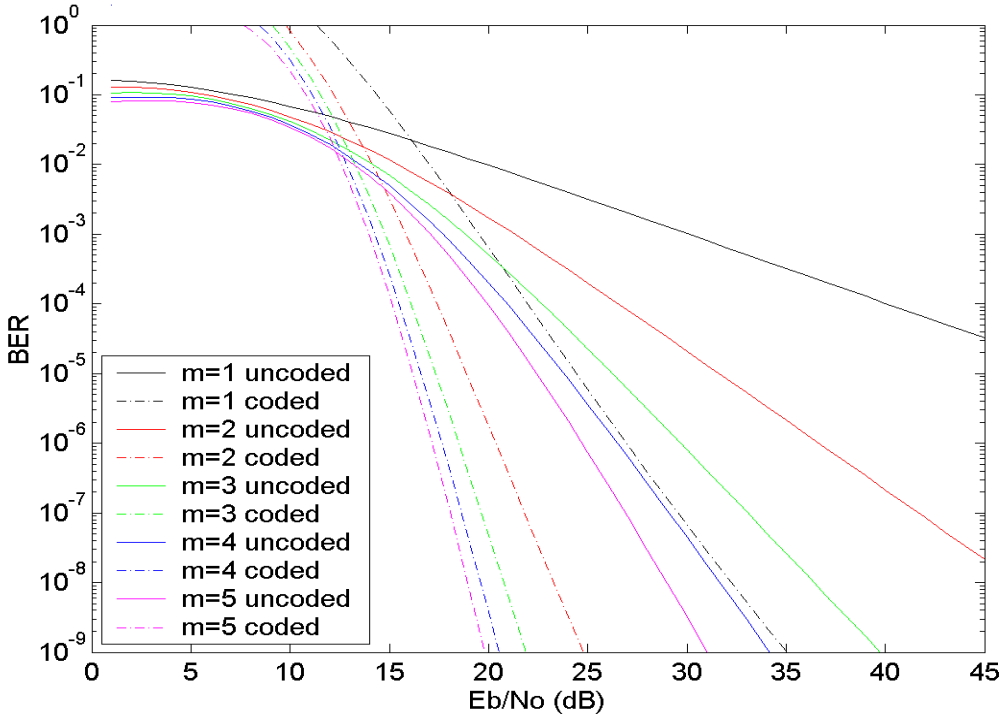

Figure 44. Uncoded vs. HDD 64-QAM in Nakagami-m fading for $r = 2/3$

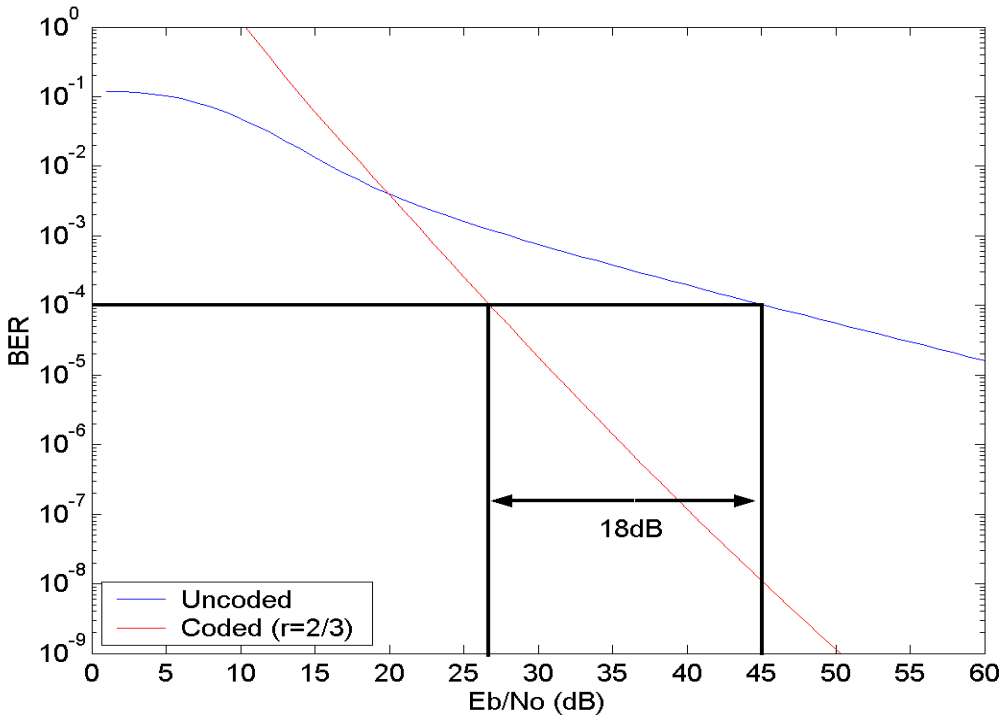

Figure 45. 64-QAM Modulated OFDM in Nakagami-m Fading w/ HDD $r = 2/3$

The analysis is performed for all 48 data sub-carriers called for in the IEEE 802.11a standard for 64-QAM at $r = 2/3$ and $1/2 \le m \le 5$ and averaged to obtain the composite OFDM system performance at 48 Mbps as in Figure 45. For this code rate and modulation we note positive coding gain is realized at about 21 dB between 10^{-2} and 10^{-3} BER. The coding gain increases quickly after this point and reaches 18 dB at BER 10^{-4} where the absolute performance of the system is 27 dB received average SNR.

At this point only the 54 Mbps data rate remains to be analyzed. To obtain this data rate 802.11a uses 64-QAM with convolutional coding at rate $r = 3/4$. The results of this analysis are presented in Figures 46-48.

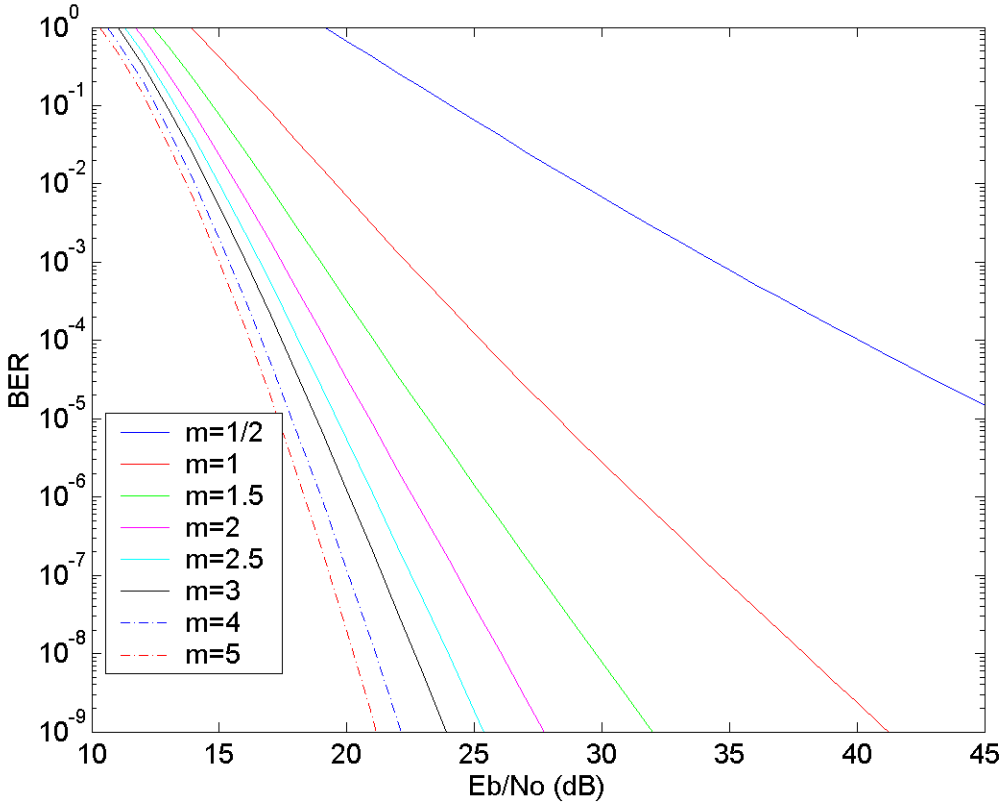

Figure 46. 64-QAM in Nakagami-m Fading with HDD for $r = 3/4$

In Figure 48 we note that positive coding gain for the OFDM system level analysis begins at $E_b / N_0 \approx 27\,\text{dB}$ and $\text{BER} \approx 10^{-3}$. At BER 10^{-4} the coding gain has reached 13, dB and we observe an absolute performance of 32 dB.

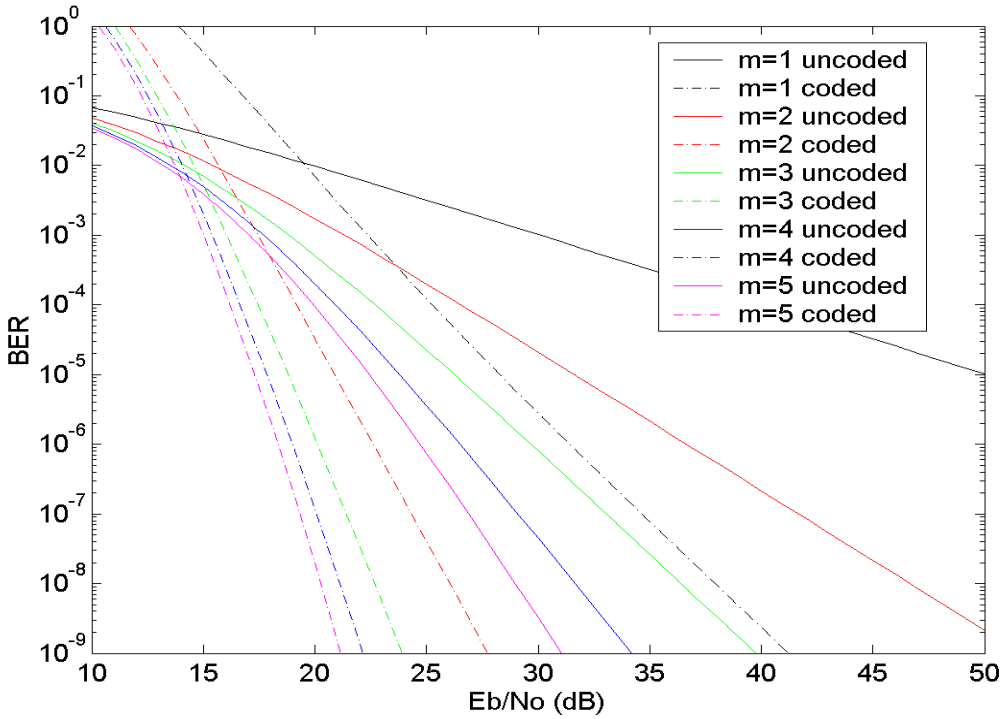

Figure 47. Uncoded vs. HDD 64-QAM in Nakagami-m fading for $r = 3/4$

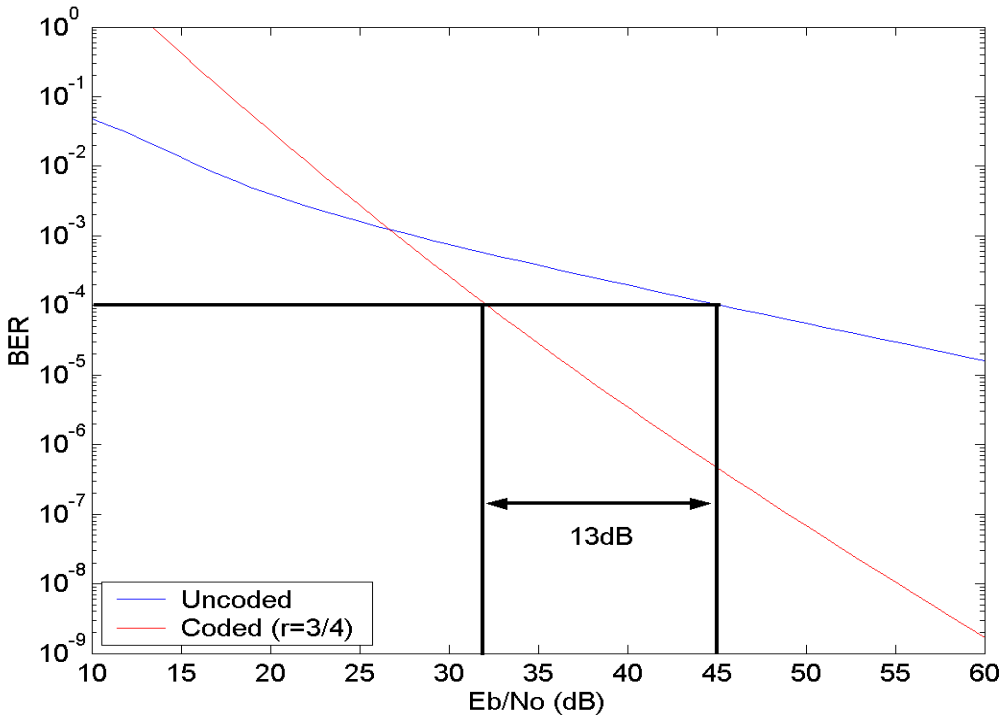

Figure 48. 64-QAM Modulated OFDM in Nakagami-m Fading w/ HDD $r = 3/4$

4. HDD Summary

In this section we have conducted the analysis for OFDM in all of its 802.11a-compliant forms. We have re-evaluated our original equations for the performance of BPSK, QPSK, 16-QAM, and 64-QAM in Nakagami-m distributed fading by incorporating FEC coding at the data rates specified in the standard. This analysis was based on the demodulator being classified as a hard decision Viterbi decoder. At the end of each sub-carrier modulation section we presented in Figures 33, 36, 39, 42, 45, and 48 the bottom line analysis of the composite OFDM system performance at that code and data rate. In Table 8 we summarize these results.

Modulation and Code Rate		**Data Rate (Mbps)**	**Point of Positive Coding Gain (BER and SNR)**		**Coding Gain @ BER 10^{-4}**	**Absolute Performance @ BER 10^{-4}**
BPSK/QPSK	$r = 1/2$	6/12	10^{-2}	10 dB	23 dB	17 dB
BPSK/QPSK	$r = 3/4$	9/18	10^{-3}	23 dB	12 dB	28 dB
16-QAM	$r = 1/2$	24	10^{-2}	11 dB	24 dB	18 dB
16-QAM	$r = 3/4$	36	10^{-3}	24 dB	13 dB	30 dB
64-QAM	$r = 2/3$	48	5×10^{-2}	21 dB	18 dB	27 dB
64-QAM	$r = 3/4$	54	10^{-3}	27 dB	13 dB	32 dB

Table 8. IEEE 802.11a System Performance Summary for HDD

C. SOFT DECISION DECODING

In the previous section we showed how OFDM system performance can be improved considerably through the addition of FEC coding techniques. The hard decisions made represent two levels of quantization. That is, demodulated bits are represented as one of two discrete values. Since this is a two level quantization, the use of Hamming distance as the metric is sufficient. In soft decision decoding (SDD), the

demodulator no longer delivers hard decisions, rather it provides the decoder with multiple quantized noisy signals called "soft decisions" [9]. In theory true SDD occurs when an infinite number of levels can be represented. Since this process requires a metric that can provide enough resolution to separate these various levels, the Hamming distance is no longer a sufficient metric. Another metric, one that provides the needed resolution to represent multiple quantized levels, must be employed. The Euclidean distance is one such metric. The primary difference, therefore, between hard and soft decision Viterbi decoding is that in soft decision we use a different metric, for example that of Euclidean distance instead of Hamming distance. Since the computation of the Euclidean distance often results in a non-integer value (the square root of a number for instance), real convolutional decoding chips use other monotonic metrics such as the Euclidean distance squared that are easier to implement [9] since the result of the squaring process yields an integer which is more readily realized in hardware. In using such a metric, maximum correlation with a given codeword is sought instead of minimum distance, so the path through the Trellis that is most likely is the one with the greatest path metric.

With a binary convolutional code, true soft decision Viterbi decoding cannot be accomplished in combination with non-binary modulation techniques. Therefore, any attempt to analytically develop the performance analysis for OFDM with 16 or 64-QAM would be guesswork at best. For this reason, we are forced to concede that a performance analysis of the two M-QAM sub-carrier modulation techniques in the IEEE 802.11a standard with SDD is not possible at this point. The performance of 64-QAM with approximate SDD is simulated in [17], however, since our study is an analysis of OFDM in which we derive our results analytically we will not employ such methods. This leaves only BPSK and QPSK, which can be readily developed and analyzed. Although we cannot conduct such analysis of 16 and 64-QAM, we do know that since the performance of BPSK and QPSK in general is superior to that of M-QAM, we may consider the results of the analysis of BPSK and QPSK to be the best-case performance for SDD. In the case of QPSK we may consider it a binary modulation technique in that it may be seen as two pulse amplitude modulated (PAM) functions in phase quadrature. Therefore,

as before, since the expressions for probability of bit error are identical for BPSK and QPSK, we may develop them as one.

We begin by developing the performance of BPSK and QPSK with SDD in Nakagami-m fading. After this is accomplished we will again revisit the data rates specified for the 802.11a standard along with their respective code rates. As with HDD, we will examine BPSK/QPSK at six and nine Mbps, respectively, for code rate $r = 1/2$ and 12 and 18 Mbps, respectively, for code rate $r = 3/4$.

1. SDD Performance Analysis

Equation (4.5) is still used as the upper bound for performance for SDD just as it was with HDD. In developing the performance of SDD in Nakagami-m fading for BPSK/QPSK, we note that according to [1], only P_d in Equation (4.5) changes. The coefficients listed in Table 7 remain relevant to the current analysis. How then do we obtain a new expression for P_d to represent SDD? We begin by assuming maximum ratio combining (MRC) at the demodulator and by modeling the output of the demodulator as the Gaussian random variable v_l with mean $\bar{v}_l = \alpha_l^2 \sqrt{E_{b_c}} = \alpha_l^2 \sqrt{E_b r}$ and variance $\sigma_{v_l}^2 = \alpha_l^2 (N_0/2)$ as in [1]. Assuming as before that the all-zero path is the correct path and that the v^{th} path differs from the correct path in d bits, then a decoding error occurs when [1]

$$v = \sum_{l=1}^{d} v_l > 0 \tag{4.18}$$

where the index l runs over the set of d bits in which the correct path and the v^{th} path differ. Since v is the sum of d independent identically, distributed (IID) Gaussian random variables v_l, then v is also a Gaussian random variable with mean

$$\bar{v} = \sqrt{E_b r} \sum_{l=1}^{d} \alpha_l^2 \tag{4.19}$$

and variance

$$\sigma_{\nu}^{2} = \frac{N_0}{2}\sum_{l=1}^{d}\alpha_l^2 \tag{4.20}$$

The probability that the v^{th} path will be selected over the correct path is given in [1] as

$$P_d = \Pr(\nu > 0) = \Pr\left(\sum_{l=1}^{d} v_l > 0\right) \tag{4.21}$$

Therefore, since ν is a Gaussian random variable, Equation (4.21) can be evaluated by means of the Gaussian integral function given in Equation (2.19) where the mean and variance are given in Equations (4.19) and (4.20), respectively. Thus, we obtain

$$P_d(\gamma_b) = Q\left(\sqrt{\frac{\overline{\nu}^2}{\sigma_{\nu}^2}}\right) = Q\left(\sqrt{\frac{\left(\sqrt{E_b r}\sum_{l=1}^{d}\alpha_l^2\right)^2}{\frac{N_0}{2}\sum_{l=1}^{d}\alpha_l^2}}\right) = Q\left(\sqrt{\frac{2E_b r}{N_0}\sum_{l=1}^{d}\alpha_l^2}\right) \tag{4.22}$$

Recall that in Chapter III we defined $\gamma_b = \alpha^2(E_b/N_0)$. In this case, we must now adjust this definition to reflect the summation of d Nakagami-squared random variables by defining

$$\gamma_b = \frac{E_b}{N_0}\sum_{l=1}^{d}\alpha_l^2 \tag{4.23}$$

Therefore, Equation (4.22) can be expressed

$$P_d(\gamma_b) = Q\left(\sqrt{2r\gamma_b}\right) \tag{4.24}$$

We note that Equation (4.24) is a conditional probability. As we have done previously, we can now obtain an expression for P_d by integrating Equation (4.24) over the PDF of the new γ_b, which we will designate as $f_{\Gamma_b}(\gamma_b)$. In other words we evaluate

$$P_d = \int_0^{\infty} P_d(\gamma_b) f_{\Gamma_b}(\gamma_b)\, d\gamma_b \tag{4.25}$$

The conditions, however, have changed. We can no longer utilize the equation for the PDF of γ_b given in Equation (3.16), restated here as

$$p_{\gamma_b}(\gamma_b) = \frac{m^m}{\Gamma(m)\overline{\gamma}_b^m}\gamma_b^{m-1}e^{-\left(\frac{m\gamma_b}{\overline{\gamma}_b}\right)} \tag{4.26}$$

since we now seek the PDF of the sum of d Nakagami-squared random variables as shown in Equation (4.23). Therefore, we must obtain $f_{\Gamma_b}(\gamma_b)$ before we can evaluate Equation (4.25).

It is shown in [15] that the PDF of the sum of two independent random variables is given by convolution:

$$f_Z(z) = \int_{-\infty}^{\infty} f_X(x') f_Y(z - x')dx' \tag{4.27}$$

where $Z = X + Y$ and X and Y are independent random variables. Since we must sum d independent random variables, evaluating a d-fold convolution is not mathematically tractable. Therefore, a simpler method for obtaining $f_{\Gamma_b}(\gamma_b)$ is to make use of characteristic functions to simplify the mathematics. However, since our PDF is non-zero only for positive arguments, we can utilize the Laplace transform, defined as

$$\mathscr{L}\{f(t)\} = F(s) = \int_0^{\infty} f(t)e^{-st}dt \tag{4.28}$$

We can now make use of the well known property of transforms that states that convolution in the non-transform domain is equivalent to multiplication in the transform, or the s, domain. Therefore, we obtain an expression for $f_{\Gamma_b}(\gamma_b)$ by raising the resulting Laplace transform to the d^{th} power and performing an inverse Laplace transform on the result. Taking the Laplace transform of Equation (4.26), we get

$$\begin{aligned}
&\mathscr{L}\{p_{\gamma_b}(\gamma_b)\} = P_{\gamma_b}(s) = \int_0^{\infty} p_{\gamma_b}(\gamma_b)e^{-s\gamma_b}d\gamma_b \\
&= \int_0^{\infty} \frac{m^m}{\Gamma(m)\overline{\gamma}_b^m}\gamma_b^{m-1}e^{-\left(\frac{m\gamma_b}{\overline{\gamma}_b}\right)}e^{-s\gamma_b}d\gamma_b \\
&= \left(\frac{m}{\overline{\gamma}_b}\right)^m \frac{1}{\Gamma(m)}\int_0^{\infty}\gamma_b^{m-1}e^{-\gamma_b\left(s+\frac{m}{\overline{\gamma}_b}\right)}d\gamma_b
\end{aligned} \tag{4.29}$$

In order to solve Equation (4.29) we make use of the following mathematical identity from [18]

$$\int_0^\infty x^{y-1}e^{-\mu x}dx = \frac{1}{\mu^y}\Gamma(y) \qquad \mathrm{Re}\{\mu\} > 0, \mathrm{Re}\{y\} > 0 \tag{4.30}$$

Therefore, making the substitutions

$$\begin{aligned} x &= \gamma_b \\ y &= m \\ \mu &= s + \tfrac{m}{\bar{\gamma}_b} \end{aligned} \tag{4.31}$$

we obtain the Laplace transform of $p_{\gamma_b}(\gamma_b)$ as

$$\begin{aligned} P_{\gamma_b}(s) &= \left(\frac{m}{\bar{\gamma}_b}\right)^m \frac{1}{\Gamma(m)} \int_0^\infty \gamma_b^{m-1} e^{-\gamma_b\left(s+\frac{m}{\bar{\gamma}_b}\right)} d\gamma_b \\ &= \left(\frac{m}{\bar{\gamma}_b}\right)^m \frac{1}{\Gamma(m)} \Gamma(m) \frac{1}{\left(s+\frac{m}{\bar{\gamma}_b}\right)^m} \\ &= \left(\frac{m}{\bar{\gamma}_b}\right)^m \frac{1}{\left(s+\frac{m}{\bar{\gamma}_b}\right)^m} \end{aligned} \tag{4.32}$$

As indicated above, the sum of the Laplace transform of the PDF of the sum of d Nakagami-squared random variables is equivalent to raising Equation (4.32) to the d^{th} power. Hence, we obtain

$$\begin{aligned} \left\{\mathscr{L}\left\{p_{\gamma_b}(\gamma_b)\right\}\right\}^d &= \left\{P_{\gamma_b}(s)\right\}^d \\ &= \left[\left(\frac{m}{\bar{\gamma}_b}\right)^m \frac{1}{\left(s+\frac{m}{\bar{\gamma}_b}\right)^m}\right]^d = \left(\frac{m}{\bar{\gamma}_b}\right)^{md} \frac{1}{\left(s+\frac{m}{\bar{\gamma}_b}\right)^{md}} \end{aligned} \tag{4.33}$$

which represents the Laplace transform of the PDF of the sum of d independent Nakagami-squared random variables.

The last step in obtaining an expression for the PDF of the sum of d independent Nakagami-squared random variables is to transform Equation (4.33) back to its original domain by use of the inverse Laplace transform defined by

$$\mathscr{L}^{-1}\left\{F(s)\right\} = f(t) = \int_0^\infty F(s)e^{st}ds \tag{4.34}$$

Therefore, we have,

$$f_{\Gamma_b}(\gamma_b) = \mathscr{L}^{-1}\left\{P_{\gamma_b}(s)\right\}$$
$$= \mathscr{L}^{-1}\left\{\left(\frac{m}{\overline{\gamma}_b}\right)^{md} \frac{1}{\left(s+\frac{m}{\overline{\gamma}_b}\right)^{md}}\right\} = \left(\frac{m}{\overline{\gamma}_b}\right)^{md} \int_0^{\infty} \frac{1}{\left(s+\frac{m}{\overline{\gamma}_b}\right)^{md}} e^{s\gamma_b} ds \tag{4.35}$$

Rather than carry out the integration, we make use of inverse Laplace transform tables and note the transform pair

$$\mathscr{L}^{-1}\left\{\frac{1}{(s+a)^u}\right\} = \frac{t^{u-1}}{\Gamma(u)} e^{-at} \qquad for\, u > 0 \tag{4.36}$$

By setting

$$\begin{aligned} t &= \gamma_b \\ u &= md \\ a &= \frac{m}{\overline{\gamma}_b} \end{aligned} \tag{4.37}$$

and recalling that there remains a constant term $(m/\overline{\gamma}_b)^{md}$ in Equation (4.35) that is not accounted for in Equation (4.36), we obtain the inverse Laplace transform as follows:

$$f_{\Gamma_b}(\gamma_b) = \left(\frac{m}{\overline{\gamma}_b}\right)^{md} \frac{\gamma_b^{md-1}}{\Gamma(md)} e^{-\left(\frac{m\gamma_b}{\overline{\gamma}_b}\right)} = \frac{m^{md}}{\Gamma(md)\overline{\gamma}_b^{md}} \gamma_b^{md-1} e^{-\left(\frac{m\gamma_b}{\overline{\gamma}_b}\right)} \tag{4.38}$$

which represents the PDF of the sum of d Nakagami-squared random variables. One interesting observation from Equation (4.38) is that it resembles the PDF we originally started with in Equation (4.26) except that the exponent $m = md$. This result is fortunate in that as we substitute Equations (4.38) and (4.24) into Equation (4.25) to obtain P_d, we must evaluate the integral

$$P_d = \int_0^{\infty} Q\left(\sqrt{2r\gamma_b}\right) \frac{m^{md}}{\Gamma(md)\overline{\gamma}_b^{md}} \gamma_b^{md-1} e^{-\left(\frac{m\gamma_b}{\overline{\gamma}_b}\right)} d\gamma_b \tag{4.39}$$

which we have already done. Therefore, it is clear that if we compare Equation (4.39) to Equations (3.18) through (3.22), we can evaluate this integral by the same method by letting

$$\begin{aligned} t &= \gamma_b \\ c &= 2r \\ b &= md \\ a &= \frac{m}{\bar{\gamma}_b} \\ \psi &= \frac{c}{2a} = \frac{2r}{\frac{m}{\bar{\gamma}_b}} = \frac{r\bar{\gamma}_b}{m} \end{aligned} \tag{4.40}$$

This results in,

$$P_d = \sqrt{\frac{r\bar{\gamma}_b}{m + r\bar{\gamma}_b}} \frac{\Gamma\left(md + \frac{1}{2}\right)}{2\sqrt{\pi}\,\Gamma\left(md+1\right)\left(1+\frac{r\bar{\gamma}_b}{m}\right)^{md}} \left(1 + \sum_{k=1}^{\infty} \frac{\prod_{n=0}^{k-1}\left(md + \frac{1}{2} + n\right)\left(\frac{1}{1+\frac{r\bar{\gamma}_b}{m}}\right)^k}{\prod_{n=0}^{k-1}\left(md+1+n\right)} \right) \tag{4.41}$$

Therefore, we obtain an upper bound on probability of information bit error for BPSK and QPSK in Nakagami-m fading with soft decision Viterbi decoding by substituting Equation (4.41) and the coefficients of B_d listed in Table 7 into Equation (4.5).

2. BPSK/QPSK with SDD (6 and 9 Mbps)

We now evaluate Equation (4.5) by means of Equations (4.41) and the values for B_d at different code rates in order to analyze the performance of BPSK/QPSK at the data rates specified in the 802.11a standard. In this section we present the results of this analysis for six Mbps BPSK and nine Mbps QPSK since they both require a convolutional code rate of $r = 1/2$. In Figure 49 we plot the results of this analysis for different values of the fading figure m.

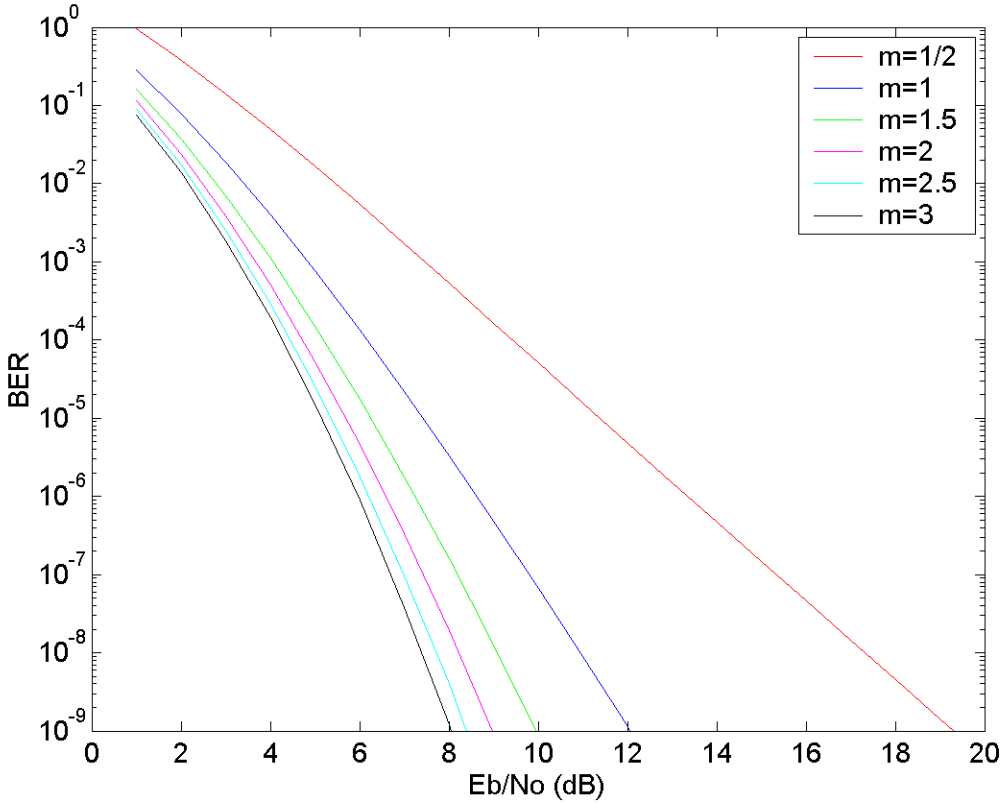

Figure 49. BPSK/QPSK in Nakagami-m Fading with SDD for $r = 1/2$

Note that due to the enormous size of some of the intermediate values involved in computing Equation (4.41), software limitations precluded the evaluation of curves for the cases of $m = 4$ and $m = 5$. The general trend is clear, however, and we can accurately estimate the location of these two curves. Fortunately, this limitation does not plague us at the higher code rate $r = 3/4$, analyzed in the next section.

By way of comparison with the case of HDD analyzed in section IV.B.1, we overlay the HDD curves corresponding to the SDD curves obtained in Figure 49 for $r = 1/2$. The benefits obtained by the use of SDD for BPSK and QPSK over HDD are indicated in Figure 50.

When we perform the analysis with SDD for all 48 data sub-carriers, we obtain the results given in Figure 51. In Figure 51 we present the results of the BPSK/QPSK modulated OFDM system with SDD against those obtained for the same data and code rate for HDD earlier in this chapter.

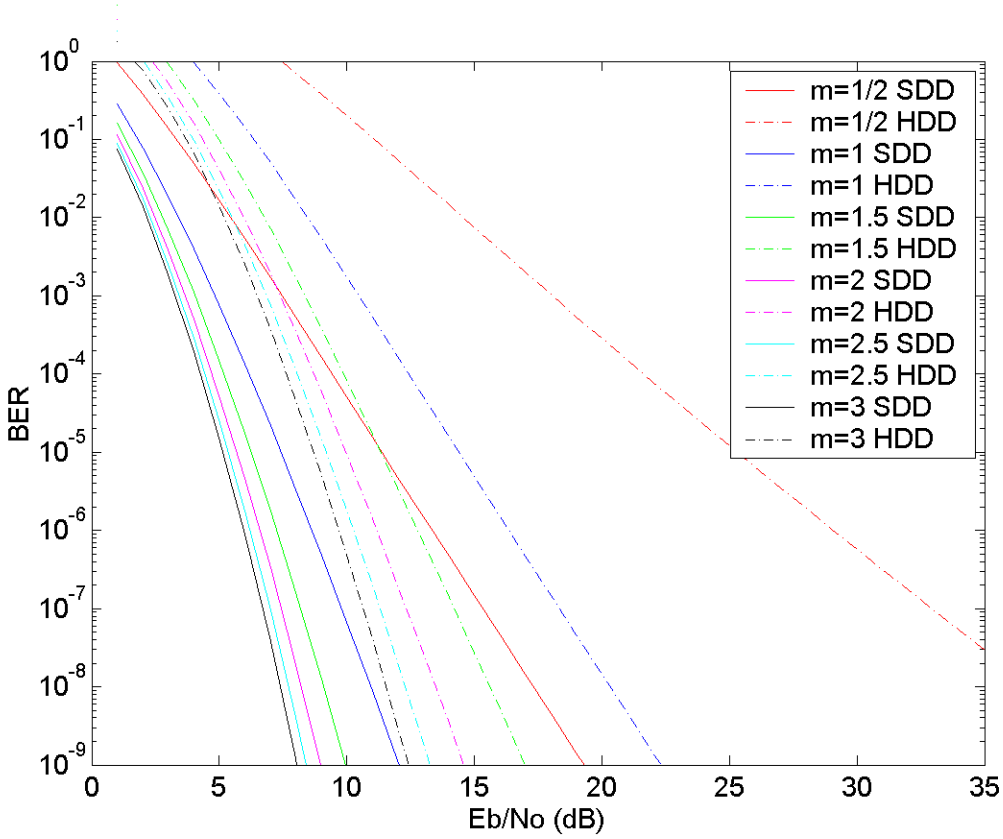

Figure 50. SDD vs. HDD for BPSK/QPSK in Nakagami-m fading for $r = 1/2$

We note from Figure 51 that the coding gain obtained for the OFDM system as a whole is significant. Where in an AWGN channel SDD generally improves performance by about 2.5 dB over HDD, under the fading conditions we have specified, we are able to obtain a coding gain of 11 dB at BER 10^{-4}. The absolute performance for BER=10^{-4} is a received SNR of just under 6 dB.

By way of summarizing the results for BPSK and QPSK for six and nine Mbps data rates at convolutional coding rate $r = 1/2$, we plot the curves obtained for uncoded BPSK/QPSK in Nakagami-m fading versus the two coded cases obtained for both HDD and SDD OFDM in Figure 52. It is important to note that the aforementioned software limitation proved to have no appreciable effect on the validity of the results obtained for SDD at $r = 1/2$ since in Chapter III we proved that the most dominant values of the fading figure were the smallest values.

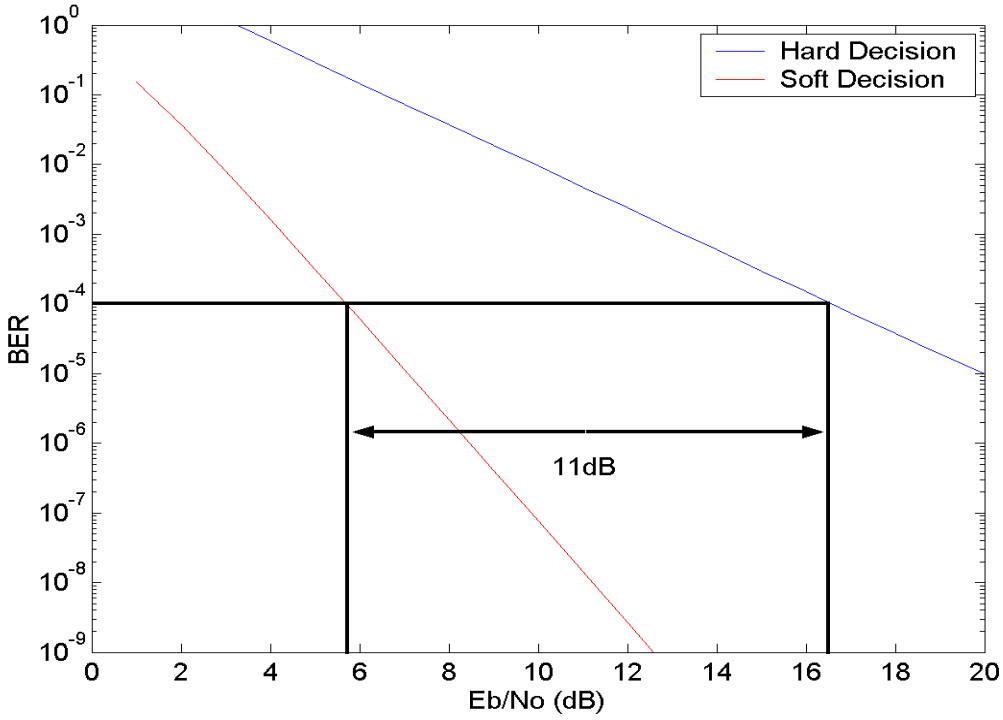

Figure 51. BPSK/QPSK Modulated OFDM in Nakagami-m Fading w/ SDD $r = 1/2$

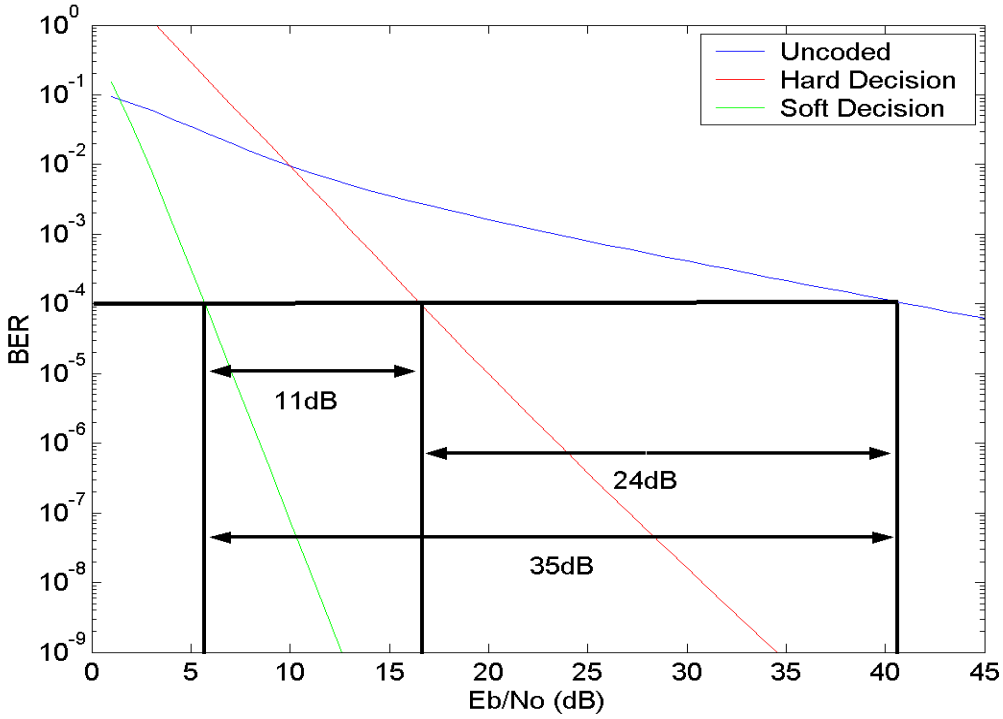

Figure 52. BPSK/QPSK Modulated OFDM; Uncoded and HDD, vs. SDD $r = 1/2$

Furthermore, in the analysis performed on uncoded BPSK modulated OFDM in Nakagami-m fading for the system of 48 sub-carriers, we proved that no matter how high we allow m to go, the least favorable fading conditions, such as $m = 1/2$ dominate the overall trend no matter how many trials we conducted. From Figure 52 we see that the coding gain is a phenomenal 35 dB when we compare the case of coded BPSK and QPSK with SDD to the uncoded case. This is a remarkable performance improvement.

3. BPSK/QPSK with SDD (12 and 18 Mbps)

At this point the only thing that remains is to analyze the performance of 12 Mbps BPSK and 18 Mbps QPSK both with SDD in Nakagami-m fading. Here again, since we are analyzing the impact of soft decision Viterbi decoding, we must evaluate Equation (4.5) by way of Equation (4.41) and Table 7. This time the analysis is performed at the code rate specified for these data rates and modulation types, rate $r = 3/4$. In Figure 53 we plot the results of this analysis for the usual values of the fading figure m. As we saw with HDD, the performance curves in Figure 53 are slightly poorer than those obtained in Figure 49 since the code rate is higher. In Figure 54, we overlay the HDD curves from section IV.B.1 for $r = 3/4$ onto these results to gain some perspective on how SDD performs relative to HDD for this code rate.

In Figure 55 we perform the analysis of the OFDM system of 48 sub-carriers at $r = 3/4$ by designating the fading figure m a uniform random variable between $1/2 \le m \le 5$. The results of the SDD case are plotted against those obtained for HDD at the same code rate. Notice that a coding gain of 15 to 16 dB is achieved over the HDD case. In terms of absolute performance, an average SNR per bit of 13 dB must be received in order to obtain a BER of 10^{-4}, up from 6 dB for the case of $r = 1/2$.

A summary of uncoded BPSK/QPSK modulated OFDM versus HDD and SDD BPSK/QPSK modulated OFDM are presented in Figure 56. The overall coding gain achieved by the use of soft decision Viterbi decoding is approximately 29 dB at 10^{-4}.

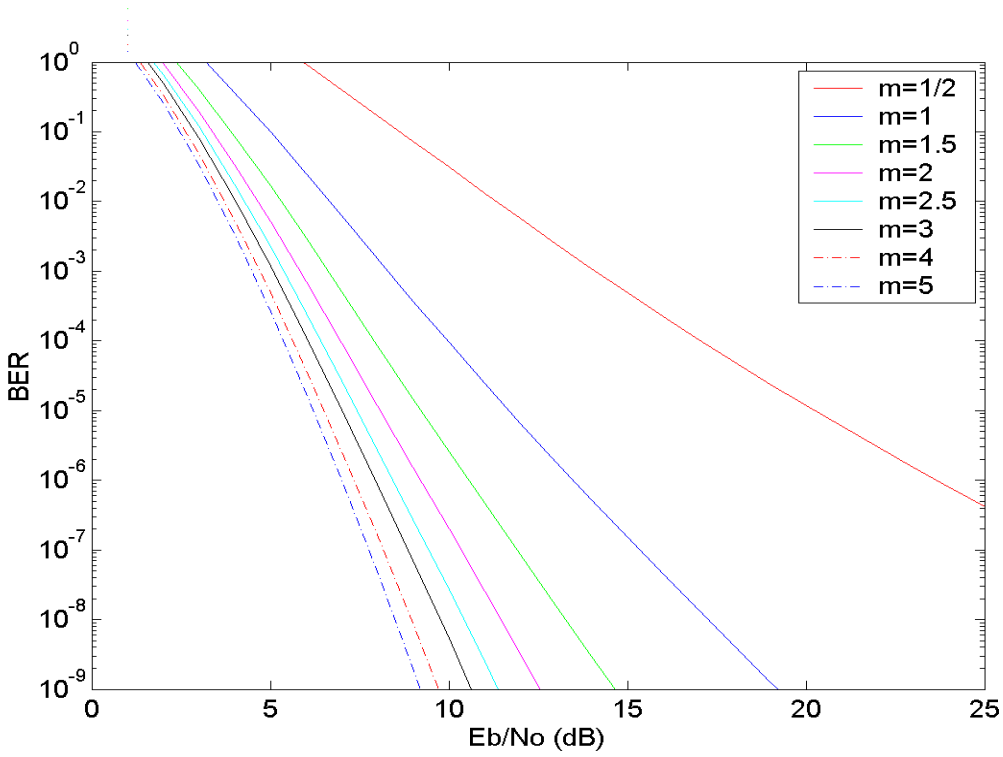

Figure 53. BPSK/QPSK in Nakagami-m Fading with SDD for $r = 3/4$

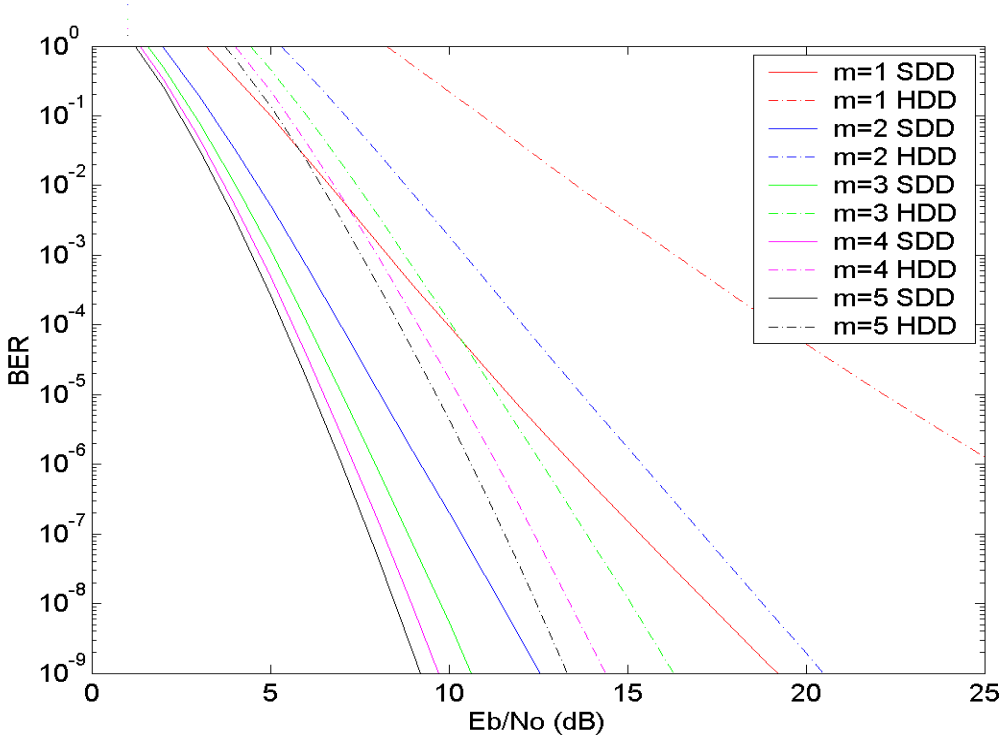

Figure 54. SDD vs. HDD for BPSK/QPSK in Nakagami-m fading for $r = 3/4$

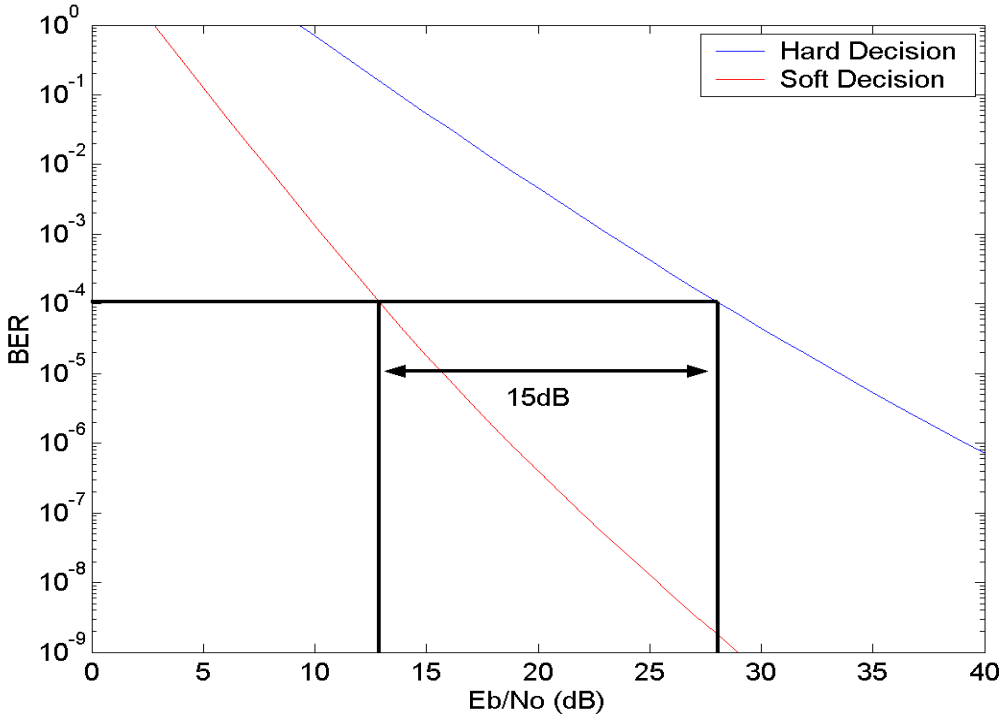

Figure 55. BPSK/QPSK Modulated OFDM in Nakagami-m Fading w/ SDD $r = 3/4$

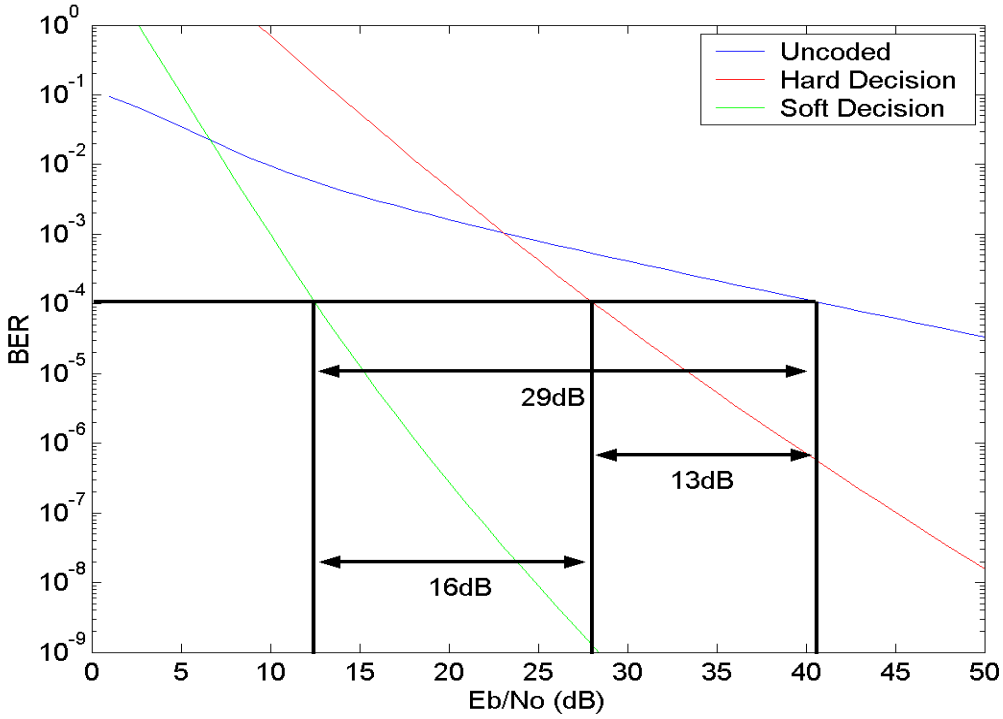

Figure 56. BPSK/QPSK Modulated OFDM; Uncoded and HDD, vs. SDD $r = 3/4$

D. FEC CODING SUMMARY

In this chapter we evaluated the performance of an OFDM system with error correction coding, specifically, the convolutional coding utilized in IEEE 802.11a-compliant systems. This was also necessitated by the fact that most real communications systems employ FEC coding to enhance performance of a digital communications system at low SNR. After a brief discussion of some fundamental trade-offs involved in employing FEC coding, we examined two distinct ways of decoding, hard decision and soft decision Viterbi decoding. In each case a different analysis technique was used based on how each technique demodulated and decoded the received bits.

Our analysis necessarily took us through each sub-carrier modulation type indicated in the 802.11a standard and every data and code rate associated with a given modulation type. What we observed in general is that employing HDD dramatically improves the performance of the uncoded system as measured by coding gain. We compiled a list of these improvements in Table 8.

An even greater performance improvement is obtained when we employed soft decision Viterbi decoding methods in our analysis. Many manufacturers have found the potential benefits of SDD to far outweigh the potential drawbacks of circuit complexity inherent in the multi-level quantization involved in SDD. Since we were only able to analytically derive the performance of BPSK and QPSK in Nakagami-m fading with SDD, the discussion surrounded only these two modulation types but at variable code and data rates. Coding gains between 11 and 15 dB were noted over HDD and overall coding gains on the order of 30 dB were obtained over uncoded system performance.

This concludes our OFDM performance analysis, and in the next and final chapter, we will review the results of this thesis with an eye to areas of potentially related research and make some closing statements.

THIS PAGE INTENTIONALLY LEFT BLANK

V. CONCLUSION

The goal of this thesis was to analytically assess the performance of OFDM in frequency-selective, slowly fading channels. Since there are numerous ways to implement OFDM, adopting one type of implementation was necessary in order to focus this study. The IEEE 802.11a standard is one such implementation. Therefore, the IEEE 802.11a standard formed the framework in which OFDM was studied in this thesis.

Many statistical models exist which allow us to analytically represent the fluctuations in the received signal envelope due to multipath fading, so here again it was necessary to narrow the scope by choosing a model. The Nakagami-m distribution was chosen to model channel behavior since it affords the greatest degree of flexibility and application. The Nakagami-m distribution, being a two variable distribution, has the flexibility to emulate fading conditions that are either worse than, the same as, or more favorable than Rayleigh fading, and accounts for either LOS or non-LOS communications. The benefit of such a choice is clear; the results contained herein are general enough to be further refined to suit virtually all plausible slow fading conditions.

Since OFDM is designed to operate in frequency-selective channels, it was necessary to contend with this type of channel model. The method of performing the analysis on each sub-carrier individually and assuming that any ISI was virtually eliminated by the use of the cyclic extension within the guard interval enabled us to avoid more cumbersome frequency-selective methods of analysis. The OFDM composite signal was then analyzed by having each sub-carrier encounter independent fading statistics (according to the Nakagami-m distribution) and averaging the results.

A. CAPABILITIES AND LIMITATIONS

As discussed above, since the use of the Nakagami-m distribution allows for more generality, one of the strengths of this study is its applicability. With very little effort, many of the fading assumptions made in this thesis can be easily altered to more closely match the characteristics of most any fading conditions. Furthermore, since this study closely followed the IEEE 802.11a standard, analyzing each modulation type specified including error correction coding at the appropriate code rate, it represents a completely

comprehensive study of the IEEE 802.11a standard implementation of OFDM and of the performance of 802.11a-compliant systems.

In one of the strengths of this study is found its chief limitation. Because our fading statistics provided us with so much versatility, we endeavored to represent a multitude of values for the fading figure m in the Nakagami-m distribution. The only detractor here is that the results given at the end of each sub-section are heavily dependent, as one might expect, on the range of values which m is allowed to take. If for example, fading conditions more closely resembling $m = 1/2$ prevailed in a certain application or location, averaging over the range $1/2 \le m \le 5$ would provide a slightly less conservative result. Therefore, the results presented in this thesis should not be considered to be absolute. However, it is important to note that given the results obtained in Chapter III in which we demonstrate the dominance of the smaller values of m, it is clear that such deviations are minor if not negligible when averaged over a large number of sub-carriers. A more accurate estimation of particular channel fading characteristics would help narrow the focus of the analysis.

B. FINDINGS

Though our findings are difficult to single out since they are spread out over many plots of performance curves, many of the most notable findings in this thesis were a result of the analysis performed in Chapter III for the uncoded system. After averaging the 48 data sub-carriers, we noted that at low SNR, the composite OFDM signal performance appears to represent a true "average" somewhere between the two limits on the uniform distribution assigned to m. However, at moderate to high SNR, the less favorable conditions caused by smaller values m dominate the overall composite system performance. For example, when m was allowed to vary between $1 \le m \le 5$ at moderate to high SNR, the composite signal hovered around a value of $m = 1.2$ rather than closer to five. We discovered also that no matter how favorable we allow channel conditions to get, such as by raising the limit on m to the point of $m = 50$, there is little difference in average performance and system performance is still dominated by the lower limit on m.

On the other hand, raising the lower limit on m significantly enhances performance as was the case for $1 \le m \le 5$ when compared with $1/2 \le m \le 5$. Contrary to our intuition, although the average value of m in these two ranges is close, the dominance $m = 1/2$ caused the curves representing the composite signals in these ranges to be significantly far apart. We also note that the dependence of the composite signal performance on the number of sub-carriers is negligible once the number of sub-carriers exceeds about 35.

Another important finding is the magnitude of the coding gain obtained by the addition of error correction coding as analyzed in Chapter IV. While we expected moderate coding gain in AWGN with no fading by employing FEC coding, the coding gain from uncoded to HDD and SDD OFDM is enormous; on the order of 30 dB at times for BER=10^{-4} for the range $1/2 \le m \le 5$.

Upon review of Table 8, we also note that the absolute SNR required for BER=10^{-4} does not monotonically decrease (signifying improved performance) from 64-QAM at $r = 3/4$ down to BPSK/QPSK at $r = 1/2$ as we might expect. Although the absolute performance does improve from one modulation to another for the same code rate, the degradation discovered going from, for example, 64-QAM at $r = 2/3$ to 16-QAM at $r = 3/4$ is counterintuitive and perhaps demonstrates a condition not considered by the standards committee. We note the same occurs when we go up Table 8 from 16-QAM at $r = 1/2$ to BPSK/QPSK at $r = 3/4$. It is also interesting to note that the absolute performance improvement between any two modulation types for a given code rate, such as BPSK/QPSK at $r = 1/2$ and 16-QAM at $r = 1/2$ is minimal; one dB in this example. Likewise, at $r = 3/4$, we note an absolute improvement of only two dB from BPSK/QPSK to 16-QAM and from 16-QAM to 64-QAM. Under fading conditions we might have expected this improvement to be much more profound.

C. RECOMMENDATIONS FOR FURTHER RESEARCH

Now that this study is complete, there are a few areas in which follow-on research would be beneficial. In terms of a performance analysis of this sort, the approach taken in this thesis can easily be adjusted to provide any number of improvements/alterations.

For instance, one can adjust the type of distribution chosen for m when emulating the composite OFDM signal from that of a uniform distribution to some other distribution such as the exponential. The range of values of m can also be adjusted to more narrowly define certain types of fading.

In addition to the analysis performed in this thesis, approximating the performance of M-QAM modulated OFDM with SDD by means of simulation as indicated in [17] would be a welcome addition. Although this would not preserve the analysis techniques involved in this study, it would serve to completely exhaust all possible 802.11a variations and give us some insight into the performance attainable for higher order QAM constellations.

A logical outgrowth of this thesis could be a performance analysis of the OFDM in different fading conditions as described by another random distribution in place of the Nakagami or applying a different OFDM standard such as DVB or ADSL.

In an application perhaps more relevant to the mission of the Department of Defense (DOD), one can explore the vulnerability of the 802.11a standard or any other OFDM implementation to either hostile jamming or exploitation by unintended recipients. With the rapid growth of the WLAN and the need for much higher data rates provided by OFDM and 802.11a, it seems clear that IEEE 802.11a standard will find more and more acceptance in the months and years ahead. The ability to tap into these systems could prove to be an invaluable source of intelligence information.

D. CLOSING COMMENTS

With the recent emergence of IEEE 802.11a-compliant hardware, an analysis such as this may prove beneficial to those designing or employing the OFDM based 802.11a standard. Although IEEE 802.11b-compliant systems are already deployed throughout the world, it is clear that the 802.11a standard which will provide data rates of up to 54 Mbps will quickly overtake the older 802.11b standard which employs complementary code keying (CCK) at maximum data rates of 11 Mbps.

For its ability to effectively combat ISI, a bothersome form of interference in fading channels, and the relative ease with which it is implemented, OFDM will likely

continue to gain broad-based acceptance as the signaling technique of the future. It is therefore critical that communications theorists endeavor to study OFDM in all its possible permutations.

THIS PAGE INTENTIONALLY LEFT BLANK

LIST OF REFERENCES

1. Proakis, J.G., *Digital Communications*, 4th ed., McGraw Hill, New York, NY, 2001.

2. Xiong, F., *Digital Modulation Techniques*, Artech House, Norwood, MA, 2000.

3. Wan L. & Dubey, V.K., "Bit Error Probability of OFDM System Over Frequency-nonselective Fast Rayleigh Fading Channels." *IEEE Electronics Letters.*, Volume: 36 Issue: 15 July. 2000. pp. 1306-07.

4. Wan L. & Dubey, V.K. " BER Performance of OFDM System Over Frequency-nonselective Fast Ricean Fading Channels." *IEEE Communications Letters*, Volume: 5 Issue: 1 Jan 2001. pp. 19 –21.

5. Miletik, I., et.al., "Performance of OFDM DS/CDMA in Fading Channels." *TELSIKS '99,* Nis. Oct. 1999. pp 588-591.

6. Beaulieu, N.C. & Abu-Dayya, A. A., "Analysis of Equal Gain Diversity on Nakagami Fading Channels." *IEEE Trans. Commun.,* Vol. COM-39, Feb 1991. pp.225-234.

7. Van Nee, R. & Prasad R., *OFDM for Wireless Multimedia Communications*, Artech House, Norwood, MA, 2000.

8. Bahai, A.R.S., & Saltzberg, B.R., *Multi-Carrier Digital Communications: Theory and Applications of OFDM*, Kluwer Academic/Plenum, New York, NY,1999.

9. Sklar, B., *Digital Communications: Fundamental and Applications.*, 2nd ed. Prentice Hall, Upper Saddle River, NJ, 2001.

10. Proakis, J.G. & Manolakis, D.G., *Digital Signal Processing: Principles Algorithms, and Applications*, 3rd ed. Prentice Hall, Upper Saddle River, NJ, 1996.

11. Tomasi, W., *Electronic Communications Systems: Fundamentals Through Advanced*, 4th ed. Prentice Hall, Upper Saddle River, NJ, 2001

12. Institute of Electrical and Electronics Engineers, 802.11a, *Wireless LAN Medium Access Control (MAC) and Physical Layer (PHY) Specifications: High-Speed Physical Layer Extension in the 5 GHz Band*, 16 September 1999.

13. Haykin, S., *Communication Systems*. 3rd ed. John Wiley & Sons, New York, NY, 1994.

14. Wicker, S.B., *Error Control Systems for Digital Communication and Storage.* Prentice Hall, Upper Saddle River, NJ, 1995.

15. Leon-Garcia, A., *Probability and Random Processes for Electrical Engineering.* 2nd ed. Reading, MA, 1994.

16. Clark, G.C., Jr. & Cain, J.B., *Error-Correction Coding for Digital Communications.* Plenum Press, New York, NY, 1981.

17. May, T. Rohling, H., and Engels, V., "Performance Analysis of Viterbi Decoding for 64-DAPSK and 64-QAM Modulated OFDM Signals." *IEEE Transactions on Communications.* Vol. 46, No. 2, Feb 1998. pp.182-190.

18. Gradshteyn, I.S. & Ryzhik, I.M., *Tables of Integrals, Series, and Products.* Academic Press, New York, NY, 1980.

INITIAL DISTRIBUTION LIST

1. Defense Technical Information Center
   Ft. Belvoir, VA

2. Dudley Knox Library
   Naval Postgraduate School
   Monterey, CA

3. Chairman, Code EC
   Department of Electrical and Computer Engineering
   Naval Postgraduate School
   Monterey, CA

4. Professor Tri Ha, Code EC/Ha
   Department of Electrical and Computer Engineering
   Naval Postgraduate School
   Monterey, CA

5. Professor R. Clark Robertson, Code EC/Rc
   Department of Electrical and Computer Engineering
   Naval Postgraduate School
   Monterey, CA

6. Professor R. Cristi, Code EC/Cx
   Department of Electrical and Computer Engineering
   Naval Postgraduate School
   Monterey, CA

7. Professor John McEachen, Code EC/Mj
   Department of Electrical and Computer Engineering
   Naval Postgraduate School
   Monterey, CA

8. Director, National Security Agency
   ATTN: S3303 Mr. Robert Eubanks
   Fort Meade, MD

9. CDR Jan Tighe, USN
   Naval Information Warfare Activity
   Fort George G. Meade, MD

10. CDR Tim White, USN
    Chief of Naval Operations, Code N201
    Arlington, VA

11. LCDR John McKinstry, USN
Joint Special Operations Command, Code J2
Fort Bragg, NC

12. LCDR Tom Newman, USN
Space and Naval Warfare Command Space Field Activity
Chantilly, VA

13. Cryptologic Research Laboratory
ATTN: Nathan Beltz
Department of Electrical and Computer Engineering
Naval Postgraduate School
Monterey, CA

14. LT Bryan Braswell, USN
Naval Information Warfare Activity
Suitland, MD

15. Joseph A. Count
Kimberly Clark, Corp.
Beach Island, SC

16. LT Patrick Count, USN, Code N232
Commander, United States Naval Forces Central Command
Manama, Bahrain